Mechanical Behavior of a Ceramic Matrix Composite Material

by

Paul P. Grosskopf

Thesis submitted to the Faculty of the

Virginia Polytechnic Institute and State University

in partial fulfillment of the requirements for the degree of

Master of Science

in

Engineering Mechanics

APPROVED:

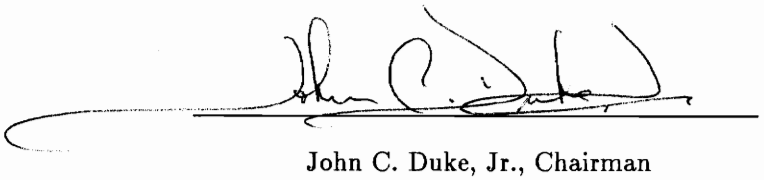

John C. Duke, Jr., Chairman

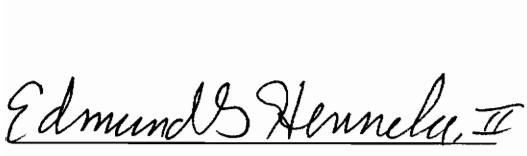

Edmund G. Henneke, II

D. P. H. Hasselman

5 November 1990

Blacksburg, VA

ABSTRACT

Monolithic ceramic materials have been used in industry for hundreds of years. These materials have proven their usefulness in many applications, yet, their potential for critical structural applications is limited. The existence of an imperfection in a monolithic ceramic on the order of several microns in size may be critical, resulting in catastrophic failure. To overcome this extreme sensitivity to small material imperfections, reinforced ceramic materials have been developed. A ceramic matrix which has been reinforced with continuous fibers is not only less sensitive to microscopic flaws, but is also able to sustain significant damage without suffering catastrophic failure.

A borosilicate glass reinforced with several layers of plain weave silicon carbide cloth (Nicalon) has been studied. The mechanical testing which was performed included both flexural and tensile loading configurations. This testing was done not only to determine the material properties, but also to initiate a controlled amount of damage within each specimen. Several nondestructive testing techniques, including acousto-ultrasonics (AU), were performed on the specimens periodically during testing. The AU signals were monitored through the use of an IBM compatible personal computer with a high speed data acquisition board. Software has been written which manipulates the AU signals in both the time and frequency domains, resulting in quantitative measures of the mechanical response of the material.

This paper will compare the measured AU parameters to both the mechanical test results and data from other nondestructive methods including ultrasonic C-scans and penetrant enhanced X-ray radiography.

ACKNOWLEDGEMENTS

The author wishes to thank the many individuals and organizations who influenced him throughout the course of this research project:

Dr. J. C. Duke, Jr. for providing me the opportunity to work on this research project as well as for making a multitude of other educational opportunities available. The creative research atmosphere and freedom of thought which he promoted will long be appreciated.

Dr. Henneke and Dr. Hasselman for graciously serving on my committee and sharing their wealth of knowledge and experience.

NASA Lewis and Alex Vary for providing financial support for this research project.

Martin-Marietta Laboratories for their generous contribution of material samples, as well as their technical assistance.

Scott Bartlett for somehow getting me into this, sticking it out through 20 'nots' per hour with me, and demonstrating the true meaning of 'Laid Back'.

Mike Kiernan for his technical assistance and for establishing much of the technical foundation upon which most of this research is based.

Mike Horne, Fred Tomasino, Anil Tiwari, Jack Lesko, and all the other friends which I have made in graduate school, for their assistance and the much appreciated diversions.

Bob Simonds, George Lough, and Bob Davis for their technical assistance in the laboratories and the shop.

My parents, whose love, guidance, and support made my pursuit of higher education possible.

And most of all my wife, Eleanor, for her infinite love and patience through these trying graduate school years. Without her understanding and support I could not have completed this goal.

TABLE OF CONTENTS

LIST OF FIGURES

1.0 INTRODUCTION

Monolithic, or single phase, ceramic materials have found many uses in industry for hundreds of years. Their resistance to degradation when subjected to high temperatures and chemically harsh environments has made them attractive materials for numerous applications. However, their usefulness as structural components has been limited due to their extreme sensitivity to small critical flaws - defects only several microns in size could cause catastrophic failure of a monolithic ceramic component.

Much attention has recently been drawn to the need for materials which can withstand higher temperatures, especially for use in the next generation of engines which will operate at much higher temperatures. The need has also been expressed for these materials to be strong, stiff, and light weight for potential aerospace applications. The past several years has seen a substantial amount of research in the development of ceramic/ceramic composites - i.e., making a "tough" ceramic with reduced dependency on small flaws which exist within the material. This toughening can be a result of several possible additions to the ceramic: a second phase of the material, particles of another material, random or preferentially oriented whiskers, or continuous fibers.

Although there exist many candidate ceramic materials to serve as matrices for reinforcement, glass has become a popular material for these studies. Glass is inexpensive, chemically inert, thermally stable, and relatively easy to process. There are also numerous glass compounds available if different matrix properties are desired. A considerable amount of work has been done on continuous fiber reinforcement of glass in the last two decades.

Several notable papers were published in the early 1970's on both randomly oriented whisker reinforced glass and continuous fiber unidirectionally reinforced glass. The amount of work being performed in this field greatly expanded in the 1980's with dozens of other researchers investigating these materials around the world. A brief review of the reports of the research which are related to this project will be presented in the Literature Review.

A silicon carbide reinforced, borosilicate glass composite material was chosen for use in this study for several reasons. It was felt that this material could be used as a "representative" material; that is, it was assumed that the material characteristics found during this study could be used to represent the general behavior of many ceramic matrix composites which have yet to be developed. It was also felt that this study could act as an introduction to the methodology required for testing ceramic matrix composite materials. In addition, there are several potential applications where this material may be chosen over either homogeneous materials or other varieties of composite materials presently available. Such applications could include chemically harsh or high temperature environments.

The materials under investigation consisted of a Corning 7740 Borosilicate glass matrix, reinforced with plain weave Nicalon (Silicon Carbide) fibers. Two lay-ups of the material were available for testing: two mats or four mats of Silicon Carbide, with all mats aligned in the same direction. The material was produced in a hot pressing operation, with the resultant panels measuring approximately 4 inches square with varying thicknesses. The material was produced and generously supplied by Martin-Marietta Laboratories in Baltimore, Maryland.

This study was initially undertaken with several broad objectives. The first basic goal was to become familiar with the behavior of ceramic matrix composite materials through the application of previously developed testing techniques. These testing techniques had been developed for application to various homogeneous and organic matrix composite materials.

Understanding of some of the material characteristics was to by gained by investigating the mechanical behavior of the ceramic matrix composite material under various loading configurations. Most of the materials in this project were tested in four point flexural loading. Although this testing method is normally used to obtain only qualitative data, it was the loading configuration specifically requested by the material supplier. For comparison to the material characteristics found as a result of the flexural testing, several samples were tested in a tensile loading configuration.

Along with mechanical testing methods, Non-Destructive Testing (NDT) techniques have played a large role in the understanding of the behavior of both resin matrix composite materials and metals. The more commonly used NDT techniques include radiographic methods, various ultrasonic techniques, acoustic emission monitoring, and liquid penetrant application. The application of these and other NDT techniques to several potential problems associated with ceramic materials is discussed in the Literature Review.

Another NDT technique used for material characterization is Acousto-Ultrasonics (AU). Originally proposed by Alex Vary at NASA Lewis Research Center, AU is a hybrid of acoustic emission testing and conventional ultrasonic testing. This technique, having been refined through several years of research at VPI & SU, NASA, and several other locations,

has been shown to correlate well with laminate strength, stiffness, and damage state in resin matrix composite materials.[1-7] It has also been applied to a variety of other materials, including: wood fiber hardboard, wire rope, human bones, and adhesive joints. [7]

An investigation of the applicability of the acousto-ultrasonic technique to ceramic matrix composites was the second goal of this project. AU measurements were taken at various points in the mechanical loading cycle and correlations with damage development and variations in mechanical properties were investigated. The AU results were also compared with the results from several other NDT techniques which were applied, including: acoustic emission monitoring (AE), X-ray radiography, and liquid penetrant inspection. The AU data, along with the mechanical testing results, will be discussed in the Results chapter.

As the material testing for this project progressed, attention was drawn to the initial development of damage in these specimens. The behavior of the material as it was initially loaded, as well as detection of damage initiation, became of interest. This information would be of great value to both the design engineer, who may be using ceramic matrix composite materials, as well as the inspector of components made of these materials. As will be discussed, a limited amount of work was performed in characterizing the material in this portion of the loading cycle.

General conclusions regarding the tests performed during this study, as well as suggested future work, will be outlined in the last chapter of this paper. Detailed information regarding the calculation of AU parameters and the computer code for these calculations is presented in the appendices.

2.0 LITERATURE REVIEW

Monolithic ceramics have many inherent advantages over other materials which make them attractive for numerous uses in industry. These attributes include: the ability to withstand higher temperatures than most metals or organic matrix composites, resistance to chemically harsh environments which degrade many commonly used engineering materials, high oxidation resistance compared to most metals, and relatively high stiffness values. Ceramic materials, however, also have several inherent shortcomings which limit their usefulness in many applications. These shortcomings include: extreme sensitivity to very small flaws within the material, low work of fracture, and worst of all, catastrophic failure modes. Although these shortcomings are many, industry has found thousands of uses for these materials through the years. Monolithic ceramic materials have not, however, been accepted for use in many structural applications because of the inability to process ceramic materials without the presence of performance limiting imperfections and the inability to reliably locate and characterize these flaws and imperfections.

There are many present and future material needs for which ceramics may possibly be used, however, the previously mentioned problems associated with many of the monolithic ceramics must first be overcome. In order to meet the demand for high strength ceramics which are capable of withstanding higher temperatures, "tough" ceramics are being developed. Many potential applications for these toughened ceramics have been reported, including uses in: radomes, space vehicle antenna windows, armor, heat exchangers, and biomedical materials.[8,9] The greatest needs lie in heat engine applications, including automotive, aerospace, and rocket engine components.[9,10] It has also been suggested that

these materials could be used in structural components in orbiting spacecraft which must endure large temperature fluctuations and the severe environment of space.[11]

In the last two decades a significant amount of work has been done to develop "tough" ceramics. Toughening of a ceramic can be achieved in several ways, including: the addition of a second phase of the same material, the addition of particles of another material to form a particulate composite, or the addition of whiskers or long fibers to create a fibrous composite material. The roles of these secondary materials are many, including:

1) To deflect an approaching crack, increasing the distance which it must travel to pass through a specimen, thereby increasing the life of the material;

2) To branch the crack, eliminating the effects of one large crack rapidly propagating through the material;

3) To reduce the stress concentration at the tip of the crack, thereby blunting it and slowing its growth;

4) To dissipate fracture energy through fibers pulling out of the surrounding matrix material and fibers bridging crack openings;

5) To prestress the material, through the residual stresses which remain after processing due to the differing coefficients of thermal expansion of the matrix and fibers. [12]

Many of these newly developed composite materials have much better performance characteristics compared to their monolithic counterparts. In many cases material properties, such as strain to failure and ultimate strength, have been increased significantly.

There are, however, many areas of concern in the development of these new materials. The reliability and quality of these materials must be guaranteed. Nondestructive testing techniques must be developed to locate and measure the size of flaws and imperfections. The quality of ceramic materials can be improved upon if these NDT techniques are implemented throughout the processing of a ceramic component. Both monolithic ceramics as well as ceramic/ceramic composite components could be inspected and characterized during processing, after production, and at various points during their service life.

NDT should not, however, be restricted to flaw detection while there are great needs in the area of material characterization. The traditional philosophy regarding the application of NDT was that the techniques were to be used strictly to locate and size imperfections within a component. It was normally left to the inspector to determine whether a given imperfection was truly a defect, based upon either an engineering criteria (fracture mechanics, for example) or subjective judgement. An alternative philosophy has recently been formulated with the development and application of NDT method which may yield information concerning the character of the material under inspection. This information may be related to material properties, relative strength, or damage state.

Acousto-ultrasonics is based upon the latter philosophy. In this method, stress waves propagate through the region of interest in the specimen. These waves interact with all aspects of the material through which they travel, including inhomogeneities, imperfections, and damage state. The received wave forms are then stored for analysis. The interaction of the waves with the material provides a considerable amount of information regarding the structure of the material. The AU method can, therefore, provide an integrated measure of the material state, rather than just detect flaws. A more complete description of the technique will be provided in the Testing Methods chapter.

The next part of this review will describe several studies reported in the literature which have dealt with materials and mechanical testing methods which are similar to those used in this study. These reports discuss flexural or tensile testing of continuous fiber reinforced glass. The final section of this literature review will identify and outline the many critical areas in the field of ceramic matrix composites in which NDT methods should be developed and possibly utilized. Particular emphasis will be placed on possible applications of the acousto-ultrasonic technique.

2.1 MECHANICAL TESTING OF CERAMIC MATRIX COMPOSITES

When discussing the history of composite materials it is common to mention that the first written description of a composite material was in the Bible, describing the addition of straw to clay to make bricks. Further analysis of this statement reveals that this early material was not only a composite material, but was a ceramic matrix composite material.

As discussed in the Introduction, ceramics have numerous attractive properties, including stability at high temperature, resistance to harsh chemical environments, and relatively low densities. However, the inherent weaknesses associated with ceramics have been known for centuries, including their brittleness and catastrophic failure modes. Toughening of these materials with fiber reinforcement has been the topic of much recent research.

A substantial amount of work has been done in the last two decades to investigate ceramic matrix composite materials. Although there are many possible ceramics to reinforce, many investigators have chosen glass as an initial matrix material to study. As previously discussed, this material has many advantages, including: chemical inertness, good thermal stability, low cost, and ease of processing. Although many studies of ceramic matrix composite materials have been reported in the literature, this section will review only studies which are of direct relevance to this project.

Some of the earliest published work on ceramic/ceramic composites, and most referenced, was by R. A. J. Sambell et al. in the U. K.[13,14] Reinforcement of several glasses with both short fibers and continuous fibers was investigated. Many of the fiber/matrix combinations investigated resulted in materials which performed poorly because of matrix cracking resulting from processing. These cracks were due to the mismatch of the thermal expansion coefficients of the fibers and matrix materials. The glass reinforced with graphite fibers had crack free matrices and excellent mechanical properties.

When investigating the mechanical performance of the whisker reinforced glasses, several conclusions were drawn about the parameters controlling the material strength. First,

the addition of fibers resulted in a greater work of fracture for all of the materials investigated. Through electron micrographs of the specimens fracture surfaces, it was shown that the increased work of fracture of the material was probably the result of fibers pulling out of the matrix material. Secondly, the better aligned the short fibers were in the matrix material, the better the resulting composite properties. Also, through tests performed at elevated temperatures it was shown that the strength controlling mechanism at high temperatures was the oxidation of the graphite fibers.

This work was notable in that it was one of the earliest to suggest that the condition of the interface between the fiber and the matrix material greatly affects the resultant composite material strength. Although electron micrographs of the graphite/glass composite showed no chemical bonding at the fiber matrix interface, it was clear that changes in the strength of this bond clearly controlled the mechanical properties. It was hypothesized that the amount of mechanical interaction between the fiber and matrix due to the residual stresses after processing was related to the performance of the overall material.

The continuous fiber reinforced materials in this study had considerably better mechanical properties than the whisker reinforced materials. Glass with continuous graphite fiber reinforcement showed much higher work of fracture and strength values compared to both unreinforced glass and randomly oriented whisker reinforced glasses. This, of course, is in agreement with the above conclusion that fiber alignment improved the material strength. Also, it was shown that both modulus and strength of the unidirectionally reinforced ceramic could be approximated through a rule of mixtures calculation.

The load-deflection curves presented by Sambell for a flexural testing configuration typically had a linear region followed by a curved region in which the modulus decreased. It was shown that the onset of microcracking on the tensile face of the flexural specimens resulted in the non-linearity of the load deflections curves. This matrix cracking occurred well below the ultimate strength of the material.

Another early study published in this field was by S. R. Levitt.[15] This study investigated the feasibility of producing fiber reinforced glass as well as some basic mechanical properties of this resulting composite. Several versions of a lithium aluminosilicate glass as a matrix material were investigated with Hercules HMS fibers used for reinforcement. The material was produced through a process which consisted of coating the continuous fiber with a slurry containing the glass powder, winding the coated fibers on a drum to form a unidirectional lamina, and then hot pressing several layers of this tape together into final form.

Results from mechanical test showed that a substantial increases in modulus of rupture (MOR) and modulus of elasticity were obtained. It also appeared that this composite followed the rule of mixtures for MOR, i.e., by increasing fiber volume the overall strength increased. The material also had excellent toughness, as determined by impact testing, and there was no degradation of strength after repeated thermal shock.

Observation of the load deflection curves for the composite revealed that at a point considerably below the ultimate strength, the curve became non-linear. The load defection curve which was initially linear deviated from linearity and a lower modulus was exhibited.

When the material was unload and subsequently reloaded, the modulus retained the lower value. The author hypothesized that the matrix had exceeded a critical strain value and the micro-cracking of the matrix resulted in a lower modulus. It was then shown that after several subsequent loading and unloading cycles there was no apparent loss of ultimate strength as a result of the matrix micro-cracking.

Prewo et al. at United Technologies have published several studies on ceramic matrix composite materials during the last decade.[16-21] They have studied a number of fiber and matrix material combinations. The fibers investigated included, monofilament boron and Silicon Carbide (SiC); yarns of graphite, alumina, and SiC; and whiskers of SiC and silicon nitride. The matrix materials which were tested included a borosilicate glass and a lithium aluminosilicate glass (LAS).

These materials were reportedly produced by a hot pressing process similar to that of Levitt.[15] The process was extended to show that it was possible to produce laminates with reinforcement in various directions. Laminates were produced in several stacking sequences with reinforcement in both the 0 and 90 degree directions.

Early investigations of these materials showed similarities with the Sambell studies, showing that the graphite reinforced borosilicate glass exhibited excellent mechanical properties. This composite had excellent thermal stability, high strength and modulus, and excellent fracture toughness. As the other studies had similarly reported, this material had a bi-linear load-deflection curve at room temperature. As the testing temperature was elevated, the ultimate strength of the material increased considerably, until a temperature was reached

(> 600° C) at which the matrix material began to soften.

In later studies by Prewo, several different material systems were investigated. SiC fibers were shown to result in similar improvements in mechanical properties over the monolithic matrix material as the graphite fiber composite. The SiC fibers, however, were able to withstand much higher temperatures before oxidative degradation than the graphite fibers. LAS glass was used as a matrix material and was shown to reach its maximum strength at a temperature over 400 degrees Centigrade higher than the temperature at which the borosilicate glass composite had obtained its maximum strength. These changes in constituent components resulted in a composite material which can be used in application which may reach a maximum temperature of over 1000° C.

The mechanical performance of this high temperature composite material was also studied. As before, the load-deflection curve of the unidirectionally reinforced material exhibited two slopes - an initial linear region followed by a second region with a lower slope. For this material, a rule of mixtures approximation was used to predict the initial modulus with good agreement. It was also shown that when a sample which had previously been loaded beyond the linear region of the curve was reloaded, the material retained the lower modulus upon reloading. After several loading cycles, the material did not have a lower ultimate strength compared to an uncycled material.

Prewo reported that the tensile fracture surfaces of specimens loaded in flexure exhibited considerable fiber pull out. Unidirectional specimens loaded in this manner failed as a result of matrix crack formation on the tensile surface of the specimens. It was also

shown that in both monotonic and fatigue loading, the material was not sensitive to the presence of holes in the sample.

Comparisons of the unidirectionally reinforced samples with the bidirectional samples showed that the unidirectional samples had both a higher ultimate strength and a higher elastic modulus. Fracture toughness for the bidirectionally reinforced specimens is also lower than that for the unidirectional specimens. It should be noted that all of the values of these properties for the bidirectionally reinforced composite were considerably higher than those of monolithic glass samples. It was also shown that the 0° samples were only slightly notch sensitive, while the bidirectionally reinforced material was notch insensitive.

Another study, presented by D. B. Marshall et al., investigated the failure mechanisms of a ceramic matrix composite material.[22] The material which was studied was a unidirectionally reinforced SiC/LAS glass produced by United Technologies.

The results of mechanical testing revealed several interesting points. The load deflection curves in both flexural and tensile loading had similar forms to those discussed above, with the onset of nonlinear behavior coinciding with matrix cracking. The difference in behavior between specimens loaded in tension and flexure being that in flexure, the cracks which began on the tensile surface did not propagate through the thickness of the specimen, as they did in tensile loaded specimens. In flexure, the cracks only propagated about half way through the specimen and then failure occurred either in compression or shear, depending on the ratio of the distance between adjacent loading and support pins to the specimen thickness. The effect of this ratio on the failure mode was explained in terms of simple elastic

beam theory; the ratio of the maximum tensile stress in the specimen to the maximum shear stress was shown to be proportional to the test ratio described above, therefore, for thicker specimens loaded in the same configuration, the magnitude of the shear stress in the elastic beam increases relative to the bending stress.

It was also shown how the behavior of these material is very complex, especially after damage begins to develop. It is clear that treating this material as linear in a classical beam calculation is in error once matrix cracking occurs. A cracked specimen is no longer linear or elastic, and classical beam theory is no longer valid. It was shown that unreasonable results are calculated if the investigator assumes that this method of material modeling is still valid after matrix cracking occurs.

Several other interesting aspects of the material were revealed through the mechanical loading. The material was shown to be relatively notch insensitive; matrix cracks did not form at locations which had previously been indented by a hardness indentor and initial matrix cracking did not occur at a lower load for the damaged specimens. Also, the matrix cracks which formed under loading closed tightly after the load was released.

2.2 NONDESTRUCTIVE TESTING OF CERAMIC MATRIX COMPOSITES

This section will discuss and identify several possible problems associated with ceramic matrix composite materials. Also, the Nondestructive testing methods which have been or could possibly be developed and utilized to characterized the various flaws will be discussed. This is by no means a complete listing of the areas of concern, but, it should prove

to be a reasonable starting point which will lead to a more complete understanding of these new materials. Emphasis will be placed upon the possible application of the acousto-ultrasonic technique.

It should be noted that no single NDT technique will solve all of the problems associated with any material system. Several techniques used in conjunction with each other may be required to fully characterize the state of a material system.

Unfortunately for the researcher, relatively little information has appeared in the literature regarding NDT of ceramic matrix composite materials. Most of the information must, therefore, be drawn from the studies of monolithic ceramics, and other materials, and then applied to ceramic matrix composites.

DISCRETE FLAWS: The literature is generally devoted to describing the areas of flaw detection and determination of critical flaw sizes for monolithic ceramic materials. The size of the largest imperfection which can exist in a component and not cause catastrophic failure is considered to be the critical flaw size. Much of the NDT research for ceramics has, therefore, been centered on locating imperfections and determining the smallest flaws which can be reliably located.

The critical flaw size in some monolithic materials has been reported to be in the 10 micrometer range in size [23]. NDT techniques have been reported which are able to locate flaws in this size range, so these techniques should be applicable to ceramic composites [24].

One of the concerns with these studies is that imperfections were fabricated into the samples by the investigators. The reliability of these techniques becomes questionable when applied to real components, manufactured out of laboratory conditions. Another problem is the rate at which the techniques can be performed; it may take hours to fully inspect even a small region for microscopic imperfections. Optimized inspection routines and statistical quality assurance methods would be necessary for industrial applications.

The purpose of using reinforcement in ceramic materials is to reduce the material's dependence on small imperfections. The size of the critical flaw for a ceramic matrix composite is, therefore, significantly larger than for its monolithic counterpart. Locating imperfections only micrometers in size is therefore less critical in these new materials.

Techniques which are of use to locate and size small imperfections include high frequency ultrasonic scans, ultrasonic scattering and attenuation measurements, and microfocus radiography [23,24,25,26].

POROSITY AND DENSITY: Large pores and density variations are material imperfections which are desirable to locate in ceramic materials. Pores or voids which would have a negative effect on the strength or toughness of the material are considered to be large. These imperfections can result from numerous process variables, such as: irregularities in raw materials, processing time and temperature, or uneven pressure distributions. New processes for the production of ceramic matrix composites are being developed which result in more uniform density and lower porosity specimens.

One such technique being developed for the production of ceramic matrix composites is Chemical Vapor Deposition (CVD) [27]. In this technique, a chemical vapor containing molecules of the matrix material infiltrates a preformed mesh of fibers. In the presence of heat and pressure, the matrix material is deposited on the ceramic fibers. The process takes hours or days to complete, but the resulting matrix is significantly more uniform and dense than composites produced by other methods.

Composites produced by CVD infiltration have been reported to have theoretical densities as high as 85-90% [28,29], however, a large number of pores may be distributed throughout the composite. Oak Ridge National Laboratories reports that pore sizes as large as several hundred micrometers exist within these composites. It has been hypothesized that further increases in density will have little beneficial effect on strength and toughness of these materials [30].

Several other processing methods are mentioned in the literature including reaction bonding, polymer precursor synthesis, and sol-gel techniques [31]. The prevalent processing method is hot pressing or tape casting which produces a laminated composite plate. This method also has the problems associated with production of uniform specimens. Large variations in the material density and large pores left in the matrix material after processing have been reported.[15] These variation will have a pronounced effect on the finished material properties. One possible reason is that during the pressing process, the reinforcement fibers inhibit the flow of viscous glass (or other matrix material). The flowing matrix material may be restrained from flowing into certain areas of the mesh such as where fiber tows cross, thereby leaving voids.[32]

NDT techniques have proven to be useful in this area. As discussed above, the location of pores larger than a critical flaw size would be necessary to assure that a component would be trustworthy in service. High frequency ultrasonic techniques and microfocus radiography could be effective in locating and determining the size such flaws. Location and characterization of clusters of small pores or density variations would also be of use in the investigation of ceramic composite materials because of their decreased dependency upon small, single imperfections. Ultrasonic scattering and attenuation measurements have been used to measure density gradients in the monolithic ceramic materials. Ultrasonic velocity measurements have been applied to monolithic ceramics and material densities variations as small as 2% have been identified. X-ray techniques have also been used. These techniques may also be applicable to ceramic matrix composite materials.[23-26,33] Although expensive, computed tomography (CT) X-ray scans can also readily distinguish variations in material density [34].

MATRIX VARIATIONS: Most candidate matrix materials for ceramic composites have been produced in monolithic form, however, it was determined that toughening would improve some aspect of their performance. The condition of the matrix material in a composite has a great influence on the final properties and characteristics. Variations or degradation of the matrix should be qualified.

The existence of different phases of the matrix material can greatly change the properties of the resultant composite. The existence of secondary phases of the matrix ceramic could have beneficial or undesirable effects on the material. In some materials

inclusions of a secondary phase are considered to be the toughening agent - the inclusions deflect approaching cracks. On the other hand, the secondary phase may also degrade the overall performance. Secondary phase inclusions may be crack initiation points; microcracks may occur in the two phase matrix at a low load. Or if too large, the grain itself may exceed the critical flaw size.

In the study of monolithic ceramics, phase constitution is usually determined through the application of metallographic and X-ray diffraction methods.[18] High resolution CT X-ray scans could probably also distinguish matrix variations. Discrete inclusions may be located through the application of high frequency ultrasonic scans. Also, to avoid unwanted inclusions in the matrix or oversized powder granules before firing the material, inspections should be carefully performed before processing. [35,36]

RESIDUAL STRESS: As in other composite systems, residual stresses are present in ceramic matrix composite materials due to the differences in the coefficients of thermal expansion between the various components of the composite system. The materials are processed at a high temperature, and after cooling, the constituents of the composite system attempt to shrink different amounts, thereby, creating residual stresses. Residual stresses may also results from processes such as rolling or pressing of the material. Machining of components to final dimensions may also leave stresses in the material. If the residual stress levels within the composite are large enough, microcracking of the matrix will result.

An understanding of these residual stress levels will be important in the design and analysis of structures constructed of advanced composite materials. A measurement of these

stress levels would prove to be of great use when determing the suitability of a part for service.[13,22,24]

ANISOTROPY: Both whisker and fiber reinforced (long fibers) composite materials will be anisotropic to a certain degree. In contrast, randomly oriented particulate composites can generally be treated as isotropic. The variation of mechanical properties in various directions may result from fiber orientation, hot pressing, or rolling of the ceramic composite during preparation.

An understanding of the degree of anisotropy is required for proper design and use of these materials. A measure of the relative material properties in various directions would be of great use. Presently, mechanical testing is the dominant method of determining material properties in anisotropic specimens. This testing, of course, results in the destruction of the specimen. Nondestructively, ultrasonic velocity measurement have been used on ceramic materials to determine anisotropy.[23,27] Acousto-ultrasonic measurements have been shown to have a direct correlation to direction in other anisotropic materials.[38]

FIBER DISTRIBUTION: Homogeneous fiber distribution throughout a matrix material is an important quality in a composite material system. However, it is possible to have areas of fiber or whisker concentration or sparsity in these materials. These inhomogeneous regions would obviously not perform as expected. A measurement of the effect of these inhomogeneities on the overall material characteristics would be necessary to assure product integrity.

Ultrasonic velocity and attenuation measurements could be used in locating these variations. X-ray methods would also be used to locate the regions of concern. CT X-ray scans have identified regions of uneven fiber distribution in other types of composite materials.[34] Acousto-ultrasonics measurements have been shown to correlate with fiber distribution and alignment.[39]

FIBER DEGRADATION: Generally the limitation of ceramic composite materials is the degradation of the reinforcing fibers. Several fibers used for reinforcement of ceramics have been shown to degrade in high temperatures and oxidizing environments [20,27]. These factors may exist during material processing or while in service.

The matrix material of a ceramic composite generally protects the fibers from the surrounding atmosphere, however, in service, microcracks may allow the degrading atmosphere to penetrate to the fibers. For example, it has been shown that SiC fibers may begin degrading at temperatures as low as 1000° C. An oxide scale forms on the fiber surface and the fiber becomes extremely notch sensitive. After such exposure, fiber strength may be reduced by as much as 75% [40]. The degradation of the fibers along with matrix microcracking will reduce the stiffness and strength of a component.

It is questionable if X-ray methods would be able to clearly show fiber degradation, however, fiber breakage could probably be located through the application of microfocus techniques. A reduction in stiffness and strength would be found if the part were loaded or proof tested, however, these methods may increase the severity of the damage which already exists within the structure. Changes in AU measurements could possibly be correlated with

the extent of fiber degradation as well as the resulting material characteristics. Surface scanning methods may also be used to detect surface cracks which may allow the degrading atmosphere to reach the fibers. These techniques include scanning acoustic microscopy (SAM), scanning laser acoustic microscopy (SLAM), and liquid penetrant inspection.

IN SERVICE DAMAGE DEVELOPMENT: A ceramic matrix which has been reinforced with continuous fibers not only has decreased sensitivity to microscopic flaws, but also has the ability to sustain damage without catastrophic structural failure. It has been shown that ceramic matrix composites with long fibers for reinforcement have a general failure pattern: elastic behavior until the formation of microcracks within the matrix, increased strain levels while microcracking appears throughout the matrix, and failure with a single predominant crack through the thickness of the specimen [21,41,42].

Because of this ability to withstand distributed damage, a measure must be made to assess a ceramic composite component's continued performance ability after damage development has begun. A measure of the sustained damage as well as the remaining load carrying capability of a specimen would have great value. The detection of the onset of non-linear behavior would also be of use in component design to assure that safe design load levels are maintained.

Because the damage states in service may be similar in nature to the imperfections discussed in other sections of this review, many of the NDT techniques previously described may also be used to characterize damage development. High frequency ultrasonic methods as well as attenuation measurements may be used to determine the amount of matrix micro-

cracking. Scanning techniques such as SAM or SLAM may detect near surface defect formation. X-ray methods, including computed tomography, could locate and image flaws throughout the material; these methods are, however, very expensive and time consuming. Acoustic emissions monitored during testing could be used to determine the point at which the specimen begins to crack. This technique, however, may be of limited use when considering composite components which have been used in service - AE could only be used to determine the previous load levels if the part is reloaded and the material exhibits the Kaiser effect. Upon reapplication of the load, however, additional damage may develop within the material.

A direct measure of the material integrity after some load history would be beneficial in that it could eliminate the need for subjective determination of the damage state from measurements made with other techniques. Correlation of measurement made with an interactive technique, such as AU, may result in a measure of the integrity of a damaged ceramic matrix composite.

IN PROCESS NDT: It has been reported that NDT evaluations have been used to determine alterations to processing methods necessary to improve the quality and reliability of ceramics and ceramic matrix composites [23,26,32,34]. Various techniques have been used including radiography, X-ray diffraction, and ultrasonic scans.

Testing of specimens has been done at various stages during processing, including NDT of raw materials (powders and fibers), green state ceramics, and on finished materials. Changes in production that have been suggested because of nondestructive evaluation have

reduced density variations, porosity, fiber misalignment, and fiber concentrations.

Because processing of ceramic matrix composites is not the main topic of this report, it will not discussed in further detail.

FIBER-MATRIX INTERFACE: It has been stated that the behavior of ceramic matrix composite material is highly dependent upon the characteristics of the fiber-matrix interface [11,14,20,21,29,40,44]. In a composite in which the constituents are of similar materials, any cracks which propagate through the material tend to "see" only one material, and therefore, the material system acts as if it were monolithic. These materials generally exhibit very brittle behavior and show little tolerance to damage. A composite material in which a strong "bond" between the fibers and the matrix exist will also result in a very brittle composite - the fibers will simply break, rather than dissipating further energy by pulling out of the matrix. These composites offer little or no resistance to a progressing crack. A frictional interface results in a better performing composite. The fibers can pull out or deflect approaching cracks, thereby increasing the energy needed to fracture the material.

Several methods of altering the fiber matrix interface to produce a better performing material have been reported. The most successful method seems to be fiber coatings. The fibers are coated with a thin layer of another material which creates a frictional bond with the matrix.

Because the fiber-matrix interface has a pronounced effect on the composite's performance, this area deserves much more research attention. Mechanical testing could

result in a measurement of the effect of alterations to the fiber-matrix interface, however, this measurement may not be realistically made on every component produced. Although many mechanical tests have been suggested for accomplishing this purpose, it would be difficult to develop a mechanical test which truly measures only the properties of the interface region.

A NDT technique which measures material characteristics with various fiber-matrix interfaces would be of great value to the composites community both as a quality control measurement and as a development tool in the production of new ceramic matrix composites. An interactive method, such as acousto-ultrasonics could possibly yield a measure of the effects of these changes, however, this has yet to be determined. It is doubtful that velocity measurements or image producing techniques could be of great value in this area.

3.0 TESTING METHODS

This chapter will describe the test methods used during this project to characterize the behavior of the ceramic matrix composite material. A brief description will be given of the two mechanical loading configurations and the nondestructive testing methods which were employed.

3.1 MECHANICAL TESTING

One of the objectives of this research project was to develop an understanding of the mechanical performance of ceramic matrix composite materials. To develop this understanding, two different loading configurations for mechanical testing were chosen - four point flexural loading and tensile loading. This section will describe the purpose for performing these tests and the details of each loading configuration. The data from these mechanical tests will be discussed in the Test Results chapter.

The flexural loading configuration was chosen for several reasons. First, the material supplier, who had developed this material, specifically requested this testing method. Secondly, flexural testing is commonly used in the ceramics field. Flexural test results are widely seen in the literature discussing ceramic matrix composites and thus, a database of similar mechanical test data is beginning to form in the literature. As a result, the test results from this project could be compared to the performance of the similar materials which have been reported in the literature. Also, as can be shown from basic beam theory, a four point flexural configuration has a "pure" bending moment applied throughout the gage

section, with the effects of shear strain limited to the regions between adjacent loading and support pins.

Flexural testing is more commonly used for ceramic materials than tensile loading. The problems associated with tensile testing are exaggerated due to the inherent weaknesses of monolithic ceramics, thereby making this test method very difficult to perform. The loads induced by gripping the ceramic specimens may cause catastrophic failure and load frame alignment is critical to avoid non-uniform loading of the specimens which may cause premature failure. Because of its simplicity, flexural testing is typically performed to compare the relative quality of materials [45], however, it is generally not recommended for generating design data [46]. To obtain accurate mechanical properties from this method, an understanding of the loading and proper interpretation of the data is required.

Although no American Society for Testing Materials (ASTM) testing standards have yet been developed for flexural testing of ceramic matrix composite materials, several other related standards were consulted in establishing a testing procedure. These included ASTM D790, "Standard Test Methods for Flexural Properties of Unreinforced and Reinforced Plastics and Electrical Insulating Materials" [47] and ASTM C158, "Standard Methods of Flexural Testing of Glass (Determination of Modulus of Rupture)" [48]. Based upon the recommendation of these standards, testing parameters were determined which satisfied both ASTM standards. The resulting configuration is shown in Figure 1 and the testing parameters were defined as:

$$L = \text{Support Span} = 3 \text{ in.}$$

$$L/2 = \text{Loading Span} = 1.5 \text{ in.}$$

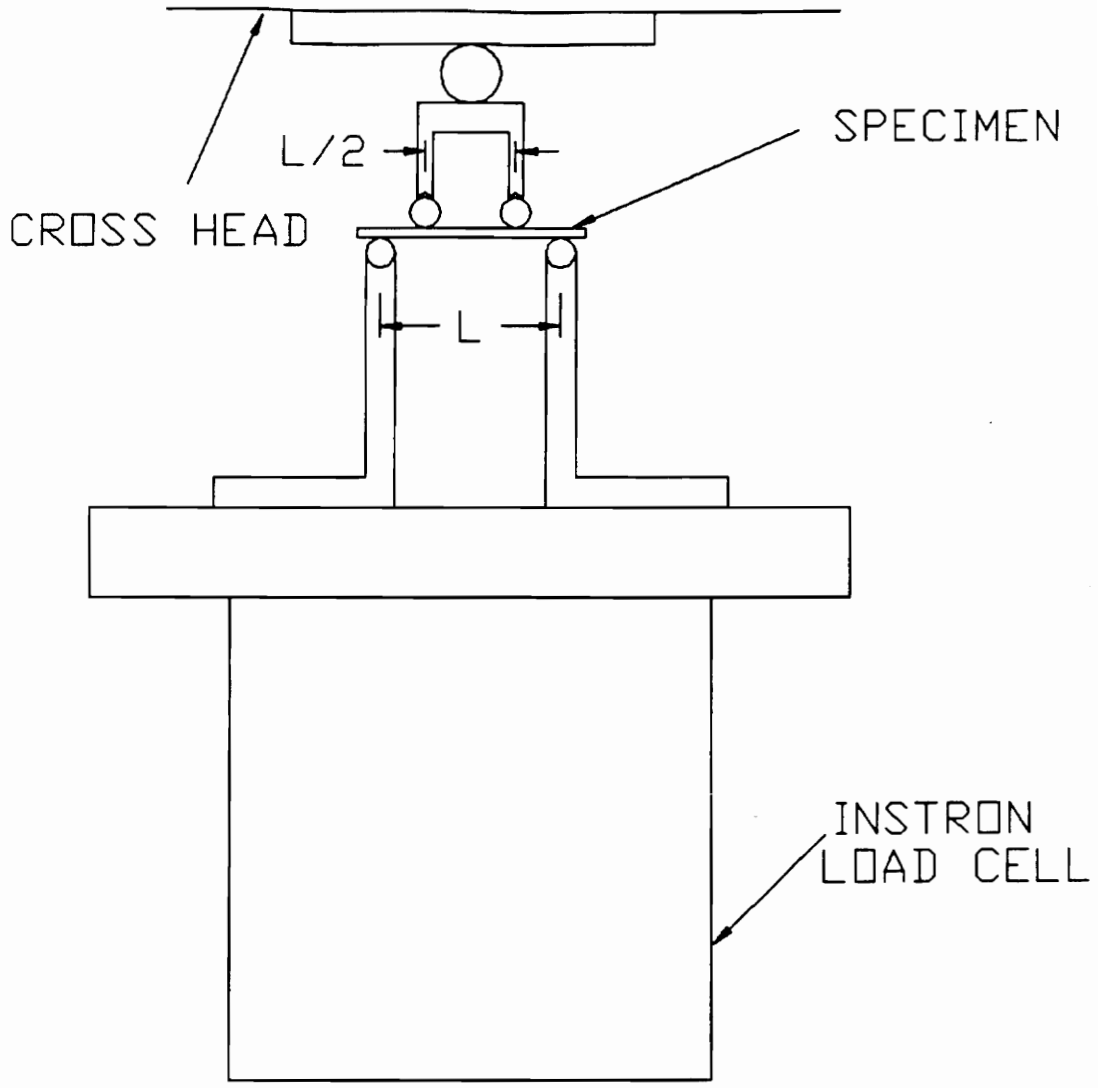

Figure 1. Four-point Flexural Testing Configuration

$$R = \text{Crosshead Displacement Rate} = .05 \text{ in./min}$$

$$r_l = \text{Radius of Loading Pins} = .1250 \text{ in.}$$

$$r_s = \text{Radius of Support Edges} \approx .1875 \text{ in.}$$

The loading pins and support edges were made of hardened steel to prevent excessive deformation. The loading pins could rotate about their axes to minimize frictional loading and the load bearing edges were free to pivot laterally to compensate for any irregularities in the specimens. The load was applied through a spherical steel joint to assure uniform loading of both loading pins.

The chosen configuration resulted in a support length to specimen thickness ratio (L/D) of approximately 18 for the four layer specimens. This value is just over 16, the lowest ratio recommended for obtaining flexural strength data by the ASTM D790 standard. To minimize the effects of shear deformation, it has been suggested [45,47] that an L/D ratio of at least 60 be used to obtain accurate modulus data for both three and four point flexural testing. Although a larger L/D ratio would have been desirable, the size of the panels limited the specimen length and, therefore, limited the support span length. Also, because the specimens were tested in an "as received" condition, the specimen thickness was fixed. For the thinner, two layer specimens, an L/D ratio of approximately 30 resulted.

As suggested in the testing standards, the specimen width was specified to be 0.500 in. ; a tolerance of $\pm$ 0.010 in. was stipulated. The specimens were cut with an Isomet (Beuhler) sectioning saw which was modified to cut large panels. A fixture was mounted to the arm of the Isomet, allowing the existing micrometer on the arm to be used to accurately

control the resulting width of the specimen. This cutting method was successful in that no detectable damage developed as a result of cutting the panels and the specimen dimensions were close to the specified size. The specimen average width varied between 0.490 in. and 0.510 in. and the maximum variation of the width of a specimen from its average width was approximately $\pm$ 0.010 in.

During some of the flexural loading tests, the center displacement of the specimen was monitored through the use of an LVDT-type displacement transducer mounted to the support base of the flexural testing fixture. The instrument was an RDP brand DC-DC type displacement measuring transducer, with a spring return arm to assure contact with the specimen throughout the test. The alignment of the instrument was checked with a plumb bob hung from the load frame crosshead and a calibration check was performed by measuring the displacement of the crosshead with both the LVDT and a dial-type displacement gage and comparing these measurements with the displacement output from the load frame. The spring rate of the LVDT was negligible compared to the testing loads, and the end of the transducer arm was fitted with a socketed ball bearing to allow for possible lateral movement of the specimen. The displacement range of the instrument was $\pm$0.5 inches.

In addition to the four point flexural loading, several specimens were tested in a tensile loading configuration. This test was performed to try to correlate mechanical properties found in flexure with tensile properties, to demonstrate any differences in mechanical performance or failure modes between the two test procedures, and to induce an alternative type of damage for correlation with the nondestructive measurements. No testing standards for tensile testing of ceramic matrix composites have been developed, therefore, the

same size samples as specified for the flexure loading were used. The loading configuration is shown in Figure 2. Several crosshead speeds were used during testing.

Gripping the samples for application of a tensile load was of great concern. A layer of protective material between the specimen surface and the serrated grip surfaces was required to minimize damage in the samples and to help avoid movement of the sample within the grips. Coating the ends of the specimens with a polymer coating was attempted. This method was unsuccessful because the coating did not adhere well to the glass surface and it crept under load. The configuration which was used during the remaining tests consisted of two layers of emery paper between the specimen and the grip surfaces - a fine grit paper surrounded by a course grit paper. Even with the protective layers of emery paper, some specimen damage occurred during the application of grip pressures due to the surface irregularities and the material non-uniformities. This gripping damage was, however, limited to the outer portion of the gripped regions of the specimens. After several tests, it was determined that gripping approximately 0.75 in. of each end of a sample in this manner resulted in very little slipping with most specimen failures occurring in the gage section.

During tensile loading, the elongation of the specimen could be measured through the use of an Instron extensometer. This device was attached to the gage section of the specimen with several rubber bands and spanned a one inch long region.

Both forms of mechanical testing were performed using an Instron, screw driven load frame with selectable crosshead speeds. The load in all of the tests was monitored with a standard Instron reversible (tension-compression), strain gage type load cell with a 1000

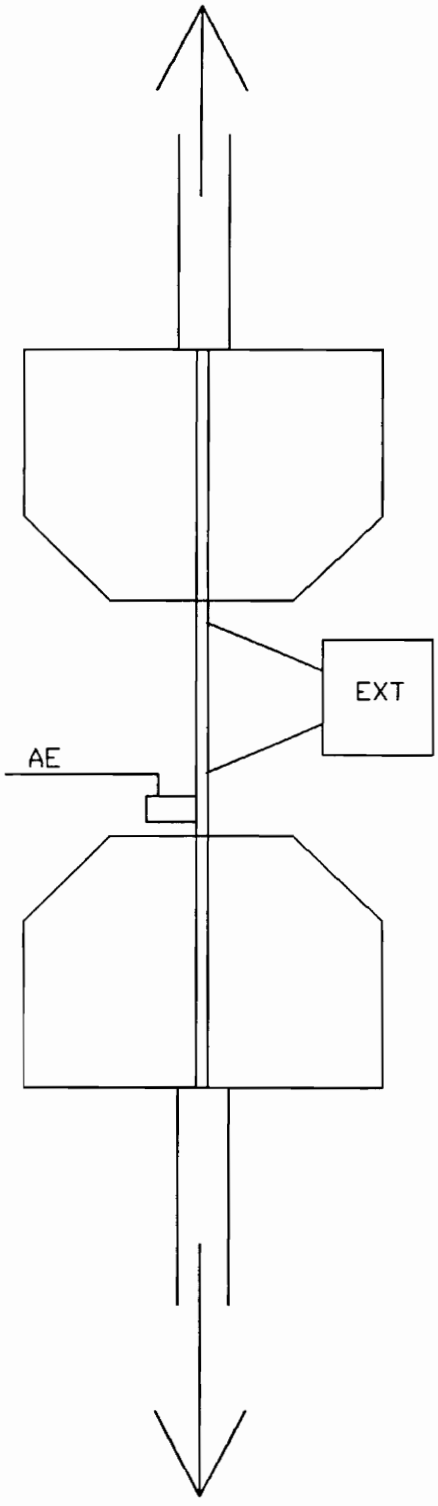

Figure 2. Tensile Testing Configuration

pound (454 kg) load range. Crosshead displacement measurements where available through the Instron control system.

Surface strains were monitored during selected flexural and tensile tests using resistance strain gages; these were Micro-Measurement brand gages, model CEA-250UW-350. This type of gage was suggested by the gage manufacturer for composite materials and for the desired testing configurations. The large gage size (0.25 X 0.25 in.) was chosen to obtain an integrated measure of the surface strain over an area which was larger than the imperfections which were revealed by the preliminary nondestructive tests, thereby assuring that the measured strain was not greatly biased by the effects of a single sub-surface flaw. Most specimen surfaces were left in the "as-received" condition for testing, that is, no polishing was performed. The specimens which had strain gages mounted on them were lightly polished by hand only in the region were the gage was to be mounted. These specimens were also cleaned with acetone and Micro-Measurements Conditioner and Neutralizer to assure good bonding of the gage to the surface.

Data from all of the mechanical measurements discussed above were output to a Hewlett Packard X-Y-Y type pen plotter, an Instron chart recorder, or an IBM PC based digital data acquisition system.

3.2 NON-DESTRUCTIVE TESTS

Several nondestructive testing techniques were applied during the mechanical testing process. These methods included: ultrasonic C-scans, X-ray radiography, acoustic emission

monitoring, liquid penetrant inspection, and acousto-ultrasonics. A brief description of each of these techniques in terms of their application in this project will be given; however, a more complete description of these techniques and their applications is available in several reference handbooks.[49-51] The results from the nondestructive tests will be discussed along with the mechanical test data in the Test Results chapter.

Ultrasonic C-scans: Ultrasonic C-scans were produced of the uncut, untested panels. This technique consisted of scanning the panel with a 15 MHz focused ultrasonic probe in a pulse-echo configuration. The reflected signals were received by the same transducer and the portion of the received signal which was reflected from the bottom of the tank was gated. Variations in the intensity of the gated ultrasonic pulse as a function of position were then recorded in the form of a gray scale image. Appropriate gain settings were employed to result in a peak signal amplitude in the range required for the gray scale imaging equipment.

X-ray Radiography: X-ray radiographs of the panels before cutting and of the specimens at various stages in the testing were produced. A Hewlett Packard Faxitron cabinet x-ray device was used. The radiographs were produced in a contact configuration, that is, the specimens were in direct contact with the recording film during the radiographic process. Settings for the equipment which resulted in the best quality radiographs were found to be 60 keV with a 2 minute exposure time for the four ply samples, and 50 keV with a 2 minute exposure time for the two ply specimens. Single sided Kodak x-ray film was used.

To make the cracks in the specimens which contained damage appear with greater contrast in the radiographs, an x-ray attenuating penetrant mixture containing zinc oxide,

water, acetone, and Kodak Photoflo was applied to the surfaces of the specimens. The penetrant mixture was to be drawn into the surface cracks through capillary action, therefore, an appropriate dwell time was allowed after application. Residual penetrant was removed from the surface of the specimens with acetone prior to radiographing.

Acoustic Emission: Acoustic emissions were monitored during mechanical loading in several tests. A measure of the amount of emission energy generated at any time in the loading cycle was desired. A simple root mean square (rms) voltmeter measure of the emissions was developed.

A one inch AET piezoelectric transducer with a center frequency of approximately 150 kHz was used for most experiments, although a smaller diameter, Physical Acoustics resonant type transducer was also available which had a 300 kHz center frequency. The transducer used during an experiment was attached to the specimen with several rubber bands and acoustically coupled to the specimen surface with the application of Echogel Sonotrace 30 acoustic couplant.

The voltage output from the AE transducer was amplified with a Tektronics type 1A7A high gain, differential amplifier and input into an rms voltmeter. The amplifier allowed for band pass filtering of the acoustic emission signals, thereby reducing the low frequency noise produced by the load frame and the high frequency noise generated by the acousto-ultrasonic equipment. The voltmeter was a DISA brand, type 55D35 RMS voltmeter with a frequency range of 1 Hz to 400 kHz. Several integrator time constant settings on the voltmeter were used, however, the minimum time constant setting of 0.1 seconds was

typically used to attain the shortest possible response time. The rms voltage output was recorded on a Hewlett Packard pen plotter.

Liquid Penetrant Inspection: Liquid penetrant was applied to the surface of several specimens at various stages in the loading cycle. After thorough cleaning of the surface, the Magnaflux brand penetrant dye was applied. The penetrant relies upon capillary action to be drawn into the open surface cracks of the specimen; therefore, an appropriate dwell time [52] was allowed before the excess dye was removed with a cleaner and a developer sprayed on the specimen. Penetrant remaining in the cracks was then drawn to the surface by the developer for observation. Liquid penetrant application was performed on specimens under mechanical load and in an unloaded condition.

Acousto-Ultrasonics: A complete description of the acousto-ultrasonic method from both a historical and an applications stand point can be found in several sources.[1-7,53,54] A brief description of the technique as it was used in this project will be presented.

The AU technique involves the introduction of stress waves in a sample at one location and detecting them at another. The stress waves simulate waves which result from strain energy released during loading, similar to acoustic emissions. These stress waves are altered by the various aspects of the medium through which they travel, therefore, the characteristics of the detected waveform are affected by the characteristics of the material between the source and receiver locations. Unlike AE analysis, the location and characteristics of the stress wave source are known and analysis of the received waveform can be used to assess the condition of the material.[7]

If the stress waves travel in the structure, in the load carrying direction, the resultant measure is of the performance capability of the region of the structure between the transducers in the direction of propagation. This is unlike conventional ultrasonic C-scans, for example, where variations of the received ultrasonic waves traveling perpendicular to the plane of the sample must be interpreted by the investigator as to how they will affect structural performance in the load bearing direction. One of the basic concepts behind the AU technique is that a region of material which transmits the stress wave energy efficiently will also efficiently transfer the strain energy resulting from loading. Conversely, regions of the material which highly attenuate the AU signals will not likely transfer the strain energy from loading efficiently and will be more susceptible to failure.

A schematic of the AU system is shown in Figure 3. A Panametrics 5052UA Ultrasonic Analyzer is used to generate a broad band electronic pulse. A Panametrics 5 MHz, 0.25 inch diameter piezoelectric transducer converts the electrical pulse into mechanical vibrations which are propagated into the material through an ultrasonic couplant. Echogel Sonotrace 30 ultrasonic couplant was used to reduce the acoustic impedance mismatch between the transducer and the material. A similar transducer, with couplant, was used to receive the signal and convert it into a varying electrical potential. A Panametrics ultrasonic preamplifier is then employed to amplify the received signal. The signal may then be further amplified or attenuated through the 5052UA receiving unit. The signal is then captured and stored by an IBM compatible PC based data acquisition system with a Sonotek STR*825 A/D board operating at a sampling frequency of 25 MHz. The received AU waveforms are available for analysis using the signal processing procedure outlined in Appendix A. This

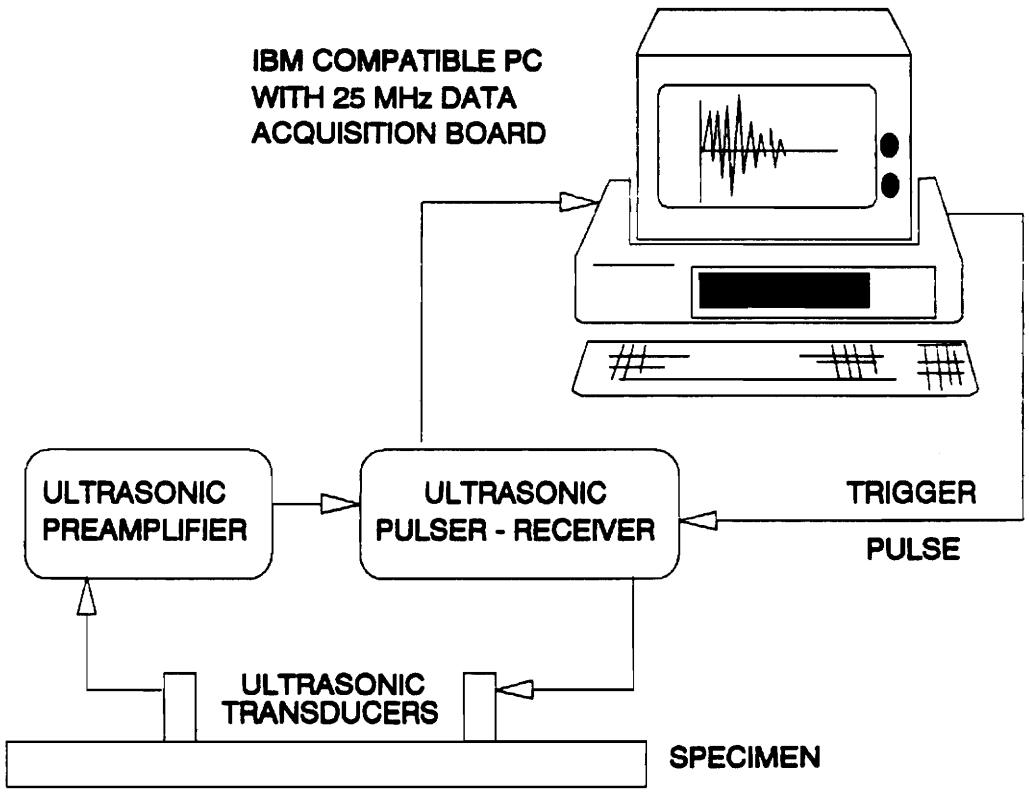

Figure 3. Schematic of the Acousto-Ultrasonic Testing System

analysis procedure results in several parameters which are available for possible correlation with mechanical performance.

The 5 MHz transducers were chosen because they were the highest center frequency transducers which produced an acceptable amplitude AU signal through the composite material. The highest frequency was desirable because it appeared that the high frequency components were the most sensitive to changes in the material in previous studies. The 0.25 inch diameter transducer was chosen because the transducers casings completely fit within the specimen width. The distance between the centers of the two transducers can be an arbitrarily chosen length, as long it is held constant for measurements which are to be compared. The center to center distance between the transducers was typically 0.75 inches throughout this study. This distance was chosen to conveniently fit the flexural testing configuration. Scanning patterns were established for when AU measurments were taken along the length of a specimen; the scanning patterns used in this study are depicted in Figures 4 and 5.

Acousto-ultrasonic measurements were performed at various points during the loading process for several specimens. The AU data and results of the correlation of the AU parameters with mechanical performance will be discussed in the Test Results chapter.

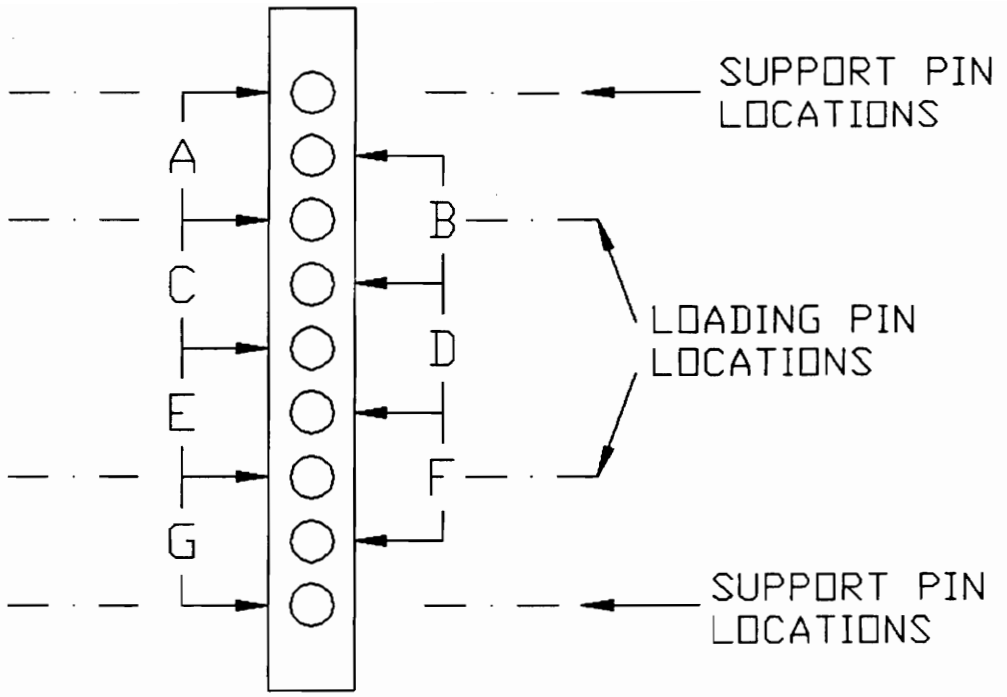

Figure 4. AU Scanning Pattern

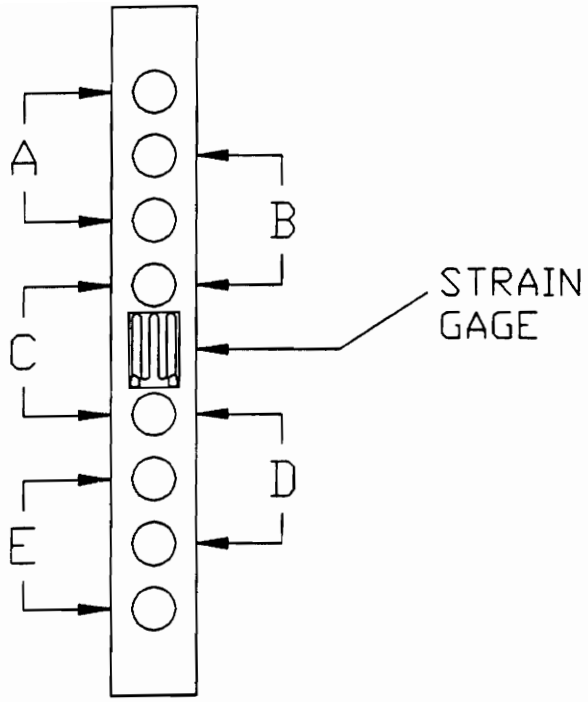

Figure 5. AU Scanning Pattern for Specimens with Strain Gages

4.0 TEST RESULTS AND DISCUSSION

4.1 INITIAL PANEL INSPECTION

Upon receipt of the panels, several nondestructive testing methods were employed to determine the condition of the composite material. Radiographs and ultrasonic C-scans were produced of each panel prior to specimen preparation. These techniques were employed as described in the Test Methods chapter. The radiographs showed a large number of imperfections in some of the panels, many appearing to be relatively large in size (a maximum diameter of approximately 0.25 in. was measured). The number and size of these flaws varied greatly between the panels, although all of the panels contained some imperfections. It was assume that these regions were voids or air pockets in the matrix material. The radiographs also yielded some information as to the orientation of the Nicalon fiber mats, which was used to accurately align the panels during cutting. Example radiographs of the panels containing the greatest and least number of voids are shown in Figures 6 and 7. The ultrasonic C-scan results were similar to the radiographs for all of the panels, however, the areas of sound attenuating material which were measured appeared larger than the imperfections detected in the radiographs. The larger "poor" regions in the C-scans were assumed to be associated with several features: the edges of the voids scattered the ultrasonic pulse making the voids appear larger in the scans, porous regions with many small air pockets trapped by the fiber mats could have greatly affected the ultrasonic results but were not noticeable in the radiographs, or other differences could have affected the C-scans such as non-parallel specimen surfaces.

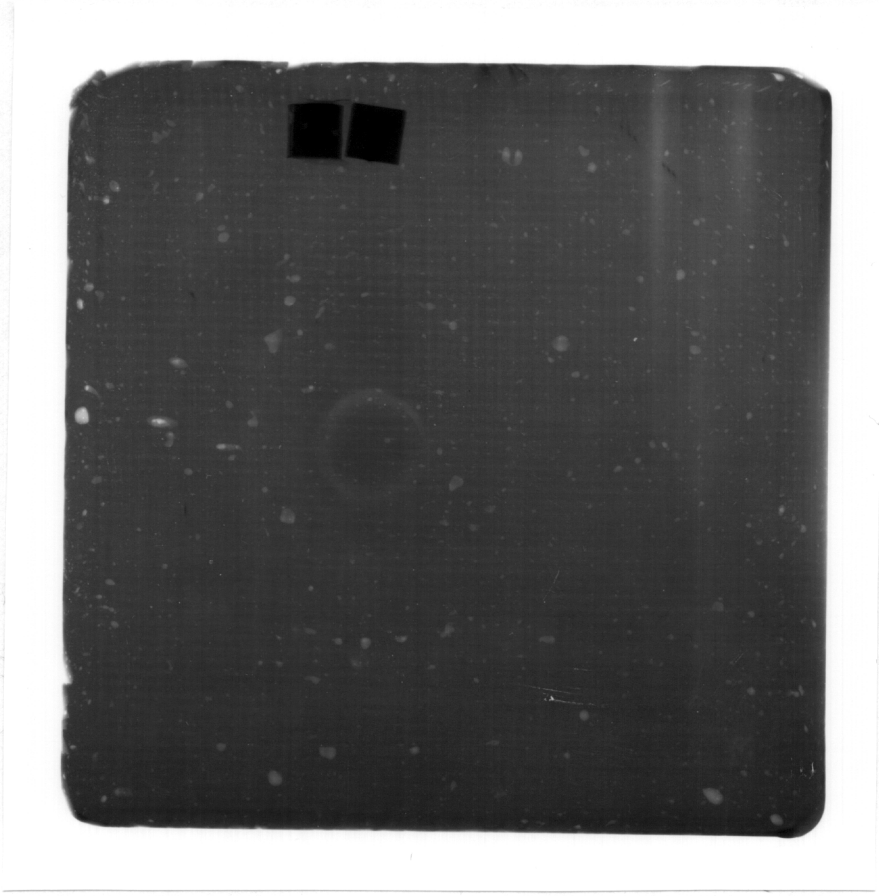

Figure 6. Radiograph of an Uncut Panel (Least Voids)

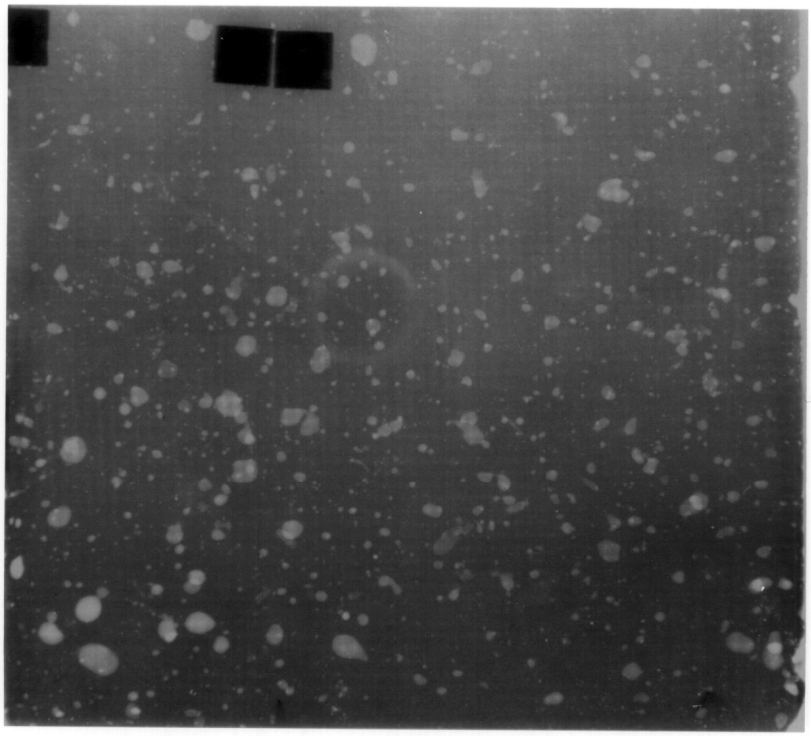

Figure 7. Radiograph of an Uncut Panel (Most Voids)

Cutting the panels confirmed that the imperfections which appeared in the C-scans and radiographs indeed were air pockets. Several large air bubbles, as well as numerous smaller ones, were revealed along the cut lines at the same locations as they appeared in the radiographs. The thickness of an open void was typically less than the thickness of one lamina within the composite panels. Open voids along the cut lines can be seen in the photographs of failed specimens, Figures 20 and 21, which will be discussed later in this chapter.

Several preliminary acousto-ultrasonic measurements were made on the uncut panels to assure that they were suitable for the planned research activities. AU tests were performed at random locations on several panels to assure that the received signals were of a reasonable amplitude.

To set up and practice the mechanical testing methods, specimens from a glass matrix composite panel which had been produced early in the development process were used. These samples had been damaged during the cutting process in the ESM machine shop and were deemed unacceptable for testing. This panel also consisted of 4 layers of Nicalon cloth in the same glass matrix material, however, it was much thicker and, therefore, had a much lower volume fraction of fibers than the panels used in the actual testing.

During the preparation of the samples for testing it became apparent that each panel of the material had considerable thickness variations. Each specimen was measured prior to testing; thickness and width were measured at three locations along the length of each specimen. The average thickness of the two-ply panels was 0.100 in., with maximum and

minimum thicknesses of 0.113 in. and 0.092 in., respectively. The average thickness for the four-ply panels was 0.148 in., with a minimum thickness of 0.133 in. and a maximum thickness of 0.170 in. The maximum thickness variation of a specimen was approximately 20% along its length, however, the thickness variation for most samples was considerably less. Specimen width variations were discussed previously. It should be noted that all calculations performed in this paper for a given specimen were based upon the average thickness and width of that specimen.

4.2 FLEXURAL TESTING RESULTS

As discussed in the Test Methods chapter, four point flexural testing was performed. Twenty quasistatic flexure tests were performed; sixteen tests were run on the four-ply specimens and four on the two-ply samples. While most tests were allowed to run uninterrupted until specimen failure, several tests were stopped at various load levels and the specimen was unloaded and removed from the fixture for inspection. Typically, upon reapplication of the load, the load level was incrementally increased with each loading cycle. These interrupted tests were performed with the intention of developing an understanding of the steps of damage development which occur within these materials in this loading configuration. Several tests were run on various unloaded specimens including penetrant enhanced radiography and optical inspection of the sample surfaces at 20X and 40X magnification. This section will summarize the results of the tests and discuss general trends observed during the testing process.

The behavior of the load monitored during the flexural testing process followed a

typical pattern for both the two-ply and four-ply specimens. A typical loading history is shown in Figure 8. The initial portion of the curve was linear, with the load increasing linearly with time. This region of the loading cycle will be referred to as Region I. Following Region I was a transition zone in which the material began to behave in a non-linear fashion. It was believed that in this portion of the loading cycle, the matrix began to micro-crack as described for similar ceramic matrix composites in the Literature review.[22,40,41] In this transition region, the measured load varied in a seemingly sporadic manner about a fairly constant load level, with slight increases followed by sudden drops as the cracks form. The transition zone was then followed by another relatively smooth region, which was approximately linear and lasted until specimen failure. This final portion of the loading cycle will be referred to as Region II.

Although only monitored during a few tests, the center deflection was measured with an LVDT. An example of the measured center deflection is given in Figure 9. The center deflection typically increased linearly with time, i.e., the center displacement of the specimen was approximately proportional to the crosshead displacement. Exact values of the displacement could not be accurately obtained during the Region I portion of the loading cycle because the magnitude of the measured displacement was on the order of the resolution of the instrument. A sinusoidal noise with an amplitude of approximately 30 mV, which was equivalent to 0.003 in., diminished the resolution of the measurement and can be seen superimposed on the displacement data shown in Figure 9. The source of this noise could not be located, however, it was believed to be in the digital data acquisition system. The curve in this figure, however, generally appears to be linear throughout the whole loading cycle. This behavior indicates that the displacement of the center of the specimen was proportional to

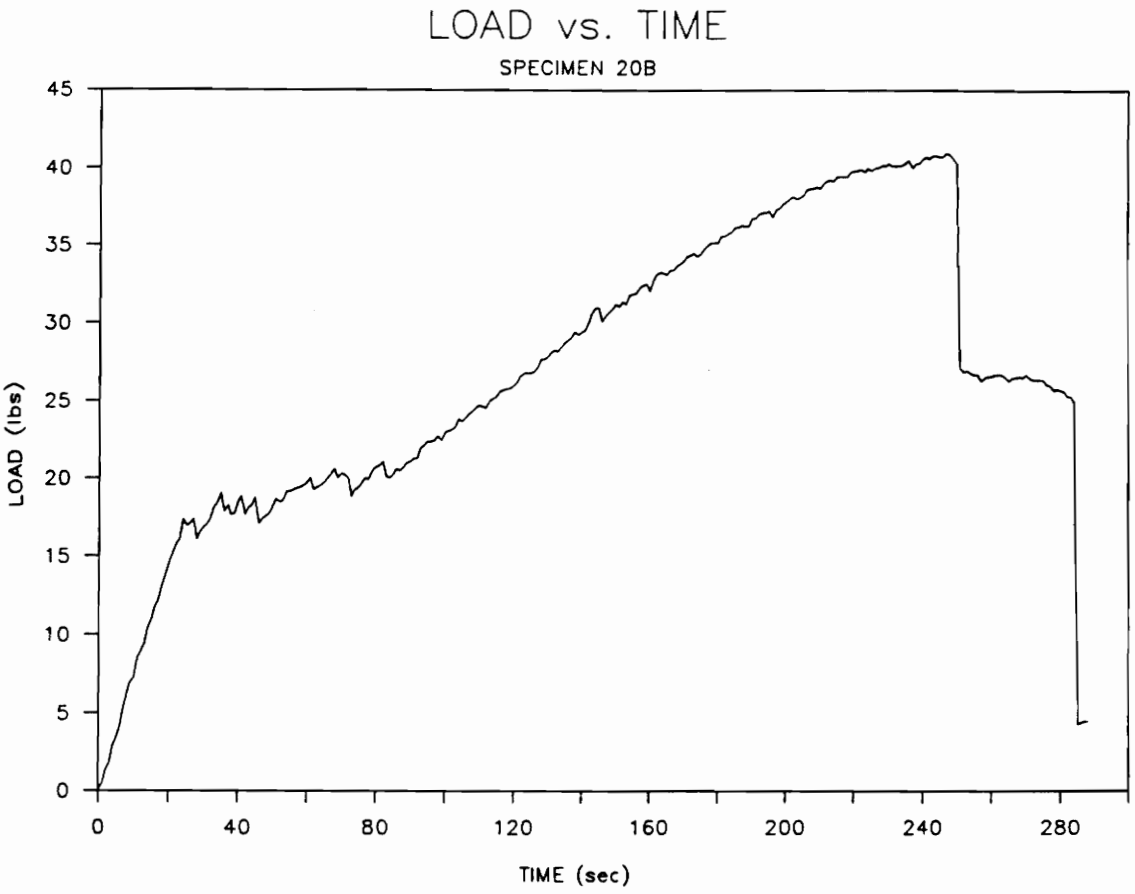

Figure 8. Flexural Load vs. Time (Specimen 20 B)

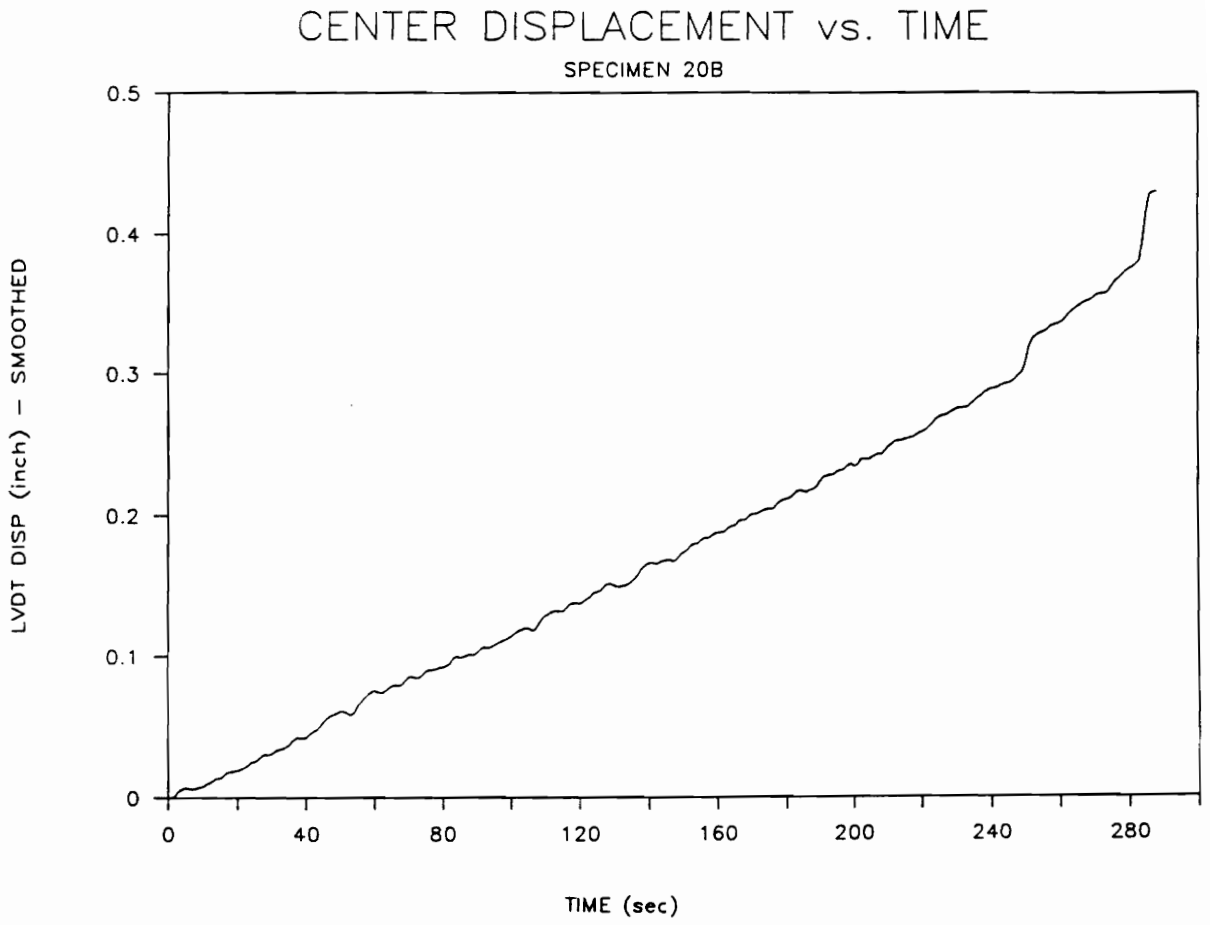

Figure 9. Center Deflection vs. Time (Specimen 20 B)

the crosshead displacement throughout the loading cycle.

Because the center deflection appeared to be proportional to the movement of the crosshead of the load frame and, therefore, proportional to time, a graph of the load plotted against the center displacement is similar in appearance to the load-time curves. An initial linear region (Region I) is followed by a nonlinear transition region and then both the load and deflection increase smoothly until failure (Region II). This behavior pattern is shown in Figure 10.

Surface strains were also monitored during several tests, with mixed success. The strain gages on the tensile surfaces of the specimens yielded data which appeared reasonable only during the initial portion of a test, that is in Region I. Typically, at the same point where the load data began to behave in a nonlinear manner, the tensile strain data became unreasonable; the strain magnitude rose or dropped erratically beyond Region I. It was hypothesized that the microcracking of the matrix on the tensile surface resulted in tensile strain data which either increased or decreased rapidly, depending upon the location of the cracks. It was surmised that if many cracks formed directly under the strain gage and were open to the surface of the specimen the measured tensile strain increased dramatically. However, if matrix cracks formed in the areas adjacent to the gage, the surface strain in the gage area dropped quickly.

The strain measurements from the compressive surface of the specimens appeared to have been more reasonable, with fewer and smaller jumps in magnitude during the loading cycle. Like the tensile strain, the compressive strain was typically linear in Region I. The

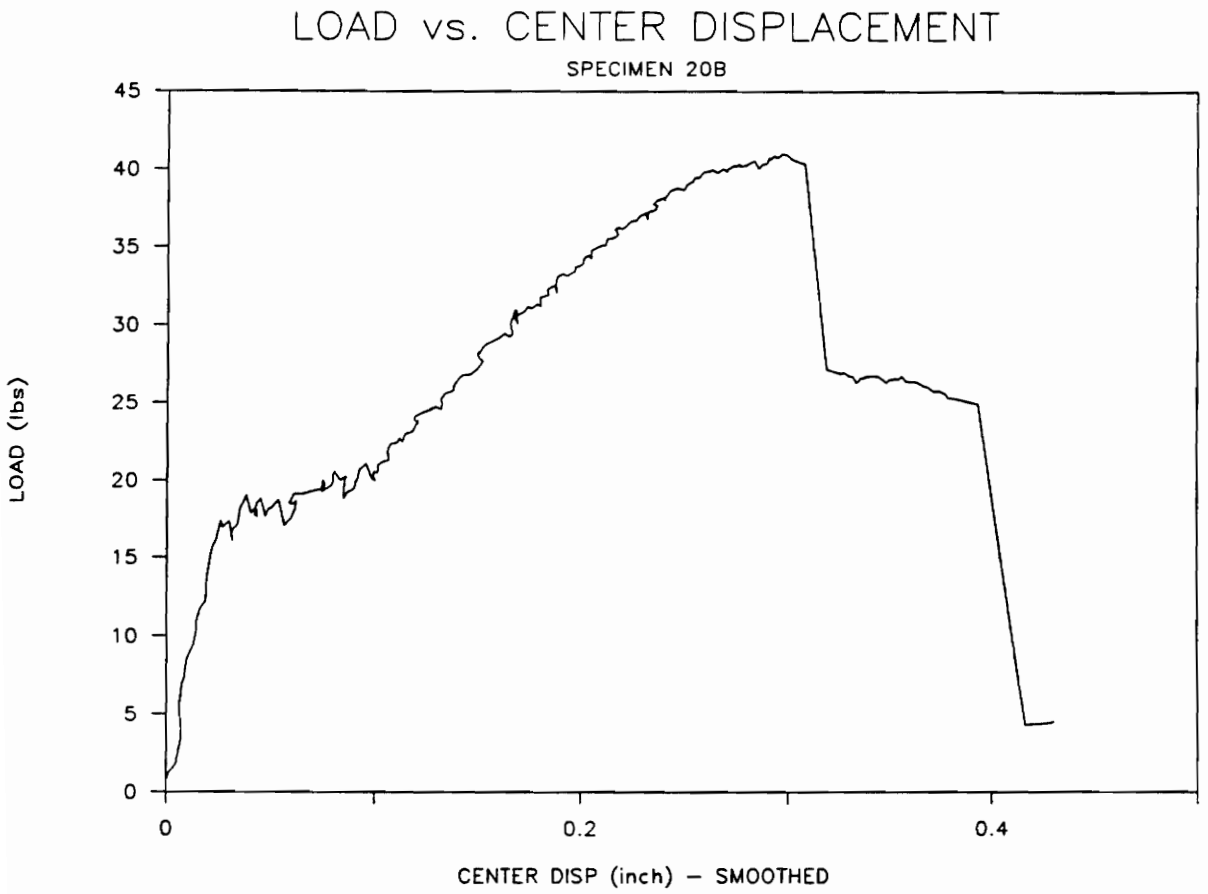

Figure 10. Flexural Load vs. Center Deflection (Specimen 20 B)

compressive strain data in this initial, linear section was typically identical in magnitude to the strain measured on the tensile surface of the specimen. After the initial linear portion of the loading cycle had been completed, the compressive strain generally leveled off to a fairly constant magnitude while the load oscillated about a constant load level. This was followed by a rapid rise in strain magnitude; the cracking of the tensile surface caused the neutral axis of the beam to shift toward the compressive side of the specimen and increase the stress and the measured strain at the surface. After the rapid rise in strain magnitude, the compressive strain increased steadily until specimen failure, with only a few increases or decreases; any rapid changes in strain occurred simultaneously with a drop in the measured load. The generally smooth behavior of the compressive strain appears to be reasonable considering that the flexural tests were run in displacement control and that the cracks which formed in the matrix typically were on the tensile face and not on the compressive surface of the sample. Examples of both tensile and compressive strains measured during a test are shown in Figure 11.

Because both the load and strain data were found to be linear in Region I, the flexural modulus in this region could be calculated, with the stress at the surface found using a classical linear-elastic beam calculation. The average initial modulus for both the four-ply and the two-ply samples was approximately the same value, 9.0 Msi (61.9 GPa) with a sample standard deviation of 0.18 Msi (1.23 GPa). This value is approximately the same as the reported modulus of the borosilicate glass matrix (62 GPa). Therefore, it appeared that in Region I the composite beam samples behaved as elastic beams with the modulus of a monolithic glass sample. This could have been a result of the layer of glass between the fiber mat and the surface of the specimens.

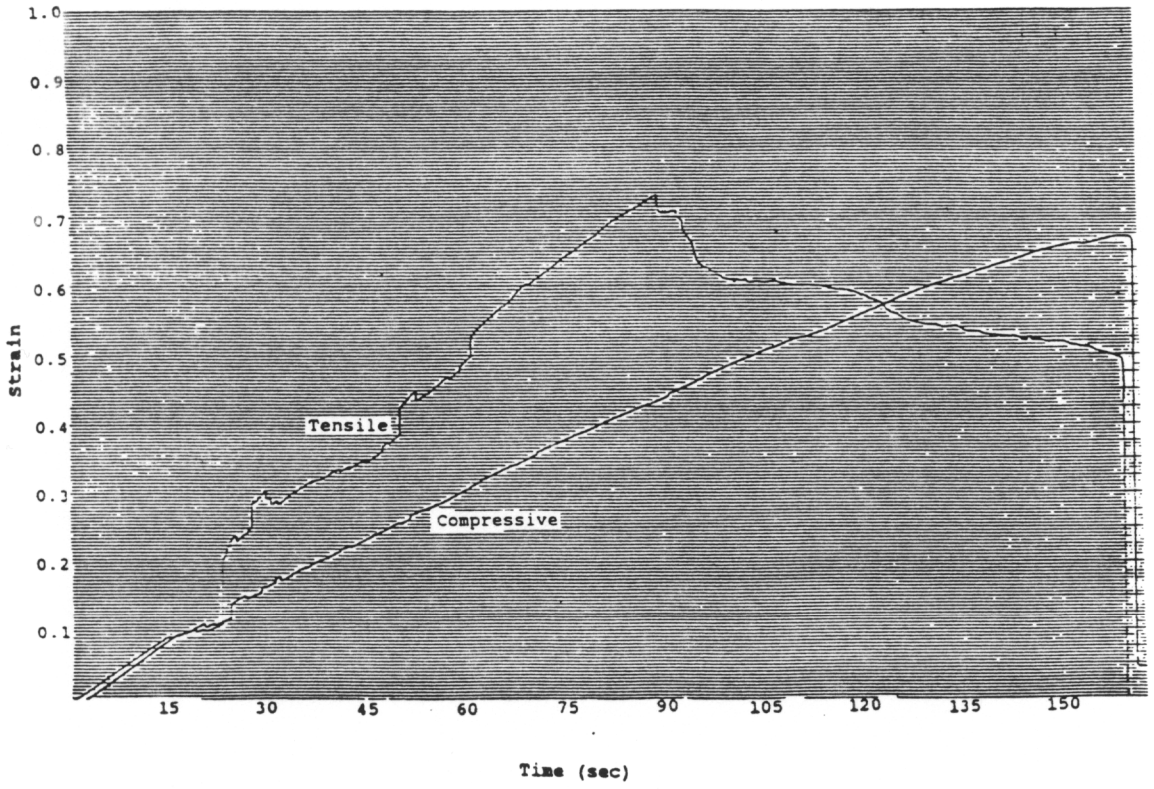

Figure 11. Typical Flexural Strains vs. Time

The onset of nonlinearity in the material occurred at a load of 18 pounds for the two-ply samples and 40 pounds for the four-ply samples. Elastic beam theory calculations revealed that the onset of nonlinear behavior occurred for both lay-ups at approximately the same stress magnitude at the outer surface of the beam (the location of the maximum bending stress), 8000 psi (55 MPa). The mean value of this stress magnitude for the four-ply specimens, excluding the data from one sample which behaved in a very non-typical manner, was 7698 psi (53.1 MPa) with a standard deviation of 318 psi (2.2 MPa). Although too few two-ply specimens were tested to obtain statistically reliable data, the mean and standard deviation for the two-ply samples were 8153 psi (56.2 MPa) and 497 psi(3.4 MPa), respectively. The dispersion in this statistical data can be attributed to several factors, including: the variation in surface roughness of the specimens, the inhomogeneities (voids) which varied between the samples, the evolution of the testing technique between sets of samples, and small errors associated with the computed stress and strain values. It appears that when this critical stress level was exceeded at the tensile surface micro-cracks formed on this surface and the material no longer behaved in a linear elastic manner. It could be presumed that the layer of glass at the specimen surface should have had the same strength as the bulk monolithic glass matrix material, however, the 8000 psi critical stress level was considerably lower than the reported tensile strength of the 7740 borosilicate matrix material (14,500 psi, 100.0 MPa). This difference in strength could be due to many things, including: the grinding and processing of the glass during fabrication of the panels may have degraded the strength of the matrix material; the borosilicate glass matrix may have contained impurities introduced during processing or due to the addition of fibers; or the surface irregularities of the specimens may have lowered the expected strength of the glass material at the surface of all of the composite samples.

It should be noted that once cracks have formed within a specimen the material can no longer be considered to be linear or elastic. The tensile surface cracks reduce the specimen uniformity and cause the stress distribution to be nonlinear through the material thickness. Any calculations which assume linear, elastic, homogeneous behavior, including classical beam theory, are in error. However, because there is no effective way to fully account for this nonlinear behavior, some calculations were performed using these assumptions while acknowledging that the calculated values are for the beam in its given state.

When a specimen was loaded beyond the linear region of behavior, the apparent modulus of the sample dropped considerably. Based upon the measured load and strain data from Region II and using elastic beam theory, the apparent value for the tangent modulus in Region II varied, depending upon the amount of damage which had developed within the specimen; values of the apparent stiffness, calculated using compressive strain data, ranged from 1.7 to 5.4 Msi (12 to 37 GPa).

Data from the incrementally loaded specimens allowed changes in the specimen behavior to be studied with increasing load. If a specimen had been loaded to a load level below the level at which nonlinear behavior begins, i.e., within Region I, upon reapplication of the load, the specimen exhibited the same elastic modulus as it had during the initial loading cycle (62 GPa). If, however, the load exceeded the critical load, upon reapplication of the load, the specimen exhibited a lower apparent modulus value due to the damage developed within the sample.

Observations of the cut edges and the tensile surface of the incrementally loaded specimens under optical magnification did not reveal the presence of cracks until the load had exceeded the nonlinear load level by 25 - 50%. Similarly, penetrant enhanced radiographs of the incrementally loaded flexure samples typically only revealed cracks at load levels well beyond the initial linear region of material behavior. Even if the penetrant was applied under load, with any surface cracks forced to be open, cracks were not typically visible in the radiographs taken in this load range. The results from these two methods applied at various levels within the loading cycle imply that even after nonlinear behavior had begun the matrix cracks which had formed under load typically closed tightly after the release of the load; however, once a large enough load was applied to the specimen, the cracks remained open. The crack closure was probably due to fiber tension and the mechanical interaction between the fibers and the matrix. This behavior is similar to that of the unidirectionally reinforced ceramic matrix materials discussed in the Literature Review [22,41].

Once the cracks were visible under magnification they typically had several general features which were similar for most tests. The cracks which were first visible formed in the outer glassy layer on the tensile face of the specimens at seemingly random locations throughout the gage section. These cracks ran transversely across the surface, however, occasionally the cracks veered off at an angle. Once visible on the cut edges, the cracks were typically normal to the surface of the specimen and only reached the first fiber layer. For the four-ply specimens, as the incremental load which the samples had been exposed to increased, some of the cracks propagated beyond the first fiber mat, but were stopped by the second fibrous layer; some of the observed cracks had propagated at odd angles within the glass layer between the mats. For the two-ply samples, prior to failure, the cracks propagated to the

first fiber mat and then turned to run along the mat, between the tows of fibers.

An interesting note is that when observing damaged or failed specimens, the cracks did not necessarily start at or run through the large voids which were present in the specimens. This observation implies that this material is relatively insensitive to the gross flaws which existed. This notch insensitivity was also exhibited by the bidirectionally reinforced material which was described by Prewo.[18]

As discussed in the Test Methods chapter, acoustic emission was monitored during most flexural tests. The resulting plot of the rms voltage history gave a recording of the number of high amplitude peaks which occurred and the relative amount of acoustic energy emitted during a particular portion of the loading cycle. An example of the monitored acoustic emission is shown in Figure 12.

Although each test resulted in a unique emission pattern, a few generalizations about the AE behavior of the material in this loading configuration can be stated. Almost no AE activity was recorded during the Region I portion of the loading cycle; typically only one very low amplitude peak was recorded in this region. Although very low in magnitude, this initial, short emission probably was a result of fixture or load frame noise. At the end of Region I, the AE activity increased considerably; during this transition region, many high amplitude peaks were consecutively recorded and the average rms voltage in this region remained relatively high. As the load was increased through Region II of the cycle, the AE activity continued with considerably fewer high amplitude peaks and an average rms voltage for the region which was much lower than in the transition zone between Regions I and II.

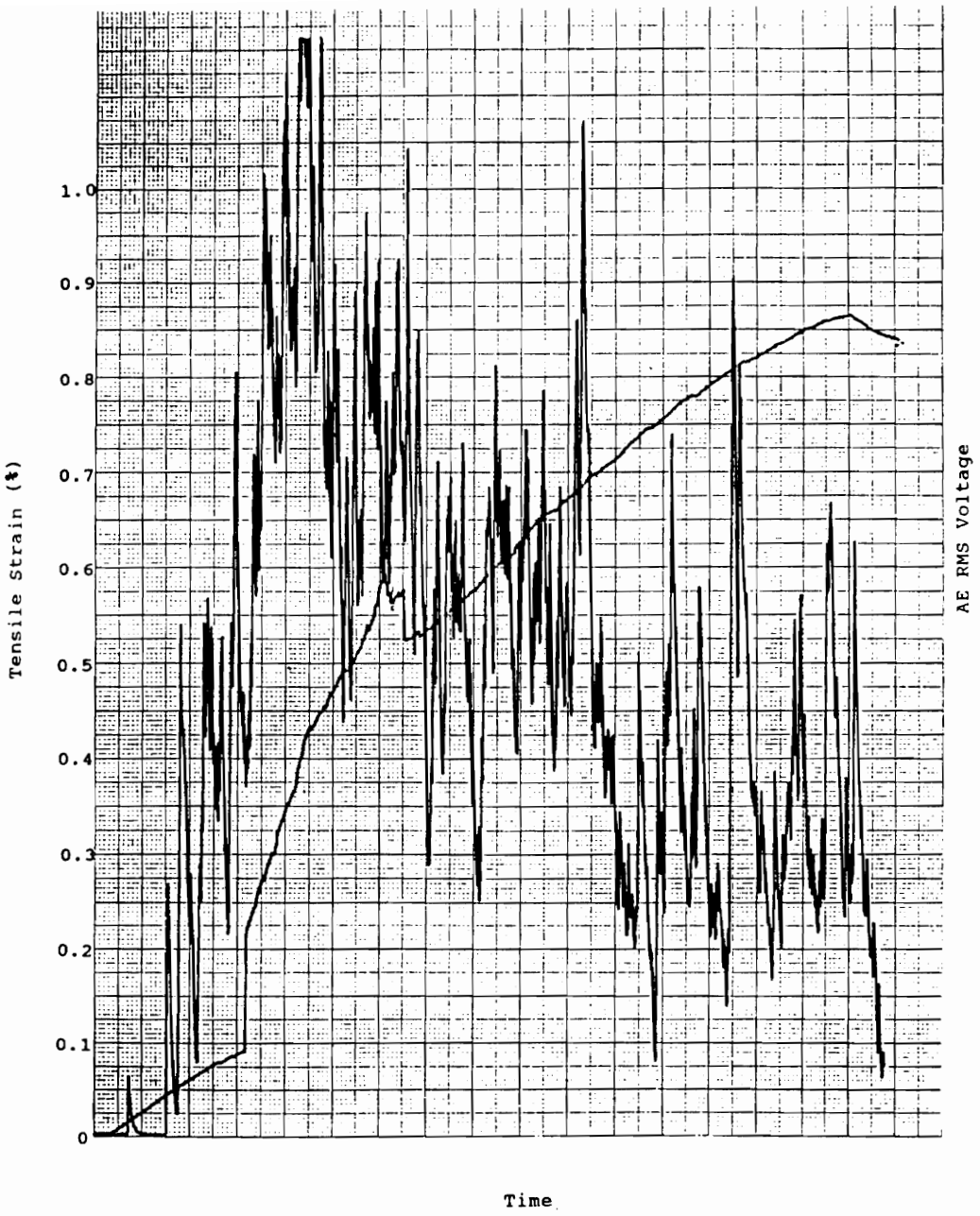

Figure 12. An Example of the Typical Monitored Acoustic Emission Pattern

Just prior to specimen failure, the AE activity increased sharply, with several very high amplitude peaks accompanying the specimen failure.

AE activity was also recorded for the specimens which were incrementally loaded. These specimens followed the same emission pattern discussed above, however, in an "interrupted" manner. Upon reloading from a given load level, the specimens emitted almost no sound until the previous deflection had been reached. Once the previous level was surpassed, acoustic emissions began again, and the data once again occurred in the described pattern. This material, therefore, exhibits the Kaiser effect.

The acousto-ultrasonic technique was performed during several flexural tests. Measurements were taken on the unloaded specimens between loading intervals during the incremental loading tests. During the uninterrupted quasistatic tests, the ultrasonic transducers were held in contact with the specimen throughout the loading cycle with two small fixtures which, in turn, were attatched to the specimen with rubber bands. Care was taken to assure that the transducer and fixture assemblies did not add any significant additional load to the specimen.

The AU results from one of the incrementally loaded tests are shown in Figure 13. During the period between loading intervals, AU measurements were performed, X-ray radiographs were made, and the surface of the specimen was examined optically. No damage was seen through the optical microscope until after 80 pounds had been applied. As is ipointed out in Figure 13, damage first became visible the radiographs after the 40 lb

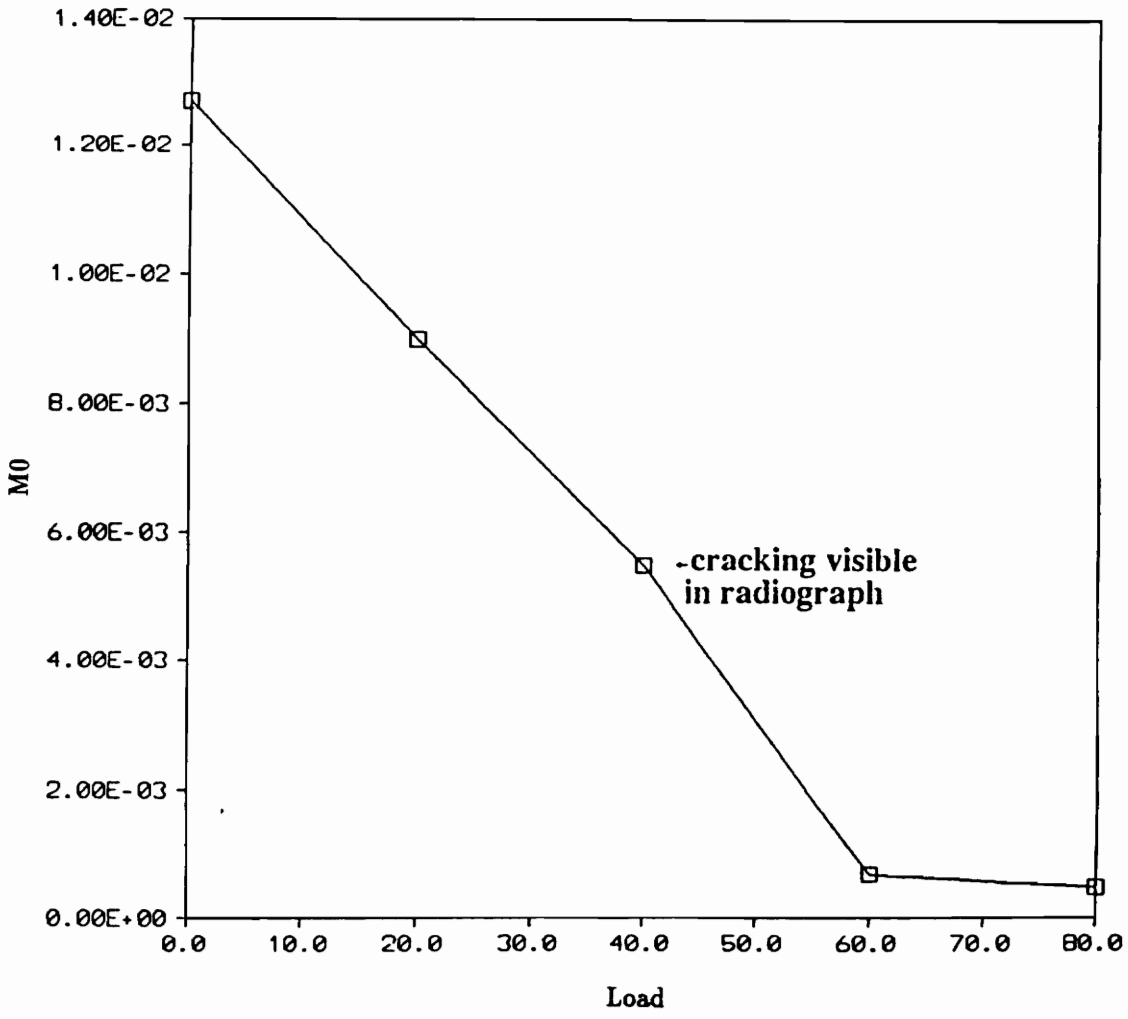

Figure 13. AU Parameter M0 vs. Load Increment (Specimen 22C)

loading and the cracks grew with each load increment. It is clear that the M0 values decreased after every loading level, including the 20 lb level. This would seem to indicate that the AU parameter M0 is very sensitive to damage development within this material.

A clear change in the mechanical performance of the specimen from Figure 13 can be seen in the incremental load-time curves shown in Figure 14. The crosshead displacement rate was held constant for each of the tests performed on this specimen. The specimen began to behave in a very nonlinear manner during the 60 lb test as shown by the sharp increases and drops in load. A comparison of the 80 lb test curve with several load-time curves for lower load levels reveals that the specimen becomes more compliant; for a given amount of crosshead displacement, the load reached during the 80 pound loading cycle was significantly lower than the load obtained during previous loading cycles.

An example of AU measurements taken during a continuous loading cycle is shown in Figure 15. The second AU measurement, taken 3 seconds into the loading cycle, is at approximately the same value as the measurement taken prior to loading. The following AU measure, 11 seconds into the cycle, was considerably lower in magnitude than the previous measurement. The third measure was taken just prior to the end of Region I of the loading cycle, where the load and strain data (Figure 16) are still linear. This point also occurred just prior to the first high amplitude AE peak recorded. The next AU data point, which was well into the transition region of the loading cycle, had an even lower value. The last AU data points had extremely low amplitudes relative to the initial AU data. No further AU measurements were made during the test because the amplitude of the received waveform was approaching the level of the noise within the system.

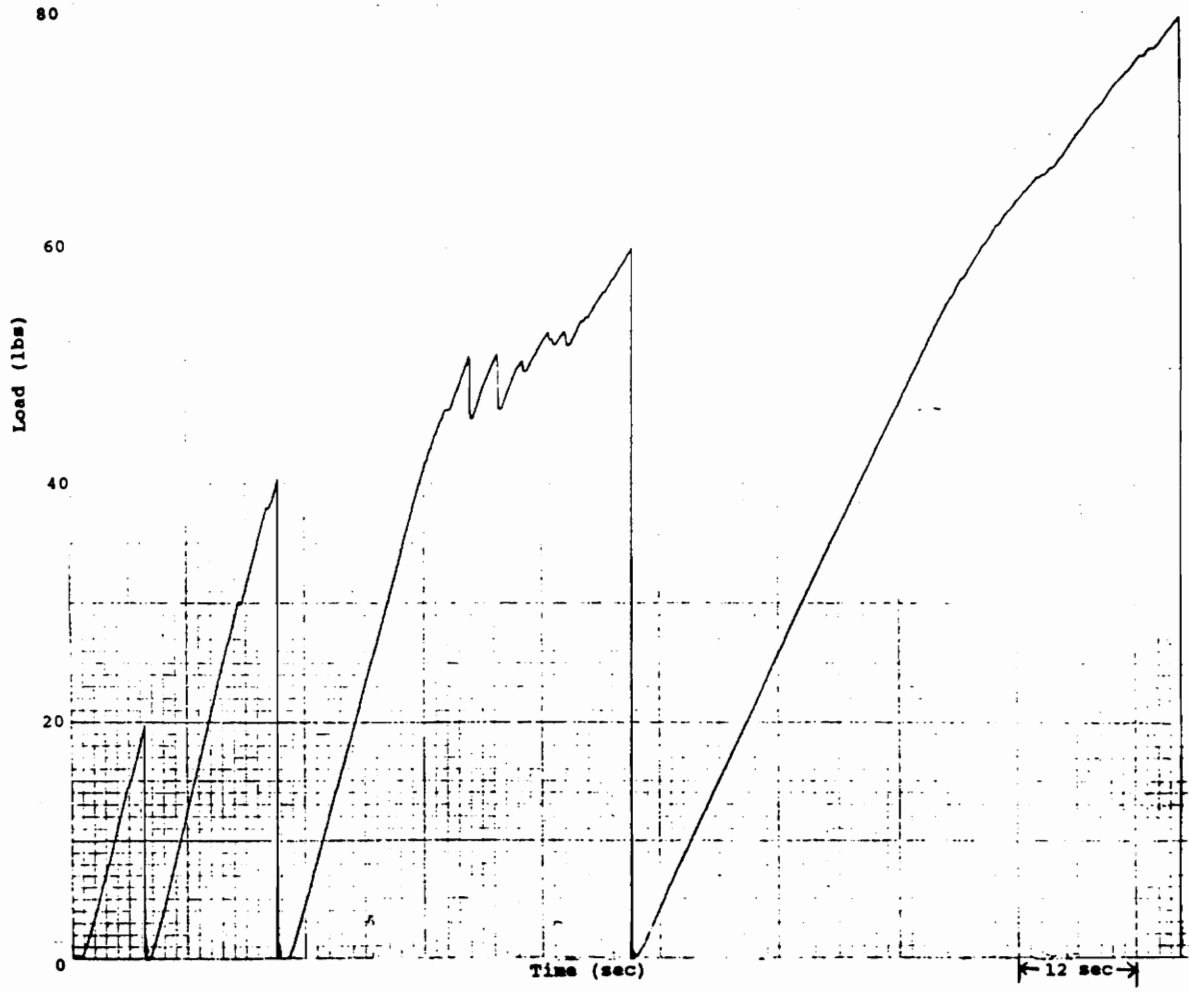

Figure 14. Incremental Tensile Load vs. Time (Specimen 22C)

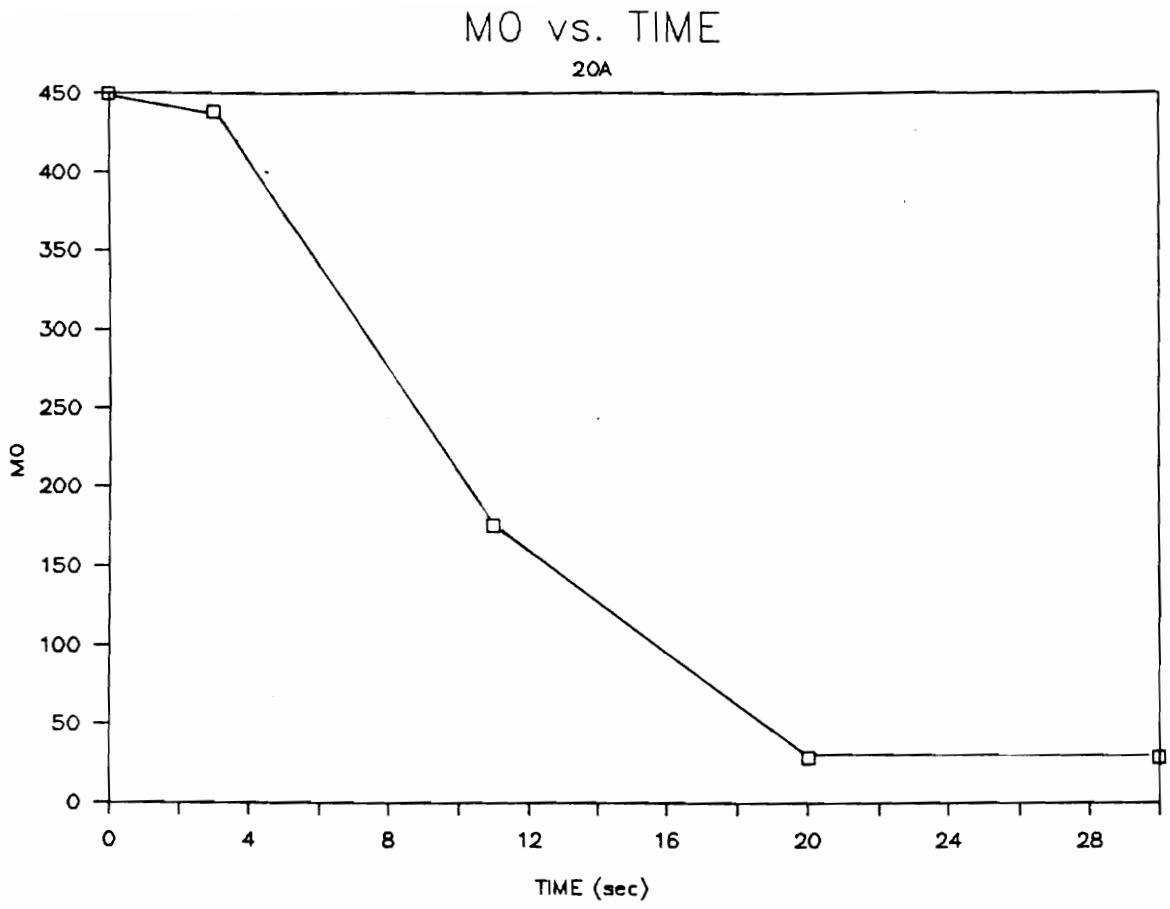

Figure 15. AU Parameter M0 vs. Time (Specimen 20A)

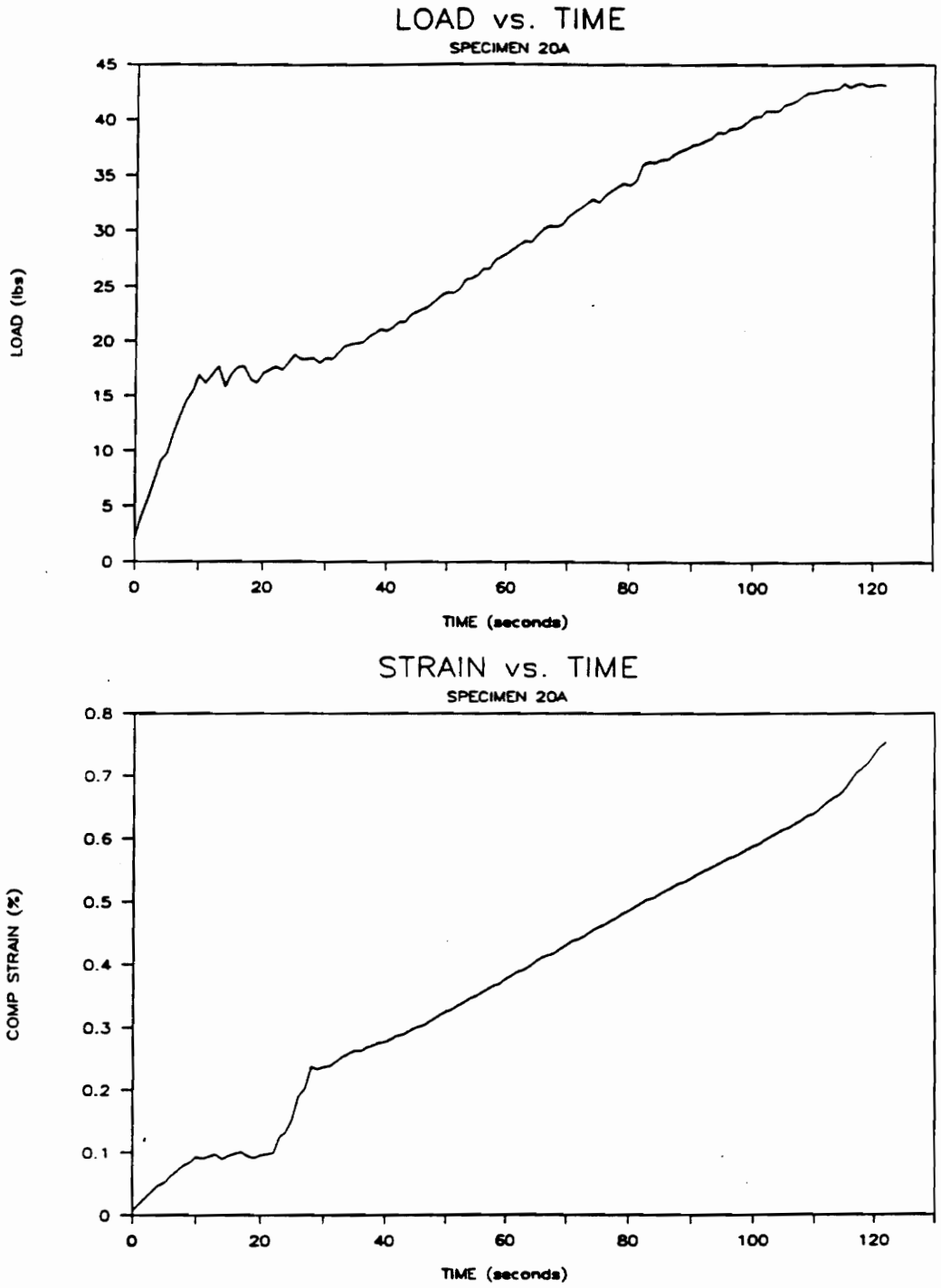

Figure 16. Load and Strain Data (Specimen 20A)

The drop in the M0 measurements during the initial portion of some of the tests was not as great as shown above; during some tests the M0 measurements increased slightly during the Region I portion of the loading cycle prior to a dramatic drop in magnitude. It was hypothesized that this could possibly be due to fiber straightening caused by the mechanical loading.

During several incremental tests, while the specimen was removed from the load frame, AU measurements were taken along the length of the specimen in the pattern described in the Test Methods chapter. Typically, between loadings, radiographs were taken and optical observations were also performed. The results of one such test are shown in Figures 17 and 18. It should be noted that because the scanning measurement regions overlapped (see Figure 5), a weighted average of the results was performed; twice the resultant value from a given location was aded to the values from the two overlapping locations and divided by four. Although in several locations M0 increased slightly at the 20 pound load step, the downward trend of M0 with increasing load can clearly be seen. It is interesting to note that an indication of a very tight crack was found in the radiographs in region "E" of the specimen; the M0 measurements from section "E" had the highest relative decrease in amplitude between the 20 and 30 pound load increments. Figure 18 illustrates the trend of generally decreasing values of M1/M0 with increasing load. This trend indicated that the centroid of the power spectrum of the received signal typically decreased as damage developed within the specimen. Therefore, the amplitude of the higher frequency components of the spectrum were decreased by a larger amount compared to the low frequency components. The change in the spectrum is illustrated in Figure 19 for a typical region ("E") on the specimen. The AU parameter M1/M0 typically followed this pattern for most tests,

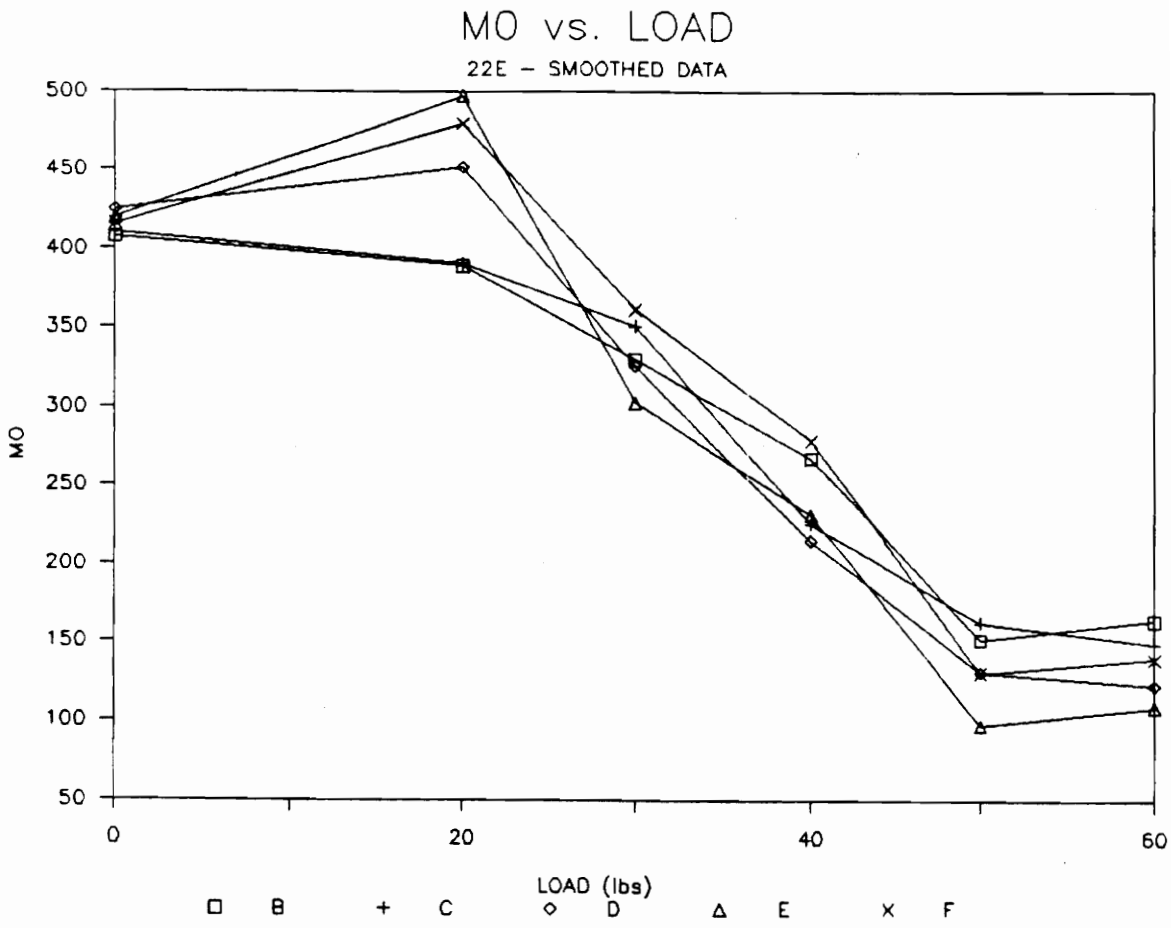

Figure 17. AU Parameter M0 vs. Load (Scanned Specimen 22E)

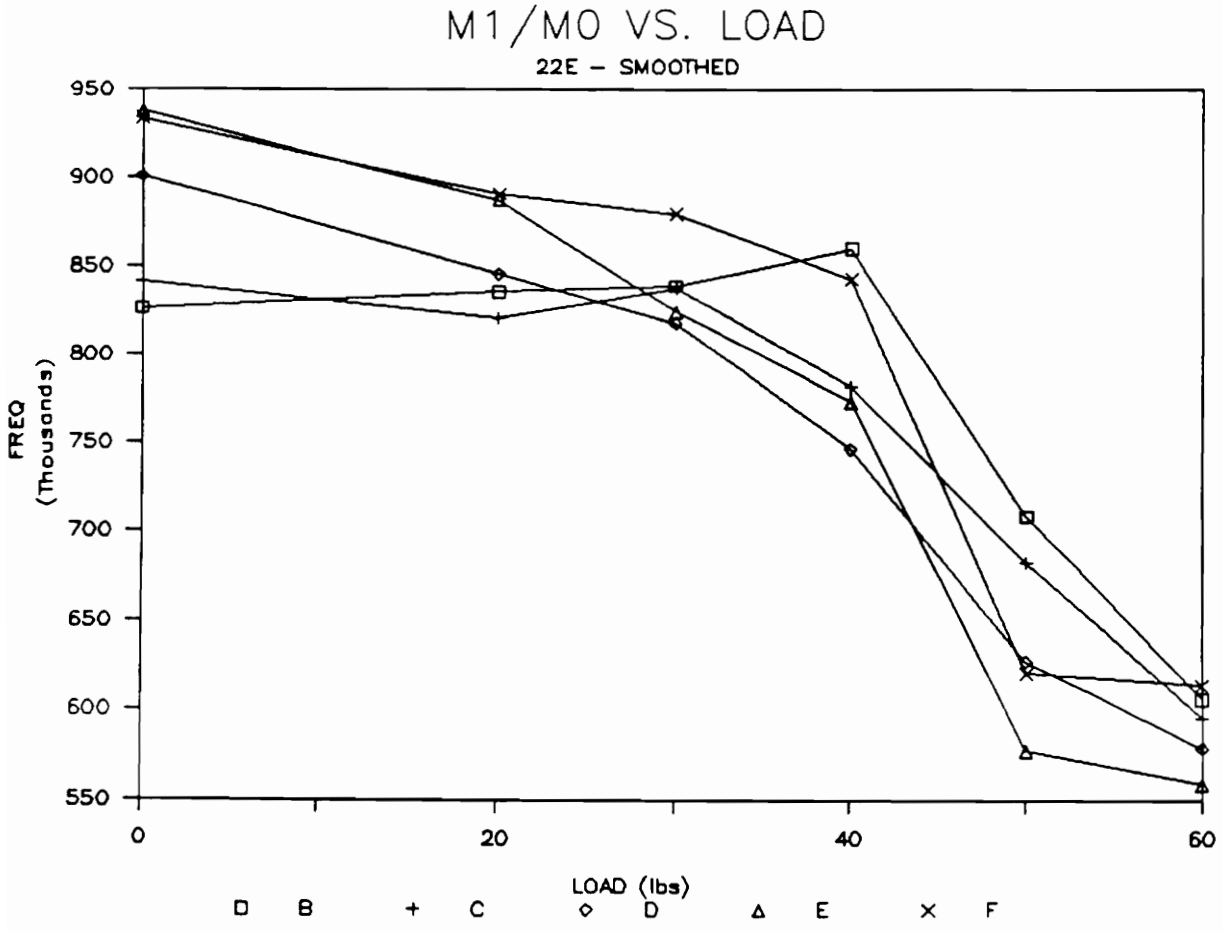

Figure 18. AU Parameter M1/M0 vs. Load (Scanned Specimen 22E)

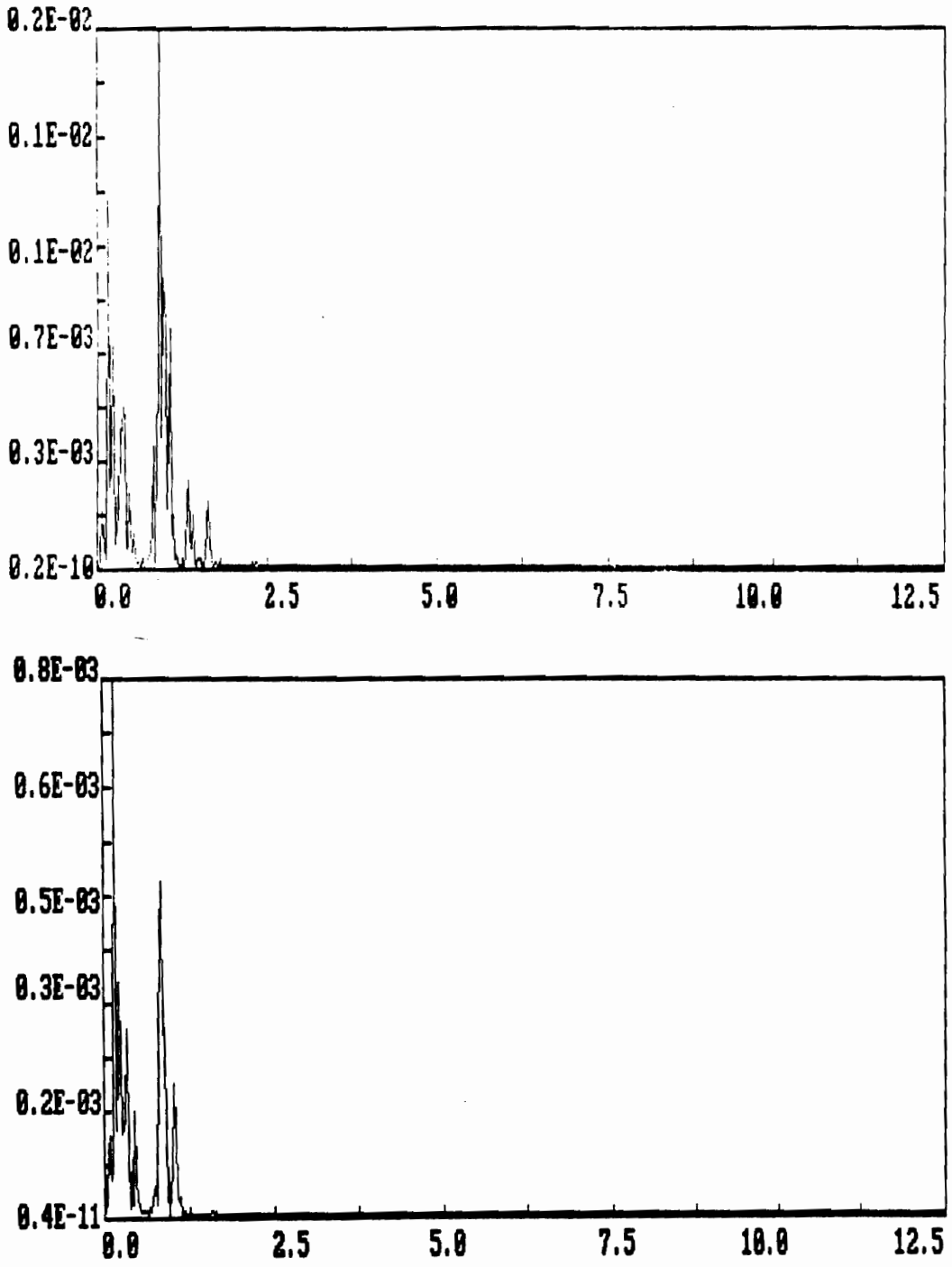

Figure 19. Power Spectrum Changes with Damage Development

however, the trend for many tests was not as clear as that seen for M0; it appeared that M1/M0 was more sensative to slight variations in the measurement technique such as pressure on the transducers, alignment of the transducers, and exact placement of the transducers.

The two-ply and four-ply specimens failed in two distinctly different failure modes. 75% of the four-ply specimens which were tested to failure, failed in a region of high shear; the specimens failed between an adjacent pair of loading and support pins. Observations of the failure regions under magnification revealed that in addition to the numerous cracks on the tensile surface which had propagated as far as the second layer of fibers, many cracks had propagated between the loading and support pin contact points. The cracks ran at steep angles, sometimes in the direction of the fiber mats, throughout this region of the specimen. In contrast, most of the two-ply specimens failed in a tensile mode, in the gage section of the specimen. It appeared that one of the many cracks from the tensile surface grew through the thickness to cause failure. Both types of failure modes had very fibrous failure surfaces, indicating that there was a large amount of fiber pull out. Examples of several failed specimens are shown in Figures 20 and 21.

It is interesting to note that the two-ply specimens typically had longer times to failure than the four-ply samples and, therefore, with identical crosshead speeds, were deflected more by the loading pins prior to failure. The loading pins for the two-ply specimens were typically displaced approximately 0.200 in., while the pins for the four-ply samples moved only 0.125 in.

Figure 20. Failed Specimen

Figure 21. Failed Specimen

Several specimens which were tested did not fail in the manners described above. Two of the four-ply samples failed in a tensile mode within the gage section. It was assumed that these failures were a result of the inhomogeneities within the samples, surface roughness, or some possible error within the testing procedure. One other four-ply sample failed in a compressive mode, with the glass layer at the surface of the specimen splitting off and a crack propagating into this region through the specimen thickness. The data from the specimen which failed in compression was left out of the above data analysis.

The average maximum load which was attained for the four-ply samples which failed in the regions of high shear was 130 pounds (59.0 kg). The four-ply specimens which failed in a tensile mode failed at a lower average maximum load of 113 pounds (51.3 kg). The two-ply samples had an average ultimate load of 43 pounds (19.5 kg). The specimens which were incrementally loaded did not appear to have a failure load which was outside the range of the results from the other specimens.

4.3 TENSILE TESTING RESULTS

As discussed in the Test Methods chapter, a series of quasistatic tensile tests were performed to compare the behavior of the material under both flexural and tensile loading. Sixteen tensile tests were performed; twelve tests were run on the two-ply specimens and four on the four-ply samples. Most tension tests were run uninterrupted until specimen failure, however, in a similar fashion to the flexural testing procedure, several tests were stopped at various load levels so that the specimen could be inspected. Typically in these tests, upon reapplication of the load, the load level was incrementally increased with each loading cycle. These interrupted tests were performed to study the development of the damage within the specimens in the tensile loading configuration. Several nondestructive tests were run on various specimens including penetrant enhance radiography, magnified optical inspection of the sample surfaces, liquid penetrant inspection, and acousto-ultrasonics. The results of the tensile testing will be summarized and general trends which were observed during the tests will be discussed in this section.

The tensile tests were performed in a displacement controlled fashion and the load was monitored throughout the test. The behavior of the load during most of the tensile tests followed a pattern that was very similar to the pattern which resulted from the flexural testing configuration. Examples of the measured load history from two tensile tests are shown in Figures 22 and 23. The initial portion of the loading curve was typically linear; this region of the loading cycle will again be referred to as Region I. As before, Region I was followed by a transition zone in which the load behavior began to behave in a nonlinear fashion. In most tests this transition zone resembled the transition zone described for the

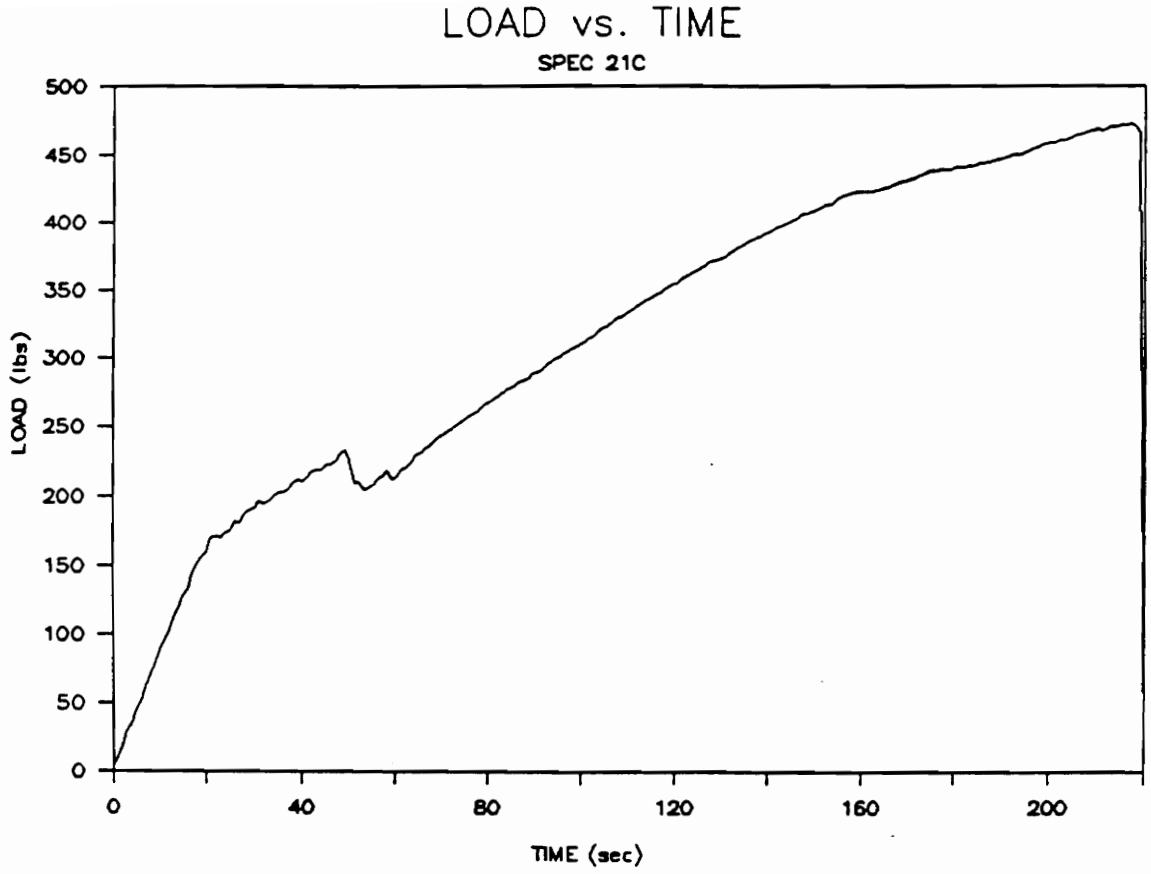

Figure 22. Tensile Load vs. Time (Specimen 21C)

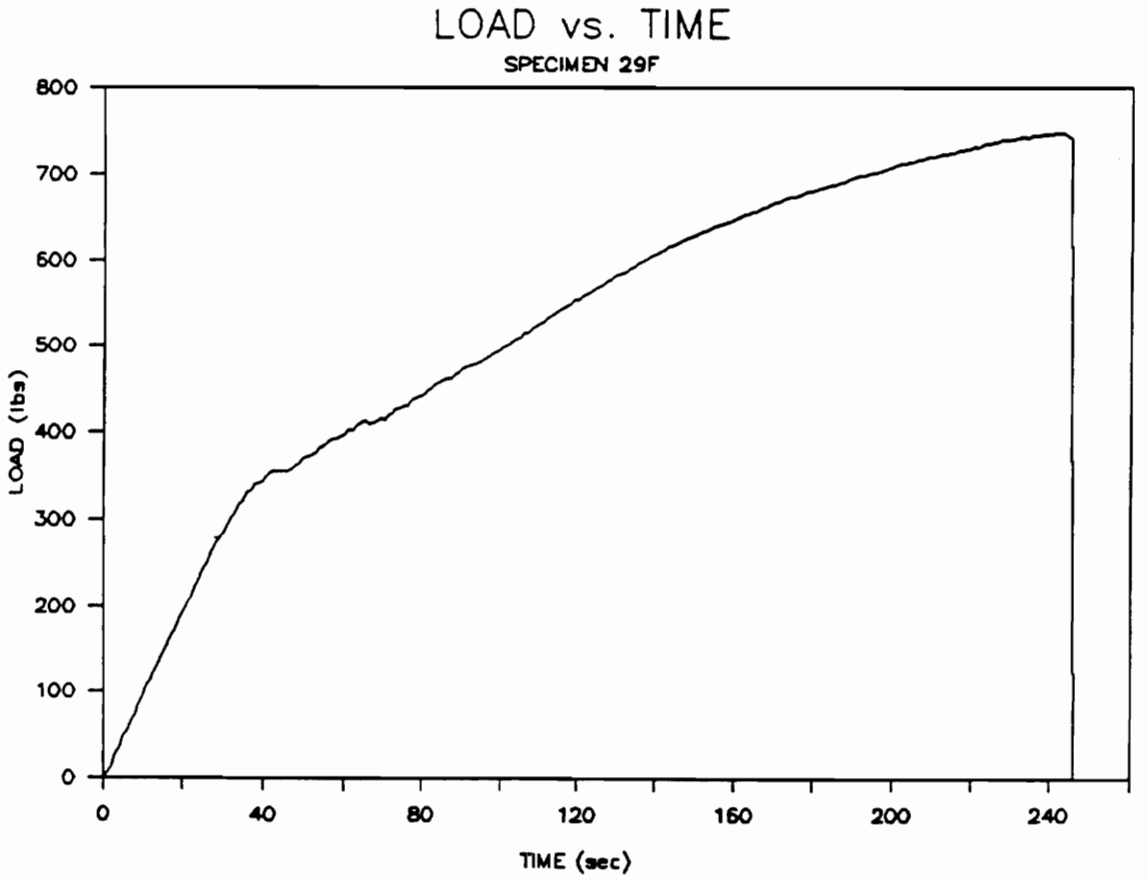

Figure 23. Tensile Load vs. Time (Specimen 29F)

flexural tests, in which the measured load exhibited rapid increases and decreases. In many of the tensile tests, the transition zone appeared to be relatively short and smooth, with little more than a change in the slope of the loading curve. Because the behavior was similar to the flexural tests, it was believed, as before, that matrix cracks formed during the transition zone. Typically, from the end of the transition zone until specimen failure, the load increased smoothly; this final portion of the loading cycle will again be referred to as Region II.

Samples which were cut from one panel (#17) had significantly different behavior than the other panels. Although the first portion of the loading curves exhibited the typical behavior, the behavior during Region II was quite different; the measured load in Region II had rapid increases and decreases in magnitude similar to those exhibited in the transition zone (see Figure 24). The average load continued to increase throughout Region II, however, this increase was considerably less than for the samples from the other panels.

A measurement of the extension in the gage section of the tensile specimens was attempted through the use of an extensometer. Two examples of the measured extension are shown in Figures 25 and 26. The extension during the initial portion of the loading cycle typically increased linearly with time; however, after Region I, the data from the extensometer varied greatly between tests. The measured extension beyond Region I many times had rapid, very large increases in magnitude, as illustrated in Figure 25; these increases, however, coincided with small discontinuities in the measured load data. It is questionable if these dramatic changes in strain were actually a result of sudden specimen extension or if the instrument slipped on the surface of the specimen as a result of the sudden release of load. The extension from some tests exhibited a smooth, but nonlinear, increase to

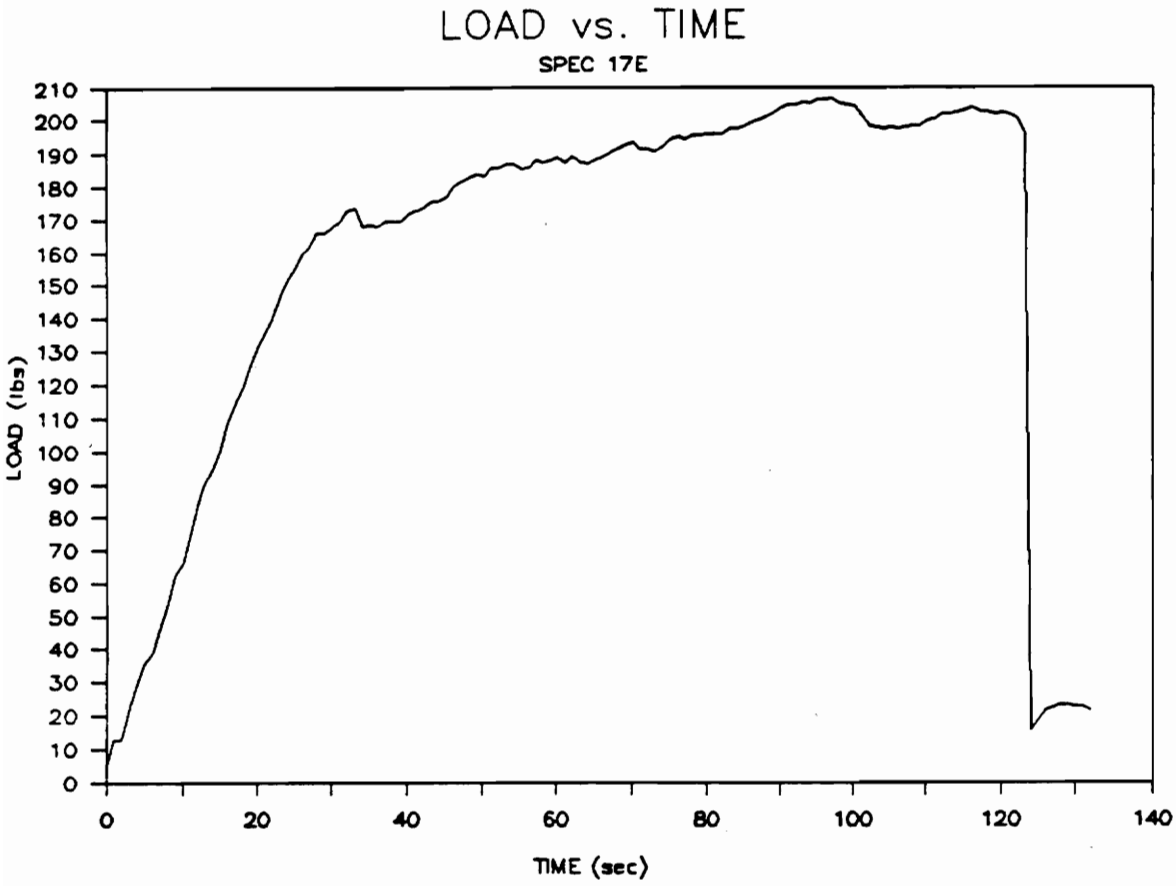

Figure 24. Tensile Load vs. Time (Specimen 17E)

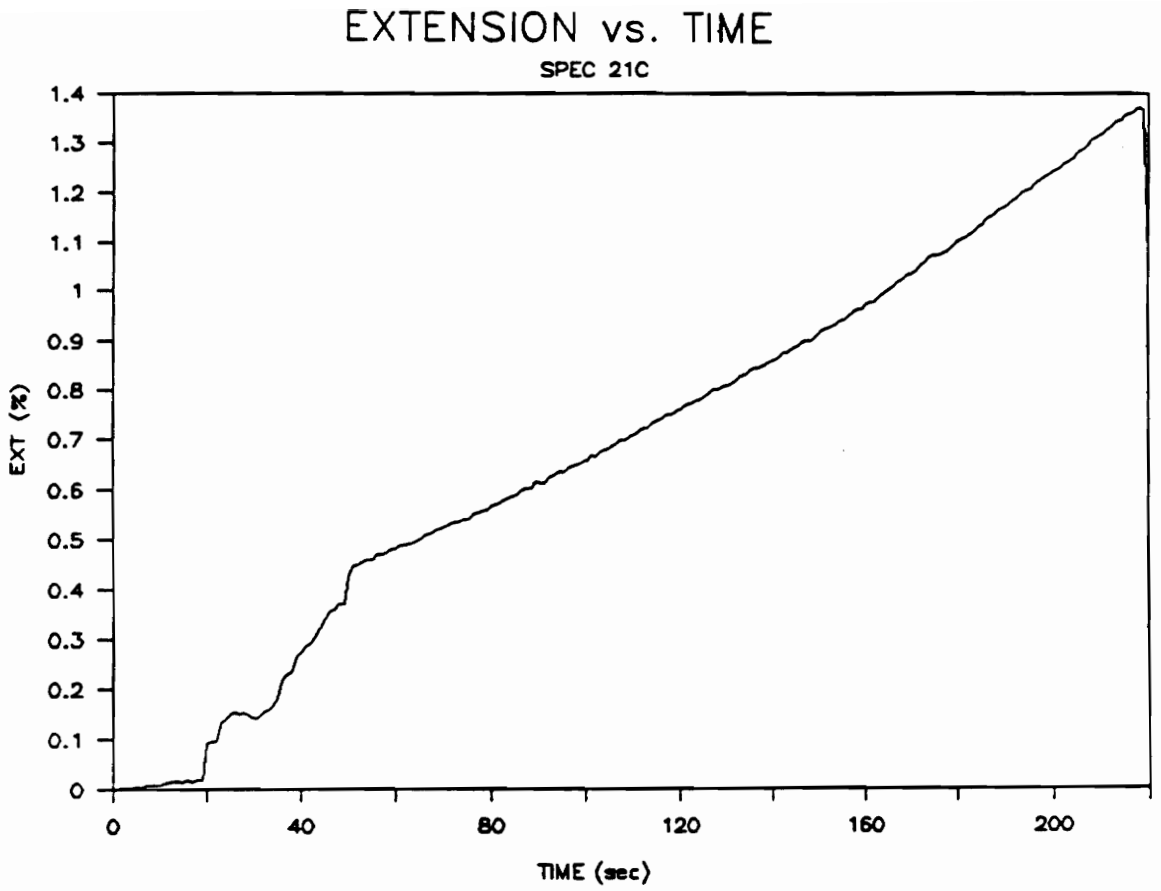

Figure 25. Extension vs. Time (Specimen 21C)

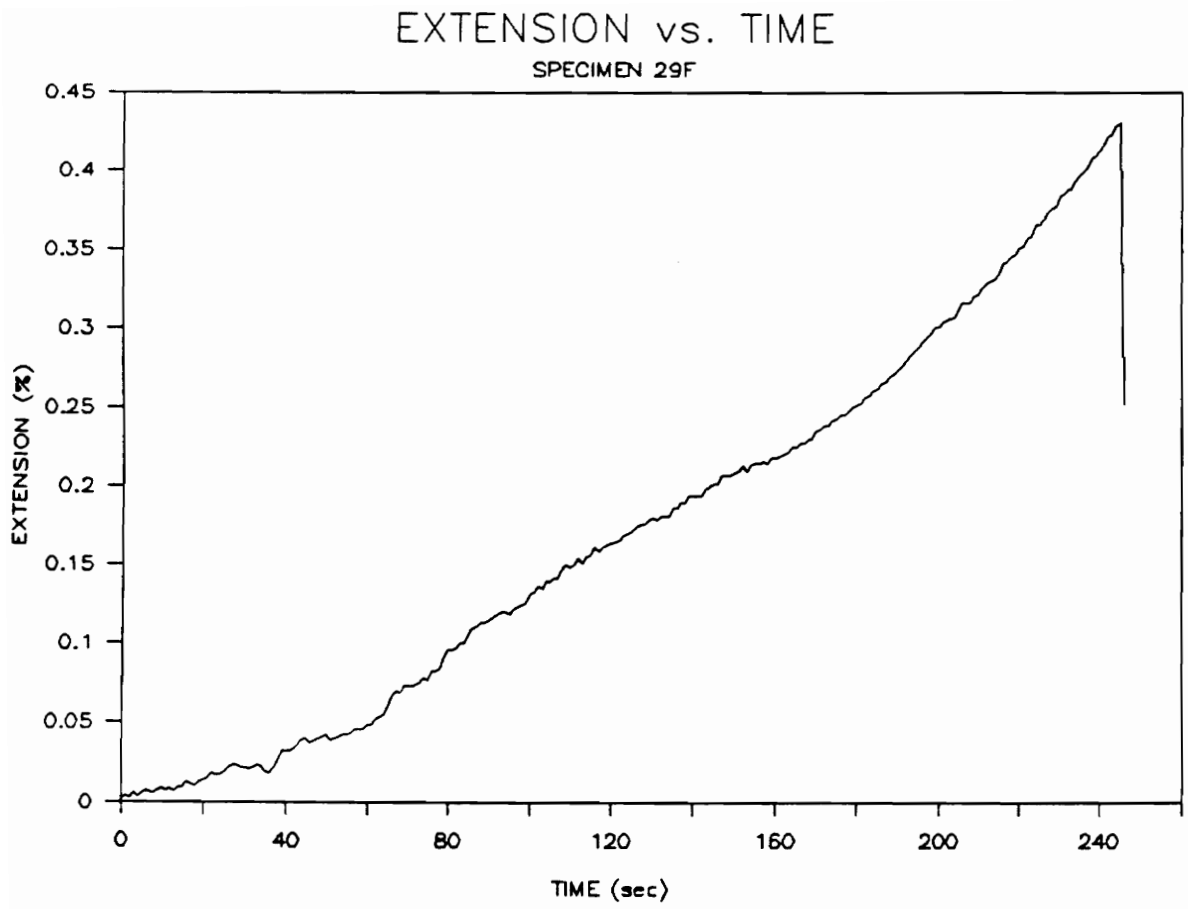

Figure 26. Extension vs. Time (Specimen 29F)

failure. It was deduced that the location of the predominant matrix cracks determined the measured extension behavior; if the largest cracks were within the span of the extensometer, the measured strain jumped as the cracks grew rapidly, or, on the other hand, if the dominant cracks formed outside the portion of the specimen which was monitored, the extension increased in a relatively smooth manner with the formation of microcracks throughout the gaged region. The measured extension at failure also varied greatly between the specimens; this value ranged from approximately 0.45% to over 2.0% elongation.

Strain gages were mounted on several specimens in order to measure strain in the direction of loading. Gages were mounted on both sides of the specimen to determine if the strain varied between the sides, indicating uneven loading of the specimen. The resulting strain gage data appeared reasonable during the initial portion of most tests, that is in Region I, during which the strain typically increased linearly. Typically, some small differences between the front and back gages were measured in Region I, however, beyond this potion of the loading cycle the strain data on each side varied dramatically. When the load data began to behave in a nonlinear manner, the strain gage data became unreasonable, in a similar manner to the measured tensile strain behavior during flexural loading; the strain magnitude rose or dropped erratically beyond Region I. This behavior was believed to be caused by the microcracking of the matrix under or around the strain gage, as described in the flexural testing results section. An example of the measured strain for a specimen loaded in tension is shown in Figure 27.

For several of the tensile tests, strain gages were mounted perpendicular to the direction of loading, resulting in a measure of the transverse strain. Because the magnitude

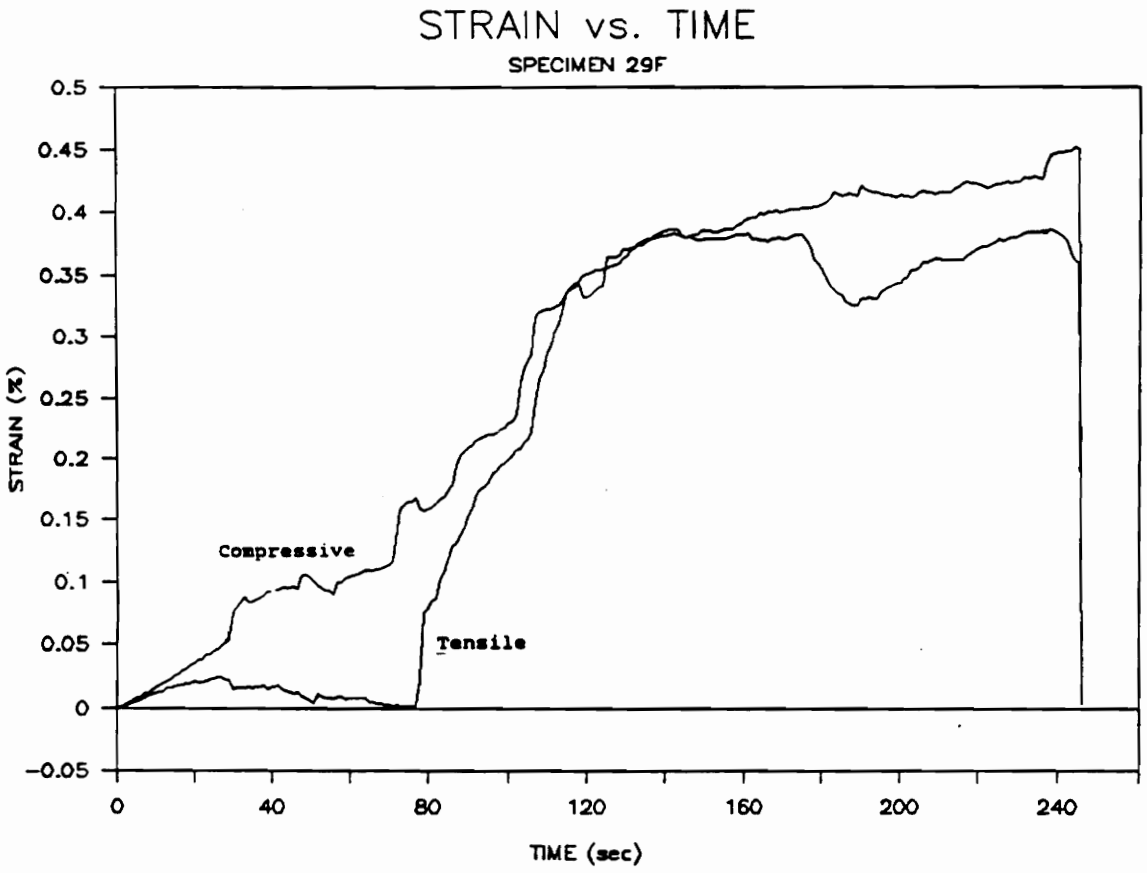

Figure 27. Strain vs. Time (Specimen 29F)

of this strain was quite low, the data contained a large amount of noise. To reduce the magnitude of this noise a weighted averaging scheme was applied to the data; two times the magnitude of the strain at a given time was added to the magnitude of the transverse strain at each surrounding point in time and the total was divided by four. The smoothed transverse strain data shown in Figure 28 followed an expected trend.[21] The magnitude of the transverse strain increased relatively linearly during Region I, after which the magnitude of the transverse strain decreased. This decrease was a result of the formation of microcracks in the matrix and the decrease in the measured load. When the load level increased again, the transverse strain magnitude also increased. As the test progressed and more damage developed within the specimen, the transverse strain data became erratic and unreliable.

Because the load, strain, and extension data were found to generally be linear during the initial portion of the loading cycle, the elastic modulus could be calculated in this region. The stress in the cross section was found assuming that it acted as a linear, homogeneous bar in tension. The calculated initial modulus for the samples varied greatly, ranging from 5.6 to 18 Msi; because of the broad range of values, no clear difference was observed in modulus values between the two-ply and four-ply samples.

The onset of nonlinear behavior for the two-ply samples occurred at very consistent load levels; elastic stress calculations revealed that the onset of nonlinear behavior occurred at an average stress of 3330 psi (23.0 MPa), with a sample standard deviation of 165 psi (1.1 MPa). The dispersion in this stress data can be attributed to the many factors discussed in the flexural results section. This value is considerably lower than the critical stress intensity found during flexure testing (8000 psi, 55.2 MPa). Although too few four-ply specimens were

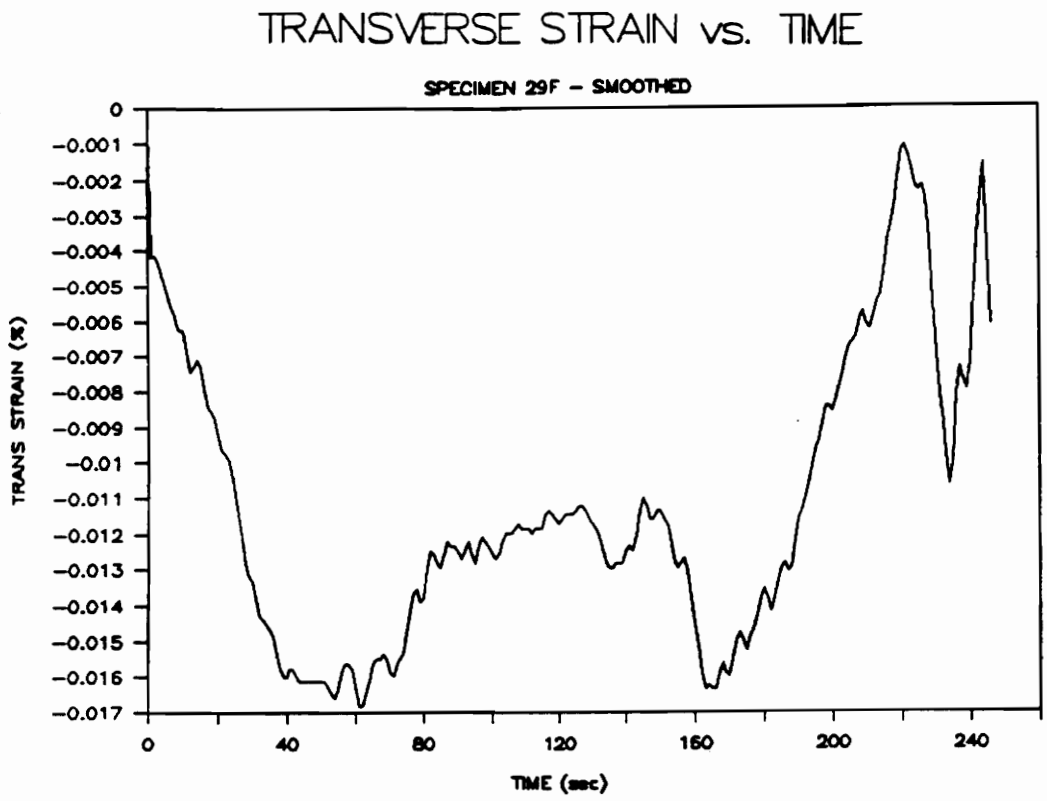

Figure 28. Transverse Strain vs. Time (Specimen 29F)

tested to obtain statistically reliable data, the mean stress level at the onset of nonlinearity was 4950 psi (34.1 MPa).

Data from the incrementally loaded specimens allowed changes in the specimen behavior to be studied with increasing load. These test reveal that if a specimen had been loaded to a load level below the level at which nonlinear behavior began, i.e., within Region I, upon reapplication of the load, the specimen retained the same elastic modulus as it had during the initial loading cycle. If, however, the load at which nonlinear behavior began was exceeded, upon reapplication of the load, the specimen clearly exhibited a lower stiffness due to the damage within the sample.

Observations of the cut edges of the incrementally loaded specimens under optical magnification did not clearly reveal the presence of matrix cracks until the load level at which the samples started to behave nonlinearly. Similarly to the flexure test results, radiographs of the incrementally loaded samples typically did not clearly reveal cracks in the specimen until after nonlinear behavior had begun. Even when the penetrant was applied while the specimen was under a tensile load, with any matrix cracks forced to be open, cracks were not typically visible in the radiographs taken of specimens loaded in this load range. One interesting observation was that when the radiographic penetrant was applied to a specimen which was loaded beyond Region I, the penetrant soaked through the specimen, revealing that the microcracks which were throughout the gage section had propagated through the specimen thickness.

Once the cracks were visible under magnification, they typically had several general

features. The cracks which were first visible in the matrix appeared at random locations throughout the gage section, typically forming perpendicular to the specimen surfaces and oriented transversely across the width of the specimen. The portion of the specimens which had been gripped were not thoroughly inspected because some obvious damage had resulted from gripping; this damage was limited to the gripped region. The cracks which typically ran transversely across the surfaces were very difficult to locate on the cut edges early in the load cycle, however, after the load level was increased, the cracks became visible on all of the edges. As seen in the flexural testing, the cracks did not necessarily start or propagate through the voids which were present in the specimens, which implies that this material is relatively insensitive to the existence of the large voids.

Liquid penetrant inspection of several of the specimens was performed. This method was applied to specimens which had been incrementally loaded to different levels of damage. Beyond Region I of the loading cycle, the penetrant clearly indicated the locations of the matrix cracks which ran transversely across the gage section of the specimens. This technique clearly highlighted the cracks in the specimens which had been loaded to levels at which cracks could not typically be located either optically or with contact radiographs. An example of a damaged specimen which was examined with liquid penetrants is shown in Figure 29. This technique was very useful in initially locating surface cracks. However, subsequent application of the method on the same specimen proved to be difficult. The penetrant dye from the first application could not be thoroughly cleaned from the cracks and it spread out from the cracks over the specimen surface, obscuring further inspection. Due to the difficulty in cleaning the specimens and the mess associated with the technique, only a limited number of specimens were inspected with this technique.

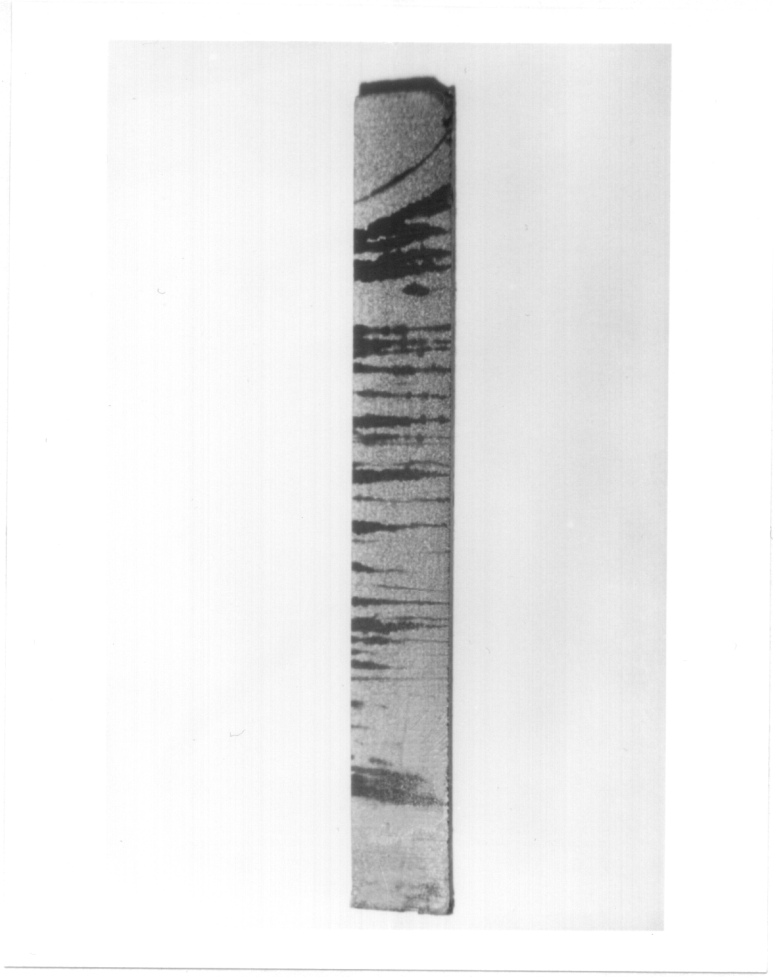

Figure 29. Liquid Penetrant Inspection of a Tensile Specimen

Acoustic emission was monitored during most of the tensile tests. This technique was applied in the same manner as during the flexural tests, with the rms voltage monitored throughout the loading cycle. An example of the monitored acoustic emission versus time in the loading cycle is shown in Figure 30.

Each test resulted in a unique emission pattern, however, a few general statements about the AE behavior of this material in the tensile loading configuration can be made. No AE activity was recorded during the Region I portion of the loading cycle; the low amplitude peak observed during Region I of the flexural testing was not observed during tensile loading. At the end of Region I, AE activity began with numerous high amplitude peaks and an average rms voltage which appeared to be higher relative to the other regions in the test. As the load was increased through Region II, the AE activity decreased considerably with almost no high amplitude peaks occurring; there was much less AE activity in this region than in the transition between Region I and Region II. There was considerably less AE activity in Region II during tensile testing than during flexural loading. Just prior to specimen failure, several very high amplitude emissions occurred. Specimens from panel 17, which had exhibited the rough load history in Region II (Figure 24), typically had considerable AE activity throughout the final portion of the loading cycle; this activity was, however, only a small portion of the activity during the entire loading cycle.

AE activity was also recorded for the specimens which were incrementally loaded. These specimens exhibited a pattern similar to the emissions behavior of the incrementally loaded flexure samples. Upon reapplication of the load for the next incremental load level,

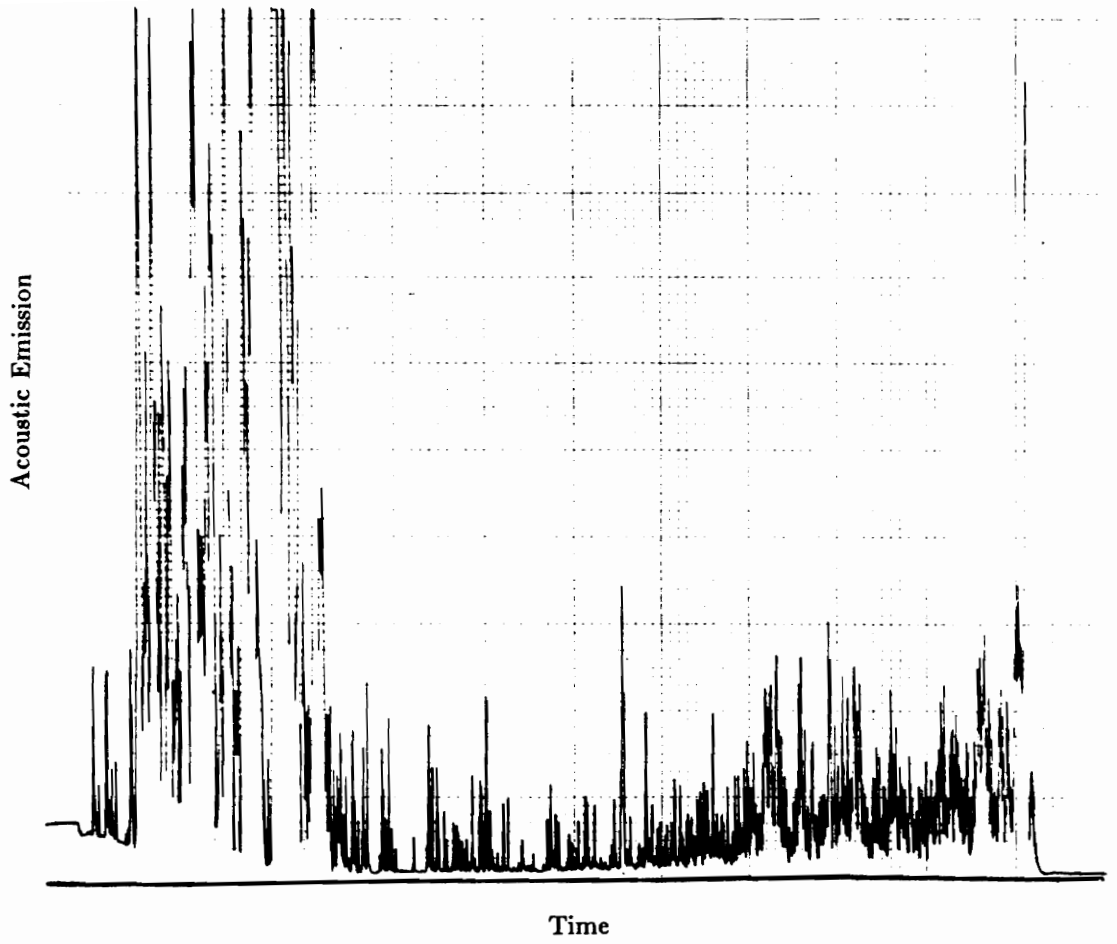

Figure 30. Acoustic Emission vs. Time (Specimen 21C)

the specimens had no acoustic activity until the previous load level was again reached, at which point the emissions began and the AE data followed the typical pattern described above. Once again, this material exhibited the Kaiser effect.

The acousto-ultrasonic technique was performed during several tensile tests. The technique was applied in a similar manner to that described for the flexural testing. During the uninterrupted quasistatic tensile tests, each ultrasonic transducer was held in contact with the specimens using several rubber bands and the center-to-center distance between the transducers was held at 0.75 in. Measurements were also taken during the incremental loading tests on the unloaded specimens between loading intervals.

Results from AU measurements taken while a specimen was under load during a tensile test is shown in Figure 31. The load and AE data which were taken during the same test are shown in Figure 32. The value of the AU parameter M0 decreased with time and, therefore, decreased with increased load. The AU parameter M0 began to decrease well before the onset of nonlinear behavior in the load data, as well as before any peaks occurred in the monitored AE data.

As shown in Figure 31 and in the AU data for the uninterupted flexural tests, only a small number of AU measurements could be taken during each test without interrupting the test using the available AU data acquisition package. A data acquisition software package which captured the waveform at a programmed time interval [55] was used during several of the tensile tests. This allowed for a shorter delay time between capturing each AU waveform.

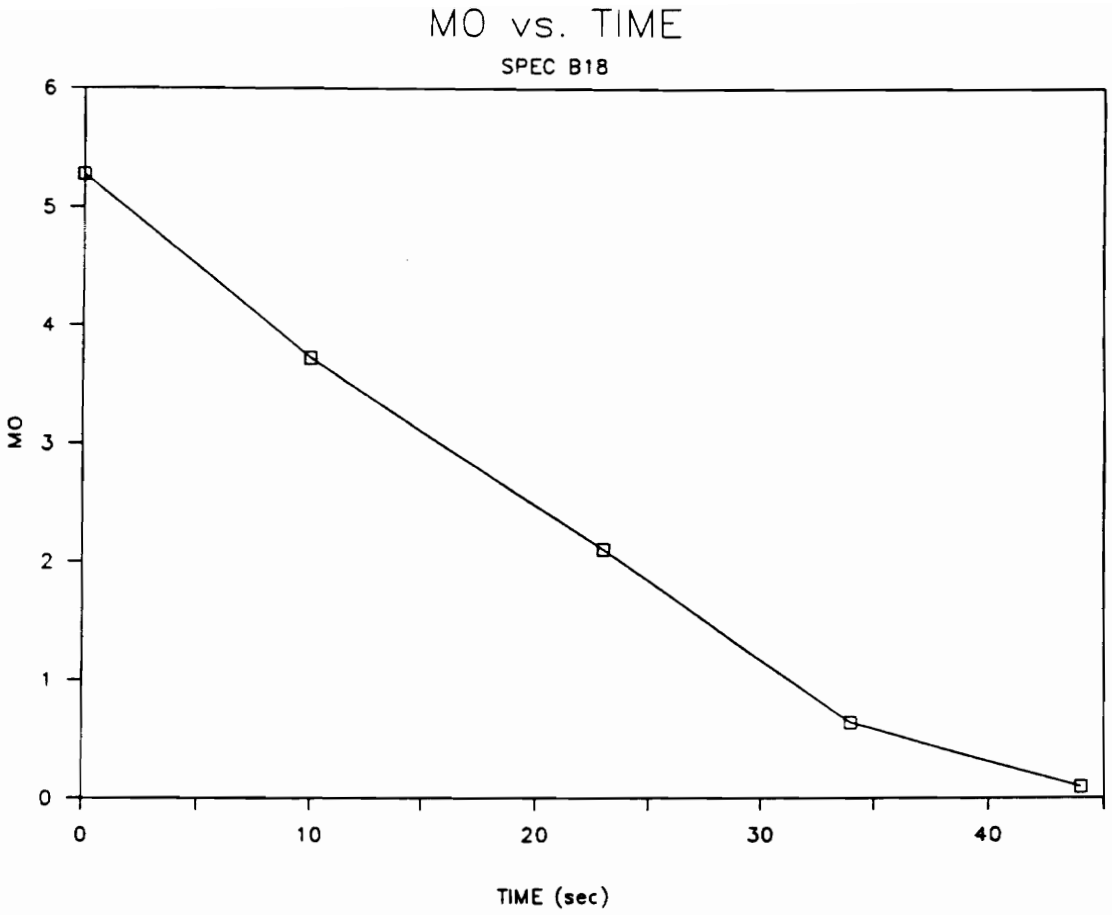

Figure 31. AU Parameter M0 vs. Time (Specimen 18B)

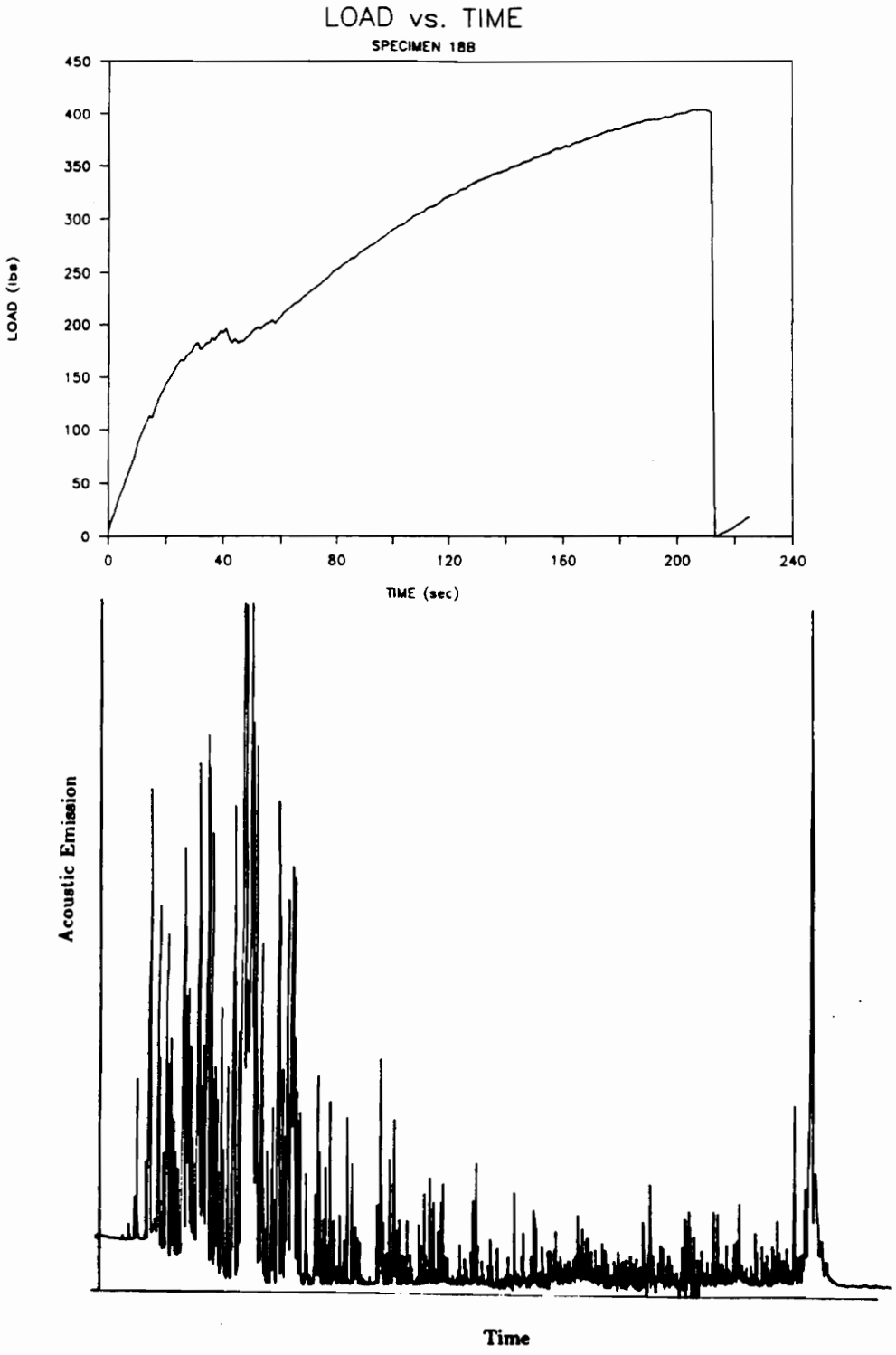

Figure 32. Load and Acoustic Emissions Data (Specimen 18B)

Examples of AU data taken using this package are shown in Figures 33 through 35. The AU data shown in Figure 33 is from the same test as Figures 22, 25, and 30. During this test the AU parameter M0 remained at approximately the same level during the first several seconds of the test and then it dropped off quickly as damage developed within the specimen. To see the variation in the AU measurements more clearly, the crosshead displacement rate was lowered to half the previous speed for the test shown in Figure 34. During this tensile test, the M0 parameter remained at a high level for a longer portion of the test before dropping off quickly, well before any acoustic emissions were registered or material nonlinear behavior was measured. These results suggest that the acousto-ultrasonic method is very sensitive to changes in this material system, with variations noted in the measured AU parameters prior to other indications of damage development.

The variations of the AU data taken during the test of a specimen cut from the panel number 17, which had exhibited different mechanical behavior, also varied from the AU patterns of the other specimens. The AU parameter M0 is plotted versus test time in Figure 35; this test data is from the same specimen discussed previously (Figure 24). The AU parameter M0 remained at a constant level for a longer period of time during the first portion of the test than during the previous tests. The relatively constant level was followed by a rapid decrease in magnitude. The drop off of the parameter M0 corresponded to the time at which the first peak occurred in the monitored acoustic emission data.

AU measurements were taken between load levels during an incremental loading test; the specimen was scanned as previously described (Figure 4). The AU data for each location along the specimen length was an average of three AU measurements; the data was then

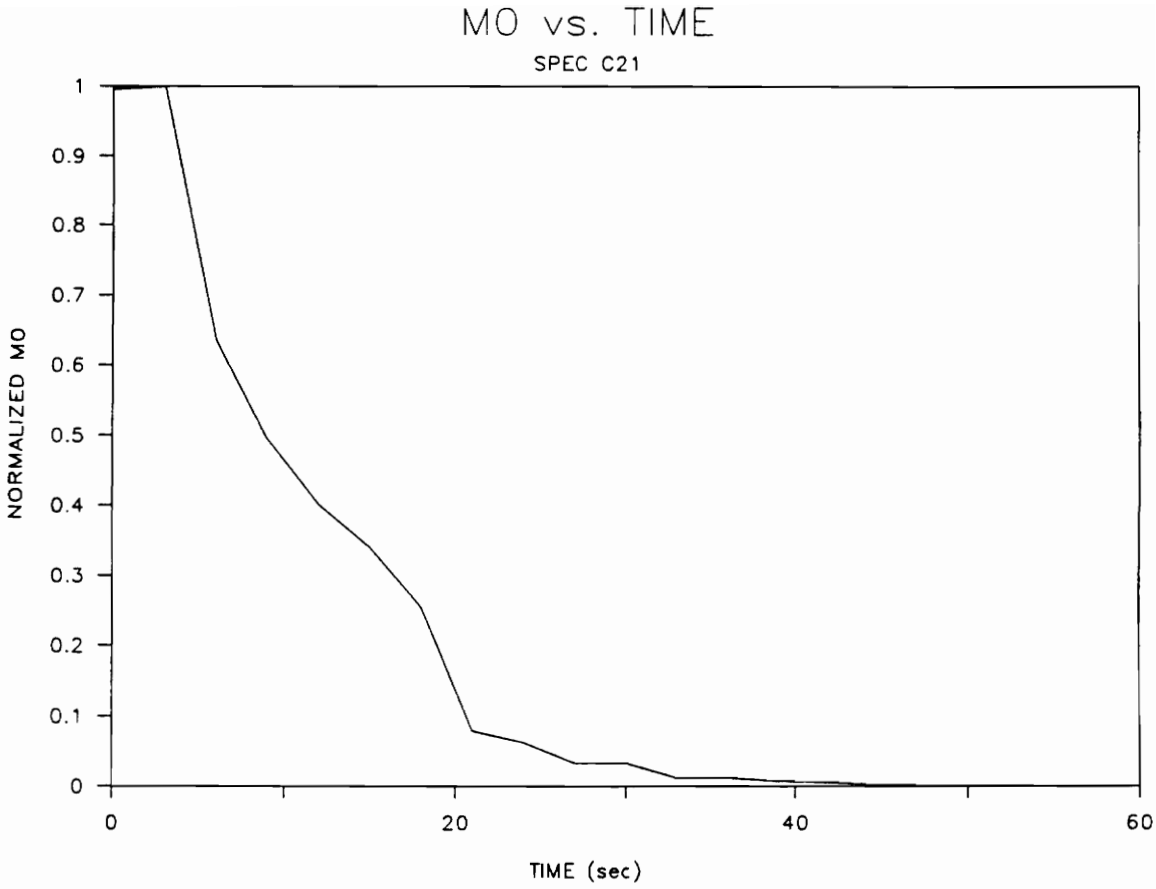

Figure 33. AU Parameter M0 vs. Time (Specimen 21C)

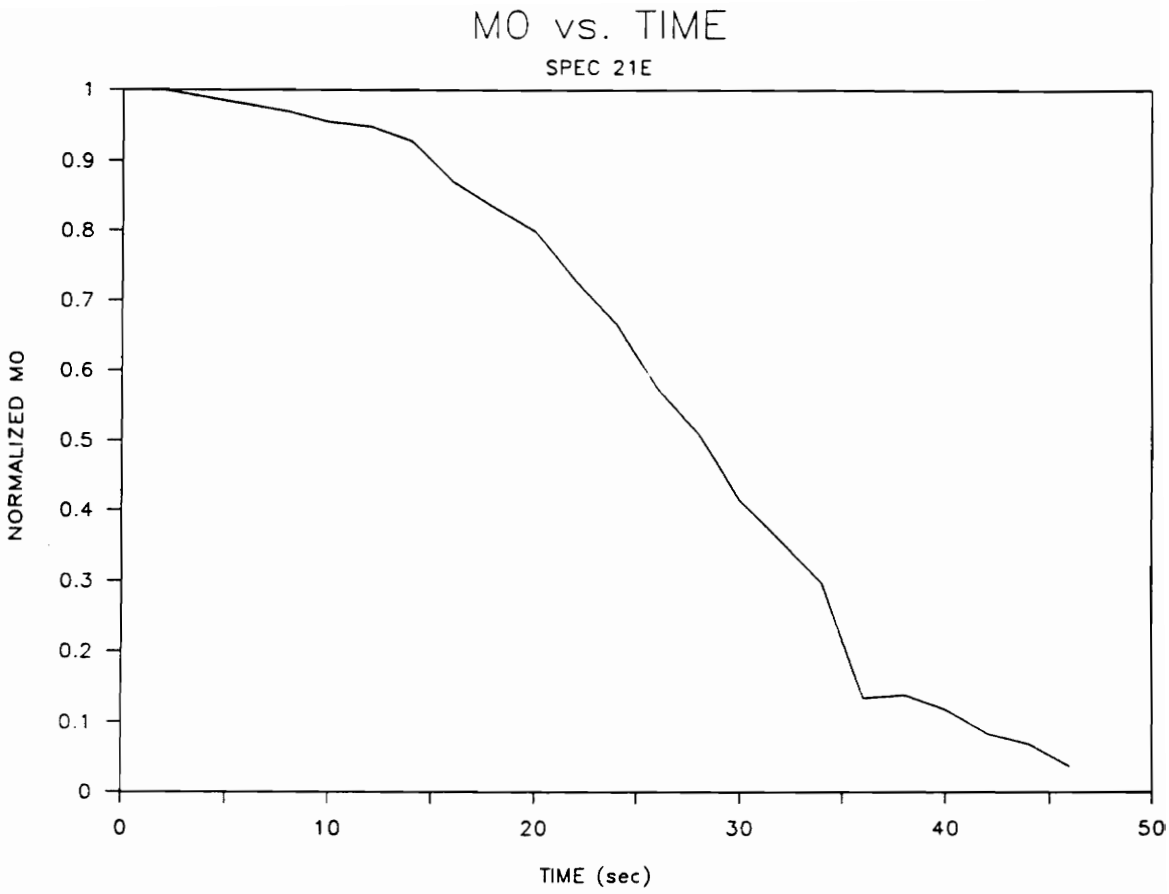

Figure 34. AU Parameter M0 vs. Time (Specimen 21E)

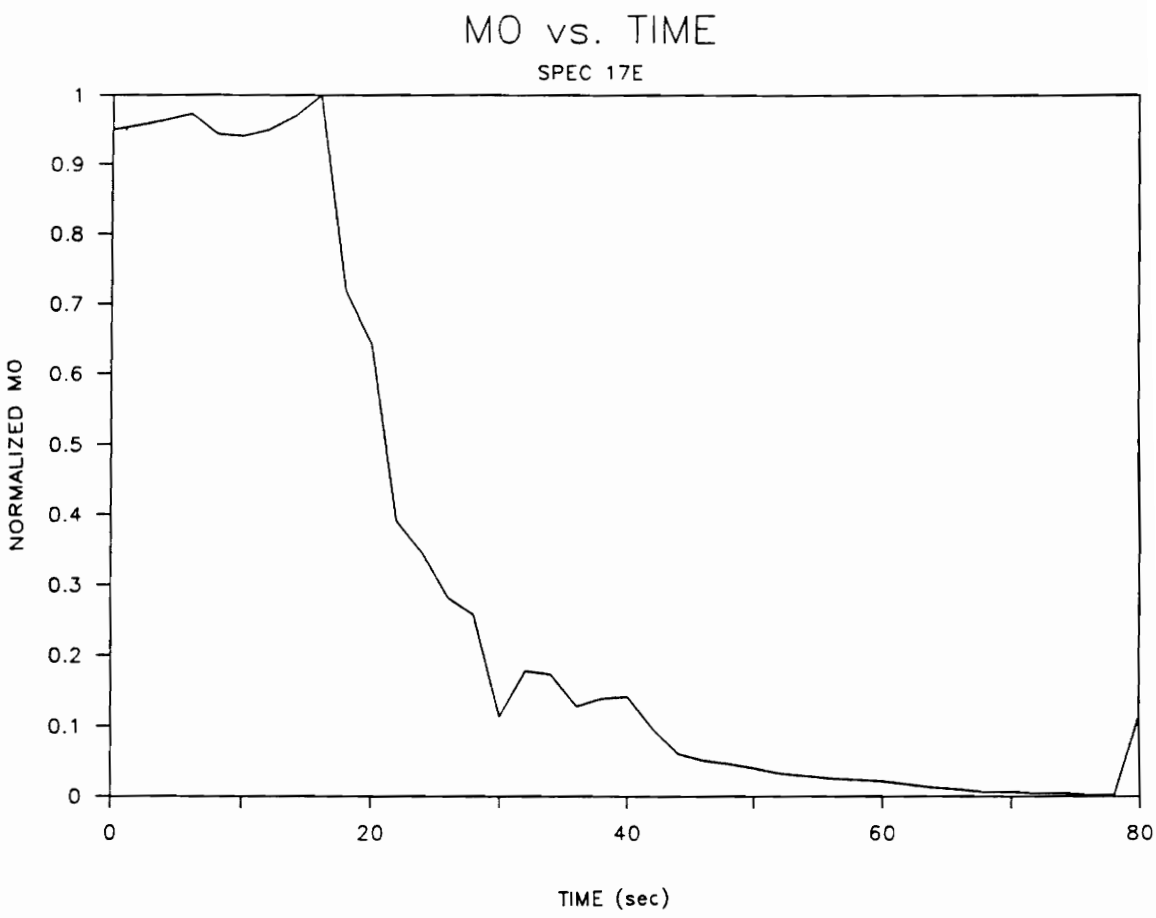

Figure 35. AU Parameter M0 vs. Time (Specimen 17E)

smoothed with the weighted averaging technique described for the scanned flexural specimens. The data for the parameter M0 are shown in Figure 36. As can be seen in this figure, the value of M0 remained approximately constant at each location after the 50 lbs loading compared to the M0 values for the specimen prior to loading. The measured values then exhibit the downward trend for each load level seen during the other tensile tests. The decrease in magnitude of M0 appears to be approximately equal in every region of the specimen, suggesting that the damage development is distributed evenly throughout the gage section. As shown in Figure 37, the parameter M1/M0 also follows the same trend; decreasing throughout the test. This shows that the centroid of the power spectrum is shifting to a lower frequency as damage develops within the specimen.

Both the two-ply and four-ply specimens failed in a similar mode. Practically all of the specimens failed in the gage region with one predominant crack causing specimen failure. The matrix material throughout the gage section of the failed specimens was thoroughly microcracked. It appeared that one of the many cracks in the matrix had propagated through the thickness of the specimen to cause ultimate failure. The failure surfaces were very fibrous, with up to 0.5 in. of SiC fibers protruding from both failure surfaces.

After a specimen had failed in tension, the material which was adjacent to the failure location still retained its load carrying capabilities. A piece of a two-ply specimen which had failed at a load of approximately 500 pounds (227 kg) was reloaded in tension; this piece then carried an ultimate load of approximately 550 pounds (250 kg) prior to failure.

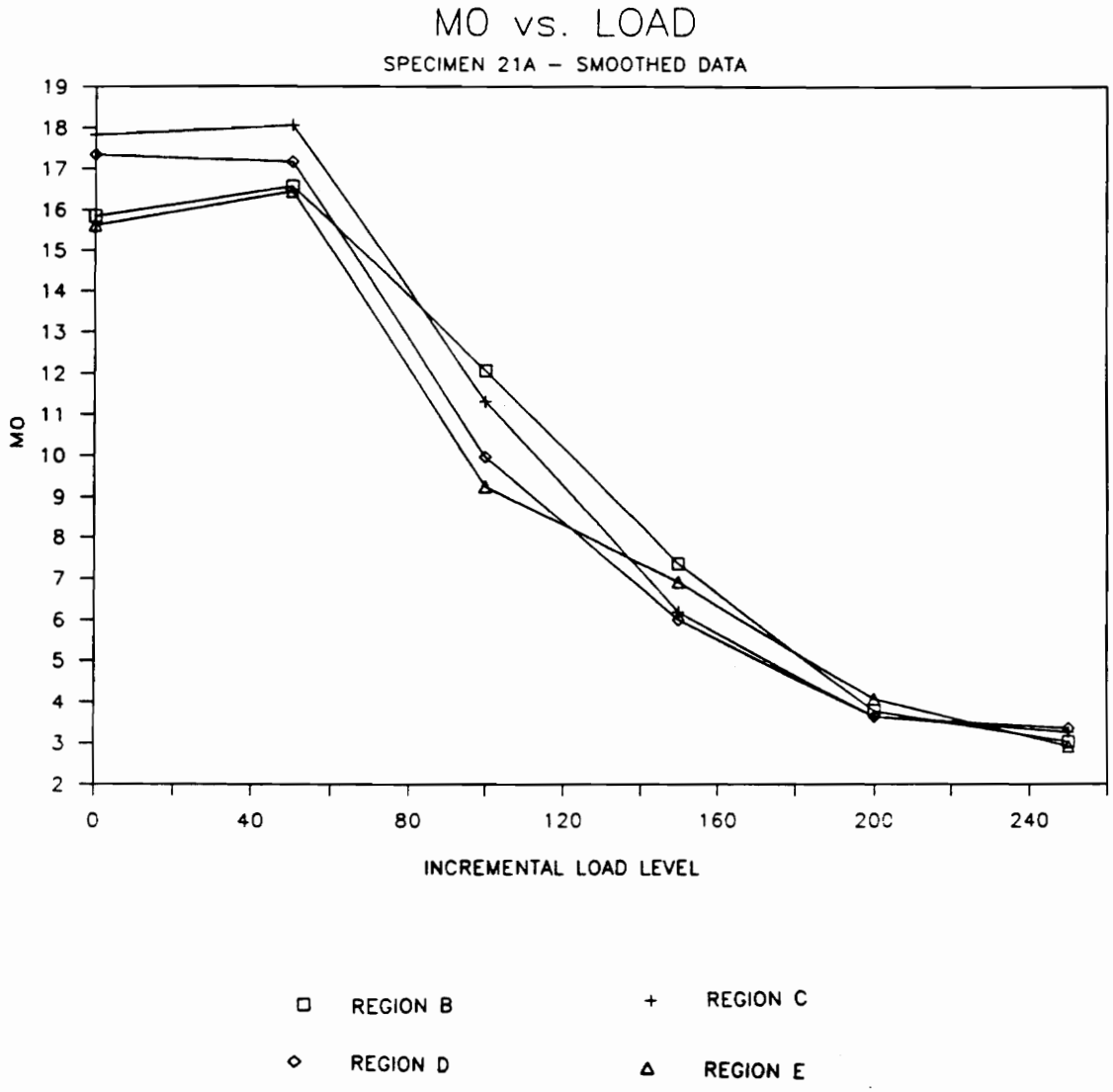

Figure 36. AU Parameter M0 vs. Load, Scanned Specimen (Specimen 21A)

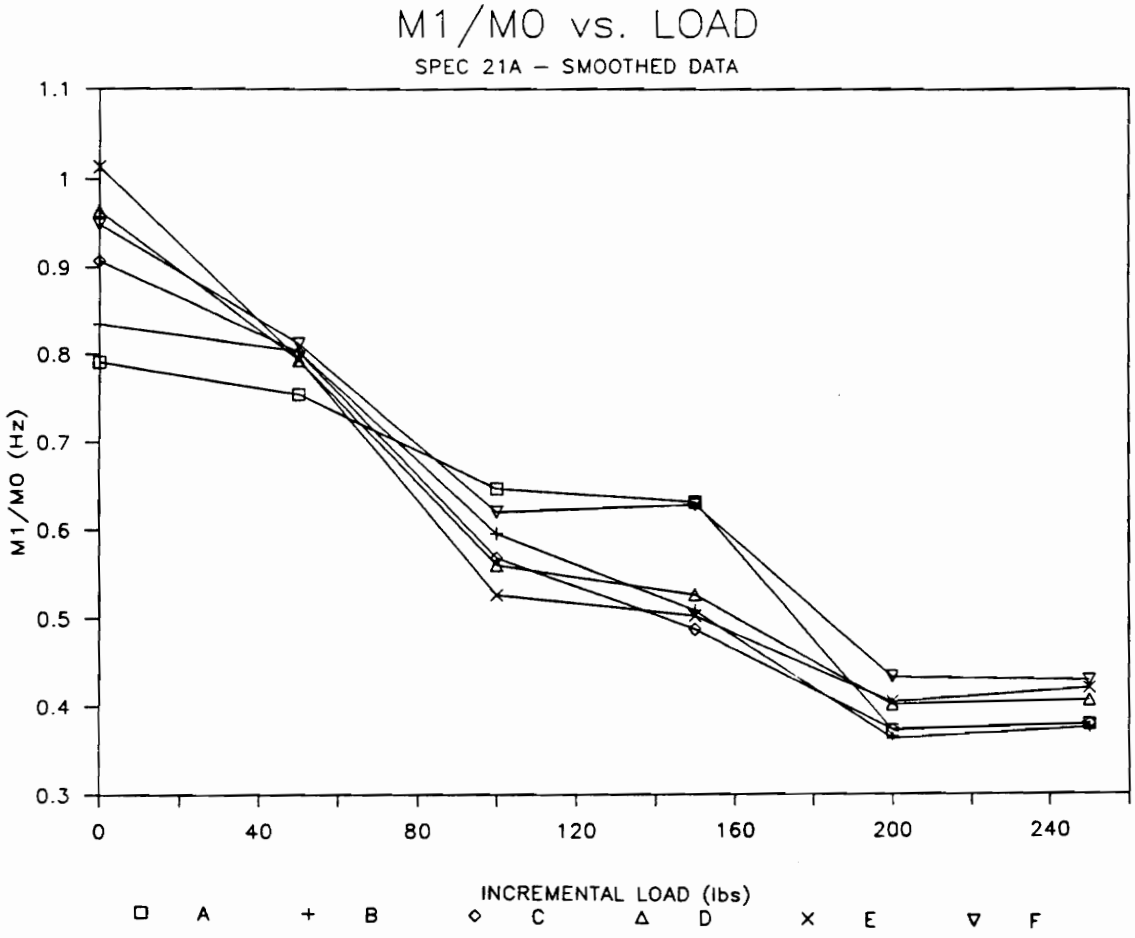

Figure 37. AU Parameter M1/M0 vs. Load, Scanned Specimen (Specimen 21A)

Considerable dispersion occurred in the ultimate load values of the two-ply specimens. The maximum load before failure ranged from 200 pounds (91 kg) to over 500 pounds (227 kg). However, when the data is presented in the form shown in Figure 38, it is clear that the maximum load at failure for the specimens cut from the same panel was very consistent. This indicates that the two-ply panels had considerable strength differences between them. The limited amount of data available for the four-ply panels indicated fairly consistent values of maximum load, with an average ultimate load of 750 pounds (341 kg). The two-ply specimens which were incrementally loaded did not appear to have a failure load which differed from the other specimens cut from the same panel.

SPECIMEN ULTIMATE LOAD, BY PANEL

PANEL NUMBER 17		
SPECIMEN		LOAD
D		218
E		206
F		220
	MEAN =	215
PANEL NUMBER 18		
SPECIMEN		
B		404
C		350
D		320
	MEAN =	358
PANEL NUMBER 20		
SPECIMEN		
D		455
E		422
	MEAN =	439
PANEL NUMBER 21		
SPECIMEN		
A		483
B		509
C		472
E		470
	MEAN =	484

Figure 38. Maximum Tensile Load at Failure for the Two-ply Specimens

5.0 CONCLUSIONS

Through the performance of numerous mechanical and nondestructive tests, the objectives of this project were fulfilled. A testing procedure was developed which allowed for determination of some of the material properties of a ceramic matrix composite material, the observation of the changes in the performance of this material with the formation of damage, and the evaluation of the applicability of several NDT techniques to this class of materials.

The application of both flexural and tensile loading configurations allowed the comparison of the mechanical behavior of the material under different loading configurations and different damage states. In both testing configurations a basic pattern of material behavior was observed through the course of the loading cycle which was divided in three regions: an initial region (Region I), followed by a transition zone, and finally Region II which lasted until failure of the specimen.

While loaded into the initial region, the material behaved in a linear, elastic manner; both the measured load and strain data appeared to be linear in this region. There was almost no measured acoustic emission activity during this region and no surface cracks were revealed through magnified observation or by the application of liquid penetrants. Upon application of a load to a specimen which had previously been loaded to a load level within Region I, the specimen exhibited the same modulus. Region I behavior ended when cracks formed in the matrix material of the specimen.

Within the transition zone which followed Region I, the measured material parameters were no longer linear; the measured load oscillated in a "saw tooth" manner, the strain data began to act in an erratic manner and the apparent stiffness of the samples dropped. Throughout the transition zone, the monitored acoustic emission was very active, liquid penetrant inspections revealed surface cracks, and dramatic drops in the measured acousto-ultrasonic parameters occurred.

In the final region of behavior, Region II, the load typically increased smoothly until specimen failure. Although still active in this region, there were considerably fewer acoustic emissions. X-ray radiographs and optical techniques showed matrix cracks distributed throughout the portion of the material loaded in tension. Upon reapplication of a load to a sample which had damage resulting from previous loading, the specimen exhibited a lower apparent modulus, but no loss in strength was observed. This material, unlike monolithic ceramics, can withstand some damage development without catastrophic failure. Also, when reloaded, this material clearly exhibited the Kaiser effect for acoustic emission activity.

The mechanical testing allowed the approximation of several properties, including flexural modulus and maximum load at failure. Tensile testing revealed differences in properties between the various composite panels which were not observed during flexural testing. Further mechanical testing should be performed to verify the measured material properties and general mechanical behavior of the material found during this project.

The application of several nondestructive testing techniques to this material system were evaluated through the course of this investigation. Contact X-ray radiographs which

were produced of the untested specimens revealed the fiber orientation and void content. This technique, however, even with the application of penetrant enhancement, did not reveal matrix cracks until well into Region II. Even with magnification, optical methods did not reveal the presence of the tightly closed matrix cracks in the unloaded specimens which had entered the transition region of the loading cycle. Inspection with liquid penetrant highlighted the surface cracks, however, this technique only reveals information about damage open to the surface of the specimens.

The feasibility of applying the acousto-ultrasonic inspection method to this class of materials was also investigated. This technique was shown to be highly sensitive to the damage which developed within the material in both loading configurations. The measured AU parameters showed clear changes prior to the detection of damage with the other NDT techniques which were applied in this study.

5.1 FUTURE WORK

Further development of this material is required to improve the quality of the composite panels produced and, thereby, improve the mechanical performance of the material. Because the intended applications for this material are in high temperatures and harsh environments, testing should be performed under these conditions to verify the capabilities of the material. As the development process for the material continues, testing of this material system with different fiber architectures and different fiber volumes should be performed to better understand the effect of these parameters on the mechanical performance.

A clear understanding of these parameters would allow for tailoring of the material for specific applications and loading requirements.

Improvements in the mechanical testing methods applied in this experiment should be made in order to assure more accurate and consistent data measurements. Better measurements would be necessary for a clear understanding of the behavior of this material and more accurate design parameters. Implementation of improved methods of measuring surface strains after micro-cracking and specimen deflections should be made. An improved flexure fixture with adjustable span-to-depth ratio would allow for flexibility in the size of the specimens which are tested. Improvements in the method of gripping the specimen in the tensile loading configuration would reduce damage developed in the gripped region of the specimens and reduce the stress concentrations at each of the gripped regions.

Because the AU technique has been shown to be useful in monitoring damage development within this material, further development of the method should be implemented. Along with the development of high temperature mechanical testing methods, the technology for application of AU in high temperature environments should be developed. Laser generation and interferometric reception of the AU signals may allow for noncontact application of the technique in harsh environments. Wave guides made of a material which can endure exposure to high temperatures may also be used to transfer the AU signals to conventional piezoelectric transducers located away from the heated testing region. Also, correlations in the changes in the measured AU parameters with the results of other NDT techniques such as SAM, CT scans, and micro-focus radiography may result in a better understanding of the changes in the material which affect the AU parameters. A more

complete understanding of the measurement technique and the effects of material damage states on the measured parameters would allow for the application of AU to ceramic matrix composites which are in-service. Further testing of the material may also result in an AU measurement technique which could be accurately correlated with the remaining load carrying capability of the material.

REFERENCES

1. Govada, A. K., et al., "A Study of the Stress Wave Factor Technique for the Characterizatiion of Composite Materials," NASA Contractor Report 174870, February 1985.

2. Henneke, E. G., et al., "A Study of the Stress Wave Factor Technique for the Characterization of Composite Materials," NASA Contractor Report 3670, February 1983.

3. Duke, J. C., et al., "Ultrasonic Stress Wave Characterization of Composite Materials," NASA Contractor Report 3976, May 1986.

4. Sarrafzadeh-Khoee, A., et al., "A Study of the Stress Wave Factor Technique for Nondestructive Evaluation of Composite Materials," NASA Report 4002, July 1986.

5. Kautz, H. E., "Acousto-Ultrasonic Verification of the Strength of Filament Wound Composite Material," NASA Technical Memorandum 88827, July 1986.

6. Duke, J. C., Jr., et al., "A Study of the Stress Wave Factor Technique for Evaluation of Composite Materials," NASA Contractor Report 4195, January 1989.

7. Duke, J. C., Jr., *Acousto-Ultrasonics, Theory and Application.* Plenum Press, New York, 1988.

8. Mecholsky, J. J., "Evaluation of Mechanical Property Testing Methods for Ceramic

Matrix Composites," Ceramic Bulletin, Vol. 65, No. 2, Feb. 1986, pp. 315-322.

9. Hyde, A. R., "Ceramic Matrix Composites," Materials & Design, Vol. XI, No. 1, 1990, pp. 30-36.

10. Mecholsky, J. J., Jr., "Engineering Research Needs of Advanced Ceramics and Ceramic-Matrix Composites," Ceramic Bulletin, Vol. 68, No.2, 1989, pp. 367-375.

11. Krynicki, J. W., "Design and Behavior of Ceramic Matrix Composite Subjected to Mechanical and Thermal Loading," Master of Science Essay, Johns Hopkins University, October 1989.

12. Rice, R. W., "Mechanisms of Toughening in Ceramic Matrix Composites," Ceramic Engineering and Science Proceedings, Vol. 2, July/August 1981, pp. 661-701.

13. Sambell, R. A. J., et al., "Carbon Fibre Composites with Ceramic and Glass Matrices - Part 1," Journal of Materials Science, Vol. 7, 1972, pp. 663-675.

14. Sambell, R. A. J., et al., "Carbon Fibre Composites with Ceramic and Glass Matrices - Part 2," Journal of Materials Science, Vol. 7, 1972, pp. 676-681.

15. Levitt, S. R., "High-Strength Graphite Fibre/Lithium Aluminosilicate Composites," Journal of Materials Science, Vol. 8, 1973, pp. 793-806.

16. Prewo, K. M., and Bacon, J. F., "Glass Martix Composites - I - Graphite Fiber Reinforced Glass," ICCM-II, Toranto Canada, 1978.

17. Prewo, K. M., and Brennan, J. J., "High-Strength Silicon Carbide Fibre-Reinforced Glass-Matrix Composites," Journal of Materials Science, Vol. 15, 1980, pp. 463-468.

18. Brennan, J. J., and Prewo, K. M., "Silicon Carbide Fibre Reinforced Glass-Ceramic Matrix Composites Exhibiting High Strength and Toughness," Journal of Materials Science, Vol. 17, 1982, pp. 2371-2383.

19. Prewo, K. M., "Tension and Flexural Strength of Silicon Carbide Fibre-Reinforced Glass Ceramics," Journal of Materials Science, Vol. 21, 1986, pp. 3590-3600.

20. Prewo, K. M., et al., "Fiber Reinforced Glasses and Glass-Ceramics for High Performance Applications," Ceramic Bulletin, Vol. 65, No. 2, 1986, pp. 305-313.

21. Prewo, K. M., "Carbon Fibre Reinforced Glass Matrix Composite Tension and Flexure Properties," Journal of Materials Science, Vol. 23, 1988, pp. 2745-2752.

22. Marshall, D. B., and Evans, A. G., "Failure Mechanisms in Ceramic-Fiber/Ceramic-Matrix Composites," Journal of the American Ceramic Society, Vol. 68, No. 5, May 1985, pp. 225-231.

23. Kupperman, D. S., and Karplus, H., "Ultrasonic Wave Propagation Characteristics of

Green Ceramics," Ceramic Bulletin, Vol. 63, No. 12, 1984.

24. Berger, H. and Kupperman, D. S., "Microradiography to Charaterize Structural Ceramics," Materials Evaluation, Vol. 43, Feb. 1985.

25. Hecht, A., et al., "Computer-aided Ultrasonic Testing of Non-oxide Ceramics," NDT International, Vol. 19, No. 6, Dec. 1986, pp. 401-406.

26. Klima, S. J., "NDE of Advanced Ceramics," Materials Evaluation, Vol. 44, No. 5, April 1986, pp. 571-576.

27. Stinton, D. P., et al., "Synthesis of Fiber-Reinforced SiC Composites by Chemical Vapor Infiltration," Ceramic Bulletin, Vol. 65, No. 2, 1986, pp. 347-350.

28. Lamicq, P. J., et al., "SiC/SiC Composite Ceramics," American Ceramic Society Bulletin, Vol. 65, No. 2, 1986, pp. 336-338.

29. Caputo, A. J., et al., "Fiber-Reinforced SiC Composites with Improved Mechanical Properties," American Ceramic Society Bulliten, Vol. 66, No. 2, 1987, pp. 368-372.

30. Personal discussion with D. P. Stinton, at VPI&SU, 1988.

31. Cornie, J. A., et al., "Processing of Metal and Ceramic Matrix Composites," Ceramic Bulletin, Vol. 65, No. 2, 1986, pp. 293-304.

32. Friant, C. L. et al., "Ultrasonic Characterization of SiC Fiber-Reinforced Glass Matrix Composite," *Nondestructive Testing of High-Performance Ceramics*, American Ceramic Society, 1987, pp. 380-387.

33. Walter, J. B. et al., "Ultrasonic Characterization of Porosity in Advanced SiC Ceramic Composites," *Nondestructive Testing of High-Performance Ceramics*, American Ceramic Society, 1987, pp. 156-162.

34. London, B., et al., "High-Resolution X-Ray Computed Tomography of Composite Materials," Materials Evaluation, Vol. 48, No. 5, May 1990. pp. 604-608.

35. National Materials Advisory Board, "Automated Nondestructive Characterization and Evaluation in Metal and Ceramic Powder Production," U.S. Army Materials Technology Laboratory, Watertown, MA., September 1986.

36. Johnson, D. R., et. al., "Needs Assessment for Nondestructive Testing and Materials Characterization for Improved Reliability in Structural Ceramics for Heat Engines," ORNL report, ORNL/TM-10354, 1987.

37. Slavin, M. J., and Gruber, J. J., "Ultrasonic Characterization of Ceramics," ASME Publication No. 87-GT-1.

38. Kiernan, M. T., and Duke, J. C., Jr., "Acousto-Ultrasonics as a Monitor of Material

Anisotropy," Materials Evaluation, Vol. 46, No. 8, 1988, pp. 1105-1113.

39. In conjunction with Dunyak, T. J., et al., "An Examination of Selected NDE Methods for Ceramic Composite Tubes," VPI & SU CCMS Report No. 89-18, 1989, pp. 16-17.

40. Mah, T., et al., "Recent Developments in Fiber-Reinforced High Temperature Ceramic Composites," Ceramic Bulletin, Vol. 66, No. 2, 1987, pp. 304-317.

41. Mah, T., et al., "Room-Temperature Mechanical Behavior of Fiber-Reinforced Ceramic - Matrix Composites," Journal of the American Ceramic Society, Vol. 68, No. 1, 1985, pp. C27-C30.

42. Briggs. A., and Bowen D. H., "Carbon Fibre Composites with Ceramic and Glass Matrices," Journal of Material Science, Vol. 7, 1972.

43. Baaklini, G. Y., "NDE Reliability and Process Control for Structural Ceramics," ASME Publication No. 87-GT-8.

44. Davidge, R. W., "Fibre-reinforced ceramics," Composites, Vol. 18, No. 2, Apr. 1987, pp. 93-98.

45. Zweben, C., et al., "Test Methods for Fiber Tensile Strength, Composite Flexural Modulus, and Properties of Fabric-Reinforced Laminates," *Composite Materials: Testing and*

Design (Fifth Conference). ASTM STP 674, S. W. Tsai, Ed., American Society for Testing and Materials, 1979, pp. 228-262.

46. Whitney, J. M., et al., *Experimental Mechanics of Fiber Reinforced Composite Materials.* The Society for Experimental Mechanics, Brookfield Center, CT., 1984, pp. 165-171.

47. ASTM D790, "Standard Test Methods for Flexural Properties of Unreinforced and Reinforced Plastics and Electrical Insulating Materials", 1984.

48. ASTM C158, "Standard Methods of Flexural Testing Of Glass (Determination) of Modulus of Rupture)" (Method B), 1984.

49. Boyer, H. E., Ed., et al., Metals Handbook, *Nondestructive Inspection and Quality Control.American Society for Metals*, Metals Park, Ohio, 1976.

50. Halmshaw, R., *Non - destructive Testing.* Edward Arnold, Great Britain, 1987.

51. Bray, D. E., and Stanley, R. K., *Nondestructive Evaluation - A Tool for Design, Manufacturing, and Service.* McGraw-Hill, Inc., New York, 1989.

52. *Nondestructive Testing, Liquid Penetrant, Classroom Training Handbook,* General Dynamics Training Handbook, Convair Division, 1977.

53. Bartlett, S. W., "Nondestructive Evaluation of Complex Geometry Advanced

Material Components," M.S. Thesis, College of Engineering, Virginia Polytechnic Institute and State University, Blacksburg, VA, March 1989.

54. Kiernan, M. T., "An Acousto-Ultrasonic System for the Evaluation of Composite Materials," M.S. Thesis, College of Engineering, Virginia Polytechnic Institute and State University, Blacksburg, VA, September 1986.

55. Horne, M. R., variation of the software written for "Scanning Measurement Testbed for Advanced Nondestructive Evaluation," M.S. Thesis, College of Engineering, Virginia Polytechnic Institute and State University, Blacksburg, VA, 1990.

Appendix A: Analysis of Acousto-Ultrasonic Signals

Processing of continuous waveforms:

Given a function, x(g), defined between g = 0 and g = T, the area under the curve can be calculated by

$$\text{Area} = \int_0^\infty x(g)dg \ .$$

E[x] is defined as the expected value of x(g), and can be expressed as

$$E[x] = \frac{1}{T} \int_0^\infty x(g)\ dg = \frac{\text{Area}}{T}$$

and the expected value of the function squared as

$$E[x^2] = \frac{1}{T} \int_0^\infty x(g)^2\ dg \ .$$

The symbol E[f(τ)] can also be used to represent the ensemble average. Given an infinitely long random function, the function may be sampled over several equal length segments, each being taken as an independent random function, $f_i(\tau)$. An average of these i functions at a given point τ (where τ is defined from zero to the segment length) may then be calculated. This function, E[f(τ)], is called the ensemble average of the independent functions. In Acousto-Ultrasonics (AU), generally the stored data is an average of between 4

and 128 waveforms, averaged together to give one data set. Although this data set is an ensemble average of many waveforms, it is generally only refered to as "a waveform".

An ensemble of data sets from the phenomenon of interest can be considered to be stationary if the mean, mean squared value, autocorrelation value (defined below), and several other parameters calculated across the data sets are constant, i.e. independent of the location τ at which they are calculated [1]. AU data is, in general, "forced" to be stationary, that is, each experiment is completed under very repeatable circumstances, therefore, the data sets can be considered to be stationary. Also, the data is not treated as being a transient waveform, rather it is considered to be a stationary (repeating) waveform of a random nature.

The autocorrelation function of a function x(t) is defined as the average value of the product of x(t) and x(t+τ). If the process is stationary, the value of the autocorrelation function, E[x(t)x(t+τ)], is independent of t and dependent upon τ. Therefore, if R_X is defined as the autocorrelation function, it can be written as:

$$R_X(\tau) = E[x(t)x(t+\tau)] .$$

$R_X(\tau)$ is an even function, therefore,

$$R_X(\tau) = R_X(-\tau).$$

If a function x(t) is periodic, with a period of T, x(t) can be expressed as an infinite

trigonometric series:

$$x(t)=a_0 + 2\left(a_1\cos\frac{2\pi t}{T} + a_2\cos\frac{4\pi t}{T} + \cdots\right)$$

$$+ 2\left(b_1\sin\frac{2\pi t}{T} + b_2\sin\frac{4\pi t}{T} + \cdots\right)$$

where,

$$a_0 = \frac{1}{T}\int_{-\frac{T}{2}}^{\frac{T}{2}} x(t)\,dt,$$

$$\underset{k\geq 1}{a_k} = \frac{1}{T}\int_{-\frac{T}{2}}^{\frac{T}{2}} x(t)\cos\omega_k\,dt,$$

$$\underset{k\geq 1}{b_k} = \frac{1}{T}\int_{-\frac{T}{2}}^{\frac{T}{2}} x(t)\sin\omega_k\,dt,$$

and

$$\omega_k = \frac{2\pi kt}{T}\,.$$

The frequency difference between adjacent coeffecient values is

$$\Delta\omega = \frac{2\pi k}{T} .$$

As shown in Newland [2], as $T \rightarrow \infty$, $\Delta\omega \rightarrow 0$, and the summation in the trigonometric series for x(t) can be replaced by an integral. The equation for the series becomes:

$$x(t) = 2\int_{-\infty}^{\infty} A(\omega) \cos \omega t \, d\omega + 2\int_{-\infty}^{\infty} B(\omega) \sin \omega t \, d\omega .$$

where,

$$A(\omega) = \frac{1}{2\pi}\int_{-\infty}^{\infty} x(t) \cos \omega t \, dt,$$

and

$$B(\omega) = \frac{1}{2\pi}\int_{-\infty}^{\infty} x(t) \sin \omega t \, dt .$$

By incorporating Euler's formula, the Fourier transform of a function x(t) can now be written as:

$$X(\omega) = A(\omega) - i \, B(\omega) = \frac{1}{2\pi}\int_{-\infty}^{\infty} x(t) \, e^{-i\omega t} \, dt$$

and the inverse Fourier transform as

$$x(t) = \int_{-\infty}^{\infty} X(\omega) \, e^{i\omega t} d\omega$$

Similiar forms of these transforms, as presented by Bracewell [3], are

$$\mathfrak{X}(s) = \int_{-\infty}^{\infty} x(t)\, e^{-i2\pi st}\, dt$$

$$x(t) = 2\pi \int_{-\infty}^{\infty} \mathfrak{X}(s)\, e^{i2\pi st} ds$$

The transforms are functionally equivalent when we set

$$s = 2\pi\omega\ .$$

Note that in the Fourier equations presented above, the functions are defined from $-\infty$ to $+\infty$.

An important proof in Fourier transforms is Parseval's theorem. This can be written as [2]:

$$\tfrac{1}{2\pi} \int_{-\infty}^{+\infty} x^2(t)\, dt = \int_{-\infty}^{+\infty} |X(\omega)|^2\, d\omega.$$

Following the argument proposed by Newland [2], if x(t) is a random signal which truly is defined from $-\infty$ to ∞, then the area under its plot is infinite. Also, a truly random

process is not periodic, therefore, it does not lend itself to Fourier analysis. To resolve this the autocorrelation function of x(t) can be analyzed instead of the original function. The autocorrelation function $R_X(\tau)$ satisfies the above requirements, being periodic in τ.

Newland [2] calls $S_X(\omega)$ the "Spectral Density of x(t)", and defines it as

$$S_X(\omega) = \frac{1}{2\pi} \int_{-\infty}^{\infty} R_X(\tau)\, e^{-i\omega\tau} d\tau$$

where $S_X(\omega)$ has units of $\frac{(\text{x units})^2}{(\text{unit of angular frequency})}$.

The autocorrelation function can be calculated from the Spectral Density function by taking the inverse Fourier transform, i.e.,

$$R_X(\tau) = \int_{-\infty}^{\infty} S_X(\omega)\, e^{i\omega\tau} d\tau \ .$$

Of special interest is when τ=0 in the autocorrelation function;

$$R_X(0) = \int_{-\infty}^{\infty} S_X(\omega)\, d\omega = E[(x(t))^2]$$

therefore, the area under the Spectral Density function is equal to the mean square of the function x(t).

Because negative frequencies have been introduced for strictly mathematical reasons, a way is needed to account for using only positive frequencies in the calculations. Because $S_X(\omega)$ is defined from $-\infty$ to $+\infty$ it is called the two sided spectral density function; $W_X(\omega)$ can be defined as the one sided spectral density function defined from zero to $+\infty$. For $S_X(\omega)$ and $W_X(\omega)$ to be functionally equivalent, the area under both spectral density functions should be equal (i.e., $E[\ (x(t))^2\ ]$), therefore,

$$W_X(\omega) = S_X(\omega) + S_X(-\omega)$$

which, because $S_X(\omega)$ is even (as a result of R_X being even), reduces to

$$W_X(\omega) = 2\ S_X(\omega)\ .$$

Because frequency is most commonly expressed in units of "Hertz" (f) in AU analysis, rather than angular frequency (ω), a correction must be made. Frequency in hertz can be related to angular frequency by $f=\frac{\omega}{2\pi}$, therefore, by equating the areas under the one- and two- sided spectral density functions, the following relationships are developed:

$$W_X(f) = W_X(2\pi\omega) = 2\pi\ W_X(\omega) = 4\pi\ S_X(\omega)\ .$$

Discrete Fourier Transforms:

Because the waveforms for AU are digitally captured prior to analysis, the Spectral Density functions defined above must also be defined for discretely sampled functions. For a function x(t) with a period T, which is sampled N times at regular intervals $\Delta = T/N$, the Discrete Fourier Transform (DFT) is given by [2]:

$$X_k = \frac{1}{T} \sum_{r=0}^{N-1} x_r \, e^{-i(2\pi kr/N)} \quad .$$

The transform X_k can be plotted at discrete frequency intervals

$$\omega_k = \frac{2\pi k}{N\Delta}.$$

The Inverse Discrete Fourier Transform is defined as [2]:

$$x_k = \sum_{k=0}^{N-1} X_k \, e^{i(2\pi kr/N)}.$$

It should be noted that the values of x can be calculated exactly from the frequency spectrum, X, only at the times at which they were discretely defined. At any other time, the values of x can be only estimated.

The discrete formulation of Parseval's Theorem is [2]:

$$\frac{1}{N} \sum_{r=0}^{N-1} {x_r}^2 = \sum_{k=0}^{N-1} |X_k|^2 \, .$$

Corrections to the software which was previously used for Acousto - Ultrasonic analysis assures that this mathematical proof holds true for the waveforms analyzed in this study. A listing of the software used for Acousto-Ultrasonic analysis in this study is given in Appendix B.

Several additional items should be noted about Fourier analysis. First, if for the given sample set x_r, the maximum frequency component of interest is ω_0, than to avoid aliasing in the transform, the sampling rate, f_0, must satisfy the following:

$$2\omega_0 < f_0.$$

This sampling frequency is defined as the Nyquist frequency. Secondly, the AU data is zero averaged to avoid a bias caused by this DC component; this component may produce a very low frequency peak in the power spectrum, thereby greatly affecting the AU parameters.

Because the Power Spectrum is defined as the transform of the autocorrelation function, it can be written as

$$S_k = \frac{1}{N} \sum_{r=0}^{N-1} R_r \, e^{-i(2\pi kr/N)}$$

where R_r can be estimated by

$$R_r = \frac{1}{N} \sum_{s=0}^{N-1} x_s \, y_{s+r}.$$

Using the formulation of Blackman and Tukey [4], the Power Spectral Density, P(f), can be calculated from the following:

$$P(f) = \lim_{T \to \infty} \frac{1}{T} \mid X(f) \mid^2$$

where X(f) is the transform of x(t) defined over the period T and zero elsewhere.

In terms of the previously used notation, the Power Spectral Density function can be calculated through the following:

$$S_{xx_k} = \lim_{T \to \infty} [\frac{1}{T} \; X_k^* \, X_k]$$

where X_k^* is the complex conjugate of X_k. For a real function, X_k^* and X_k are equal and the one-sided Power Spectral Density function can be written as,

$$W_{xx_k} = \lim_{T \to \infty} \frac{2}{T} [\mid X_k \mid^2] .$$

This formulation for the power spectral density is equivalent to the continuous formulation presented above, and is commonly called the Wiener-Khinchin relation for the mathematicians who originally proved the equivalence.

The Rice Electrical Circuit Analogy

If the electrical circuit analogy similiar to that used by Rice [5] is employed, the AU waveform can be treated as a Voltage measured across an imaginary, pure resistance of one ohm. The average power dissapated in this resistance, over a long time duration, is the mean square of the voltage, which was shown above to be equivalent to the area under the Power Spectral Density function. Because power (watts) is defined as the rate of energy transfer, multiplying by the length of the time interval (T) would result in a measure of the total energy dissapated by the waveform. A measure of energy per unit time (power), rather than that of total energy, is useful because the power found for records of unequal time lengths can then be compared.

Acousto-Ultrasonic Parameters:

The analysis parameters used in recent Acousto-Ultrasonic investigations (including this one), were proposed by Talreja [6]. He suggested that any distribution function could be described by three parameters: location, size, and shape. He then proposed the following formula with which to calculate these parameters:

$$M_r = \int_{-\infty}^{+\infty} S(f)\, f^r\, df,$$

which is equivalent to

$$M_r = \int_0^{+\infty} W(f)\, f^r\, df$$

for the two-sided Power Spectral Density function.

The parameter M_0 is the zeroth moment of, or the area under, the Power Spectral Density curve. M_0 is considered to be the size parameter. The centroid of the Power Spectrum, or location parameter, can be calculated by:

$$f_c = \frac{M_1}{M_0} .$$

Using the above integral equation, Talreja then defined shape parameters which can be used to describe the function. These parameters can be found from:

$$S_{r,k} = \frac{M_r}{M_{r-k}\, f_c{}^k} \qquad k=1,2,3... \qquad r=2,3,4... \qquad r \geq k$$

Several other statistical parameters, which have been defined by Rice [5], are also used as shape parameters. These include the expected number of zero crossing per unit time:

$$2 \left(\frac{M_2}{M_0} \right)^{1/2}$$

and the expected number of maxima per unit time:

$$\left(\frac{M_4}{M_0}\right)^{1/2}.$$

The AU parameters of most interest in this study are M_0 and f_c.

REFERENCES

1 Bendat, J. S., and Piersol, A. G., *Engineering Applications of Correlation and Spectral Analysis.* John Wiley and Sons, New York, 1980.

2 Newland, D. E., *Random Vibrations and Spectral Analysis.* Longman Inc., New York, 1983.

3 Bracewell, R. N., *The Fourier Transform and Its Applications.* 2 ed., McGraw-Hill, New York, 1986.

4 Blackman, R. B., and Tukey, J. W., *The Measurement of Power Spectra from the Point of View of Communications Engineering.* Dover, New York, 1958.

5 Rice, S. O., "Mathematical Analysis of Random Noise," Bell Systems Tech. Journal, Vol 23, 1944; reprinted in, *Selected Papers on Noise and Stochatic Processes.* Dover, New York, 1964.

6 Talreja, R., "On Fatigue Life Under Stationary Gaussian Random Loads," Engineering Fracture Mechanics, Vol 5, 1973, pp. 993-1007.

APPENDIX B

Listed below is the computer program used for acousto-ultrasonic signal analysis. This FORTRAN program is another step in the evolution of the signal analysis programs for acousto-ultrasonic studies which have been written by M. Kiernan*, A.Madhav*, and S.Bartlett*. This program is a modification of a program written by S. Bartlett [50]. The changes which were made to the program through the course of this project include several modifications, corrections, error checks, and analysis options.

```
      PROGRAM POWERAU
C
C     VIRGINIA POLYTECHNIC INSTITUTE AND STATE UNIVERSITY
C     DEPARTMENT OF ENGINEERING SCIENCE AND MECHANICS
C     BLACKSBURG, VIRGINIA 24061
C
C     THIS PROGRAM WAS ADAPTED FROM ONE WRITTEN BY ARUN MADHAV
C     FOR HISMASTER'S OF SCIENCE IN ENGINEERING MECHANICS (SEPT 1987) ,
C     AND IS A FORTRAN VERSION OF THE PROGRAM WRITTEN BY MICHAEL
C      KIERNAN FOR HIS MASTER'S THESIS IN ENGINEERING MECHANICS. (SEPT
C      86) MAJOR PORTIONS WERE REWRITTEN BY SCOTT BARTLETT FOR
C     USE IN HIS RESEARCH PROJECT, THESIS WORK, AND VARIOUS NON -
C      DESTRUCTIVE EVALUATION CLASSES.
C     IT WAS AGAIN MODIFIED BY PAUL GROSSKOPF FOR HIS THESIS WORK
C     AND IN SUPPORT OF THE ESM 4154 LAB (DIFFERENT VERSION). SEVERAL
C     OF SCOTT'S/MIKE'S/ARUN'S MISTAKES WERE CORRECTED. THE
C      PROGRAM WAS  ALSO SIGNIFICANTLY BETTER DOCUMENTED.
C
C     MODIFIED JAN 06, 1988 TO USE INPLACE FHT (REDUCE MEMORY SPACE)
C     MODIFIED JAN 31, 1988 TO USE FAST TRIG PRECALCULATION IN FHT
C     MODIFIED FEB 03, 1988 TO INCLUDE STATISTICAL EVALUATION OF TWO
C                           SIGNALS - CORRECTING PREVIOUS PROGRAMS
C     MODIFIED FEB 19, 1988 TO REINTRODUCE SCREEN GRAPHICS
```

* Past Graduate Students at VPI & SU, Department of Engineering Science and Mechanics

```
C     MODIFIED JUN 29, 1988 TO ALLOW DATA OUTPUT TO DISK OF V() & F()
C     MODIFIED JUL 19, 1988 TO USE POWER SPECTRUM INSTEAD OF THE
C                           AMPLITUDE SPECTUM USED BY A.M & M.K.
C
C     MODIFIED OCT, 1989 TO CORRECT THE CALCULATION OF THE MOMENTS
C                        AND TO USE THE DATA FROM THE THE 25MHz
C                        SONOTEK BOARD AFTER BEING "CONVERTED"
C                        AND COMMENTED OUT ALL OF THE
C                        TRANSFER FUNCTION STUFF (SORRY SCOTT)
C                        TO ONLY USE ONE CHANNEL OF DATA!!
C
C  MODIFIED JAN, 1990 TO USE THE FFT ROUTINE OUT OF NEWLAND
C  MODIFIED FEB, 1990 TO INCLUDE ZERO AVERAGING OF THE VOLTAGE DATA
C                     AND CORRECTED THE DATA OFFSET (BY 1 POINT)
C                     TO USE SINGLE SIDED SPECTRUM AND CORRECTED
C                     TO ASSURE THAT PARSEVAL'S THEOREM HELD FOR ALL DATA
C
C     MODIFIED MAY, 1990 TO ALLOW FREQUENCY WINDOWING
C**********************************************************************
C                        PROGRAM OUTLINE
C
C     1. INITIALIZE - DEFINE ARRAYS , VARIABLE TYPES , REQUEST NAMES OF
C                     INPUT AND OUTPUT FILES
C
C     2. READ CURRENT DATAFILE NAME FROM THE BATCH FILE
C
C     3. READ IN THE DATASET AND RELATED SIGNAL PARAMETERS ( SAMPLE
C        RATE, NUMBER OF DATA POINTS ... )
C
C     4. CONVERT DATASET FROM DIGITIZED DATA POINTS ( -128 TO 128 ) TO
C        THE ACTUAL VOLTAGES EVALUATED ( -0.5 TO +0.5 VOLTS )
C
C     5. ZERO AVERAGE THE VOLTAGE DATA
C
C     6. SET NUMBER OF DATA POINTS TO A MULTIPLE OF 2 (FFT RESTRICTION)
C
C     7. GATE THE SIGNAL AND PAD WITH ZEROES IF NECCESSARY
C
C     8. PERFORM THE FOURIER TRANSFORM
C
C     9. CALCULATE THE STATISTICAL MOMENTS OF THE PSD/
C        FREQUENCY DATA
C
C     10. GO BACK TO STEP 2 UNTIL ALL DATASETS IN THE BATCH FILE ARE
C           DONE
C**********************************************************
C     ACOUSTO-ULTRASONIC SIGNAL PROCESSING PROGRAM FOR DATAFILES
C     GENERATED BY THE SONOTEK STR 825 DATA AQUISTION SYSTEM
```

```
C*************************************************************
      PROGRAM POWERAU
      INTEGER GLEN,NGLEN,POP,ILOOP,SMPLRT,GSTPTA,GSTPTB
      CHARACTER*12 FNAME,FLNAME,OUT1,OUT2,OUT3
      character title1*70,title2*70,SCREEN*1,SCRPLOT*1,gating*1
      CHARACTER FRQWNDW*1
      character answer1*1, answer2*1,PERIOD*1,VTDFILE*1,PWRFILE*1
      DIMENSION AMP(0:2049),HA(0:2049),FREQ(0:2049),time(0:2049)
      DIMENSION PLTIME(0:2049),psd(0:2049)
      common V(0:4097),AR(0:2047),AI(0:2047)
C*************************************************************
C     READ IN THE DIGITIZED SIGNAL FROM DATAFILE
C*************************************************************
C     CREATE A BATCH FILE TO PROCESS DIGITIZED DATA FROM DS (INPUT).
C     THE FOLLOWING VARIABLES ARE READ FROM THE INPUT FILE:
C
C     GSTART    = GATE START INFORMATION.
C     SRATE     = SAMPLING RATE INFORMATION.
C     V(M)    = DIGITIZED VOLTAGES READ IN AS AN ARRAY (MAX = 4096)
C     NGLEN   = CALCULATED GATE LENGTH (FROM # OF DATA POINTS READ)
C*************************************************************************
     write(*,*) ''
     WRITE(*,*) '  Acousto-Ultrasonic Signal Processing Program    '
     WRITE(*,*) '  for use with output data from the Sonotek 825   '
     write(*,*) ''
     write(*,*) ' Department of Engineering Science & Mechanics     '
     write(*,*) ' Virginia Polytechnic Institute & State University '
     write(*,*) ''
     write(*,*)
C
      answer1='n'
      answer2='n'
      L2 = 0
C
     WRITE(*,*) '' INPUT the name of the file listing all of''
     write(*,*) ''  the data file names.....>>> ''
      read(*,*) fname
      WRITE(*,*) '' Input the name of the SWF OUTPUT file .....>>> ''
      read(*,*) out1
C
      WRITE(*,*) '' Do you want on-screen plots ( Y or [N] ) ...>>> ''
      read(*,*) SCRPLOT
      if (SCRPLOT.eq.''y'') screen = ''Y''
      IF (SCRPLOT.EQ.''Y'') SCREEN = ''Y''
C
      IF (SCREEN.EQ.''Y'') THEN
        WRITE(*,*) '' Do you want screen prints or just view plots?''
        write(*,*) '' To print enter a the number 1.....>>>''
```

```
        read(*,*)iprnt
      ENDIF
C
C       WRITE(*,*) " Do you want a statistical analysis [N].....>>> "
C       read(*,*) stats
C       if (stats.eq."Y") L2 = 2
C       if (stats.eq."y") L2 = 2
C       if (L2.eq.2) then
C         write(*,*) " Input the name of the STATS OUTPUT file ....>>> "
C         read(*,*) out2
C       endif
C
      WRITE(*,*) " Do you want to gate the time signals for "
      write(*,*)" the data files listed in ",fname," ?  [Y/N]....>>> "
      READ(*,*) gating
      if (gating.eq."Y") gating="y"
C
C
     WRITE(*,*)"DO YOU WANT TO FREQ WINDOW THE SIGNALS IN THE FILES"
     WRITE(*,*)"LISTED IN ",FNAME,"?(ONLY EFFECTS SWF CALCS) [Y/N]..>>"
      READ (*,*) FRQWNDW
      IF (FRQWNDW.EQ."Y") FRQWNDW="y"
      IF (FRQWNDW.EQ."y")THEN
        WRITE(*,*) "WHAT IS THE LOW FREQ FOR THE WINDOW (IN HERTZ)? "
        READ (*,*)FRQLOW
        WRITE(*,*) "WHAT IS THE HIGH FREQ FOR THE WINDOW (IN HERTZ)? "
        READ (*,*)FRQHGH
      ENDIF
C
     WRITE(*,*)" Do you want to save an ASCII file of the (Gated)"
     write(*,*)" Voltage vs. Time? [Y or N].....>>"
     read(*,*)VTDFILE
     IF (VTDFILE.EQ."y")VTDFILE="Y"
C
     WRITE(*,*)" Do you want to save an ASCII file of the Power Spect."
     write(*,*)" of the (Gated) voltage data vs. Freq.? [Y or N]...>> "
     read(*,*)PWRFILE
     IF (PWRFILE.EQ."y")PWRFILE="Y"
C
      OPEN(UNIT=7,FILE=FNAME)
      OPEN(UNIT=9,FILE=OUT1)
C       IF (L2.GT.0) OPEN(UNIT=10,FILE=OUT2)
C
      do 200 loop=1,2000
 10   READ(7,*,END = 300) FLNAME
C  FIND LOCATION OF PERIOD IN FLNAME
     PERIOD="."
     PERLOC = INDEX(FLNAME,PERIOD)
```

```
      WRITE(*,*) " PROCESSING FILE - ",FLNAME
C
      DO 15 K=0,NGLEN
        V(K) = 0.0
 15   CONTINUE
C
C     OPEN AND READ DATASET    READ READ READ READ READ READ READ
C  NOTE: THIS IS SETUP TO READ IN THE DIGISCOPE DATA AFTER IT HAS
C       BEEN RUN THRU THE "CONVERT.C" FILE WHICH LISTS EACH WAVE
C       FROM POINT ON A NEW LINE!!!!     10/3/89
C
C   NOTE: THIS IS SETUP ONLY TO DEAL WITH ONE CHANNEL OF DATA!!!
C
C   VARIABLE NAMES IN THIS SECTION:
C             SMPLRT=SAMPLE RATE FLAG (0-10)
C             SRATE=SAMPLE RATE   NOTE SRATE*1000000=SRATE IN Hz
C             NCHNNL=CHANNEL NO. FLAG (0=NO CHANNEL,1=A,2=B,3=BOTH)
C             NWAVES=NUMBER OF WAVEFORMS IN THE FILE
C             GSTPTA=GATE START POINT, CHANNEL A (IN # OF DATAPTS)
C             GSTPTB=GATE START POINT, CHANNEL B (IN # OF DATAPTS)
C             GSTART=GSTART POINT IN SECONDS USED FOR REST OF
C                  CALCULATIONS, EITHER CHANNEL A OR B
C             NGLENA=NUMBER OF DATA POINTS IN GATE, CHANNEL A
C             NGLENB=NUMBER OF DATA POINTS IN GATE, CHANNEL B
C             NGLEN= NUMBER OF DATA POINTS IN GATE OF SINGLE
C                 CHANNEL (EITHER A OR B) USED IN REST OF CALCS
C             V(K)=8 BIT VOLTAGE ARRAY (-128 TO +127)
C
      OPEN(UNIT=8,FILE=FLNAME)
      READ(8,20) SMPLRT
 20    FORMAT(I2)
       IF (SMPLRT.EQ.0)SRATE=0.195
       IF (SMPLRT.EQ.1)SRATE=0.390
       IF (SMPLRT.EQ.2)SRATE=0.781
       IF (SMPLRT.EQ.3)SRATE=1.560
       IF (SMPLRT.EQ.4)SRATE=3.125
       IF (SMPLRT.EQ.5)SRATE=6.250
       IF (SMPLRT.EQ.6)SRATE=12.50
       IF (SMPLRT.EQ.7)SRATE=25.00
       IF (SMPLRT.EQ.8)SRATE=50.00
       IF (SMPLRT.EQ.9)SRATE=100.0
       IF (SMPLRT.EQ.10)SRATE=200.0
       WRITE(*,*)SRATE
C
      READ(8,25)NCHNNL
 25    FORMAT(I1)
C
      READ(8,30)NWAVES
```

```
 30   FORMAT(4X,I1)
      IF(NWAVES.NE.1) THEN
        WRITE(*,*)"MORE THAN ONE WAVE FOUND IN FILE -ERROR"
        GOTO 300
       ENDIF
C
      READ(8,31)GSTPTA
 31   FORMAT(I4)
      READ(8,31)GSTPTB
      READ(8,31)NGLENA
      READ(8,31)NGLENB
C
      IF(NCHNNL.EQ.0)THEN
       WRITE(*,*)"NO INPUT CHANNEL SPECIFIED"
       GOTO 300
       ENDIF
      IF(NCHNNL.EQ.1)THEN
       GSTART=GSTPTA/(SRATE*1000000)
       NGLEN=NGLENA
       ENDIF
      IF(NCHNNL.EQ.2)THEN
       GSTART=GSTPTB/(SRATE*1000000)
       NGLEN=NGLENB
       ENDIF
      IF(NCHNNL.EQ.3)THEN
       WRITE(*,*)"CANNOT HANDLE 2 CHANNEL INPUT"
       GOTO 300
       ENDIF
C
      DO 50 J=0,NGLEN-1
      READ(8,55,END=60)V(J)
 55   FORMAT(F4.0)
 50   continue
C
 60   CLOSE(8)
C                  READ READ READ READ READ READ READ READ READ READ
C*************************************************************
C     CONVERT PC-DAS SIGNALS TO THE ACTUAL VOLTAGES
C*************************************************************
C     THIS SECTION CONVERTS THE DATA POINTS READ TO ACTUAL VOLTAGE.
C     TIME CAN BE COMPUTED USING SAMPLING RATE AND GATE LENGTH.
C
C       V(M)  = VOLTAGE EQUIVALENTS OF THE INPUT DATA ARRAY
C             = ( PC-DAS INPUT DATA POINTS ) * 0.5 / 128
C             where M = 0,1,2...NGLEN-1
C  VOLTTOT = THE SUM TOTAL OF ALL OF THE VOLTAGE VALUE ( TO BE USED
C               IN THE ZERO AVERAGING ROUTINE
C*************************************************************
```

```
      VOLTTOT=0.0
 70   DO 80 K = 0,NGLEN-1
        V(K)=V(K)*0.5/128
        VOLTTOT = VOLTTOT+V(K)
 80   CONTINUE
C
C          ZERO AVERAGE THE VOLTAGE DATA ( REMOVE THE DC OFFSET )
      VOLTAVG=VOLTTOT/NGLEN
      DO 71 K=0,NGLEN-1
        V(K)=V(K)-VOLTAVG
 71   CONTINUE
C*********************************************************
C     DEVELOP OPTIMUM ARRAY SIZE FOR THE FHT/DFT
C*********************************************************
C     THIS SECTION CONVERTS THE NUMBER OF DATA POINTS [GATE LENGTH]
C     TO THE NEAREST 2**P NUMBER OF POINTS.
C     NGLEN IS RESET AS GLEN, WHERE GLEN = (2**P)-1 IS NEW GATE LENGTH.
C     THIS IS DONE FOR FFT/FHT PURPOSES.  The minus 1 is included
C      because the voltage array includes V(0).
C*********************************************************
 205  IF (NGLEN.LE.512) THEN
        GLEN = 512-1
        POP=9
      ENDIF
 65   IF ((NGLEN.GT.512) .AND. (NGLEN .LE.1024)) THEN
        GLEN = 1024-1
        POP=10
      ENDIF
 75   IF ((NGLEN.GT.1024) .AND. (NGLEN .LE. 2048)) THEN
        GLEN = 2048-1
        POP=11
      ENDIF
 85   IF ((NGLEN.GT.2048) .AND. (NGLEN .LE. 4096)) THEN
        GLEN = 4096-1
        POP=12
      ENDIF
C*********************************************************
C     SIGNAL GATING SECTION AND ZERO PADDING FOR FHT/DFT.
C*********************************************************
C     THIS SECTION ADDS ZEROES TO THE VOLTAGE ARRAY BEYOND THE
C     RECORDED DATA POINTS TO MAKE THE NEW GATE LENGTH = 2**P.
C     GATING CAN ALSO BE DONE ON THE SIGNAL AND THIS GATED REGION
C     CAN BE PLOTTED OR USED LATER FOR PERFORMING FFT'S.
C
C     VARIABLES USED:
C     GSTART = GATE START TIME IN SECONDS
C     GSTIME = NEW GATE START TIME SPECIFIED BY THE USER IN SECONDS
C     GEND   = GATE END TIME IN SECONDS
```

```
C     GETIME = NEW GATE END TIME SPECIFIED BY THE USER IN SECONDS
C     TIME(I)= ACTUAL TIME ARRAY IN SECONDS
C     PLTIME(I)=TIME ARRAY IN MICROSECONDS FOR SCREEN PLOTS
C
C
C    NOTE: EVEN IF THE TIME-VOLTAGE SIGNAL IS WINDOWED, THIS PROGRAM
C       STILL USES THE ORIGINAL GATELENTH (GLEN) TO THE NEAREST N**2
C*********************************************************
 95   DO 105 I = NGLEN,GLEN
        V(I) = 0.0
105   CONTINUE
C*********************************************************
C
 90   DO 101 I = 0,GLEN
      time(i) = (I/(SRATE*1000000))+GSTART
      PLTIME(I)=(TIME(I))*(1.0E6)
101   CONTINUE
C
C     [ OPTIONAL ] PLOT ORIGINAL DIGITIZED DATA TO THE SCREEN
C
      IF (SCREEN.EQ."Y") THEN
      title1 = '    Voltage vs. Time                    Filenam
     &e: '//flname
      title2 = '    (volts)   (microsec) '
      iglen = glen
      call plotter(iglen,PLtime,V,title1,title2,IPRNT)
      ENDIF
C
      IF(GATING.EQ."y")GOTO 144
       GOTO 146
C
 144  WRITE(*,*)'Gate this signal, filename= ',flname,' ?'
      WRITE(*,*) ' Yes(1) or No(2).....>>> '
      READ(*,*) PROMP4
      IF(PROMP4.EQ.2) GOTO 146
      WRITE(*,*)' Current Gate Starts at ',time(0),' seconds'
      write(*,*) ' '
      write(*,*) ' Enter New Gate Start (in seconds ).....>>> '
      read(*,*) gstime
      write(*,*) ' '
      write(*,*) ' Current Gate Ends at   ',time(glen),' seconds'
      write(*,*) ' '
      write(*,*) ' Enter New Gate Ending ( in seconds ).....>>> '
      read(*,*) getime
      NGST = GSTIME*SRATE*1.0e06
      NGEND = GETIME*SRATE*1.0e06
       DO 115 I = 0,NGST
 115        V(I) = 0.0
```

```
      DO 125 I = NGEND,GLEN
  125       V(I) = 0.0
  175    CONTINUE
C
C     [ OPTIONAL ] PLOT GATED DIGITIZED DATA TO THE SCREEN
C
      IF (SCREEN.EQ."Y") THEN
      title1 = '  Gated Voltage vs. Time                    Filenam
     &e: '//flname
      title2 = '    (volts)       (microsec) '
      iglen = glen
      call plotter(iglen,PLtime,V,title1,title2,IPRNT)
      ENDIF
C
  146  DELTAE=0.0
      ENERGY=0.0
      POWERVT=0.0
     DELTIME=1.0/SRATE*1000000
     DO 102 I=0,GLEN
     POWERVT=POWERVT+V(I)**2
  102  CONTINUE
c
C THE NEXT LINE IS TO CORRECT THE DISCRETELY FOUND POWER FROM THE
C    VOLTAGES**2 BY THE NUMBER OF DATA POINTS (PARSEVAL'S THEOREM)
      POWERVT=POWERVT/(GLEN+1)
c
      IF (VTDFILE.NE."Y") GOTO 145
      OUT3=FLNAME(1:PERLOC)//'VTD'
C  NOTE '.VTD' STANDS FOR VOLTAGE - TIME DATA
C
          open(unit=1,file=out3)
          do 110 iloop=0,glen
             write(1,*) time(iloop),V(iloop)
  110      continue
          close(1)
C*************************************************************
C     DISCRETE FOURIER TRANSFORM
C*************************************************************
CTHIS SECTION CALLS THE ROUTINE & PERFORMS FFT ON THE TIME-VOLTAGE
C DATA. THE AMPLITUDE IS THEN CALCULATED FOR THE MOMENTS SECTION.
C
C    V(N)  = REAL ARRAY USED IN THE COMPUTATION OF THE FAST HARTLEY
C            TRANSFORM , DISCRETE FOURIER TRANSFORM RETURNED IN AI,AR
C            where N = 0,1,2,3,4,...GLEN ( GLEN = (2**pop)-1  )
C    AR(I) = REAL PART OF F() AFTER THE FFT
C    AC(I) = IMAGINARY PART OF F() AFTER  THE FFT.
C    AMP(I) = AMPLITUDE OF THE FFT OF THE SIGNAL
C    PSD(I) = SINGLE SIDED POWER SPECTRAL DENDITY
```

```
C           (THE FACTOR OF 2 MAKES IT SINGLE SIDED).
C
C   FREQ(I)  = FREQUENCY.
C      where I = 0,1,2,3,...[((2**POP)/2)-1]
C
C   SUBROUTINES CALLED:
C   FFT.FOR
C*************************************************************
 145  CONTINUE
      DO 151 I = 0,2047
        AR(I) = 0.0
        AI(I) = 0.0
        AMP(I) = 0.0
        PSD(I) = 0.0
 151  CONTINUE
C
      CALL FFT(POP)
C
C     CALCULATE THE POWER SPECTRUM FROM THE FFT
C
        TTOL = NGLEN/(SRATE*1000000)
     DO 160 I = 0,(GLEN-1)/2
        AMP(I) = (2*(AR(I)**2 + AI(I)**2))**0.5
        PSD(I) =2*( (AR(I)**2 + AI(I)**2) )/TTOL
C
        IF(AMP(I) .LT. 0 ) AMP(I) = 0.0
        FREQ(I) = (SRATE/GLEN)*I
C
 160 CONTINUE
C
      IF(PWRFILE.NE."Y")GOTO 142
        OUT3=FLNAME(1:PERLOC)//'PWR'
C       NOTE:'.PWR' STANDS FOR POWER SPECTRUM
C
        open(unit=1,file=out3)
C
C       NOTE:FREQ(I) SHOULD BE TITLED IN MEGAHERTZ!
      DO 161 I=0,(GLEN-1)/2
         write(1,*) freq(i),PSD(i)
 161  CONTINUE
         close(1)
C
C     [ OPTIONAL ] PLOT POWER SPECTRUM DATA TO THE SCREEN
C
 142  IF (SCREEN.EQ."Y") THEN
      title1 = '  Power Spectral Density vs. Frequency          Filenam
     &e: '//flname
      title2 = '   (v**2)/(Hz)        (MHz)   '
```

```
      iglen = glen/2
      call plotter(iglen,freq,psd,title1,title2,IPRNT)
      ENDIF
C*******************************************************
C   SPECTRAL MOMENT / STRESS WAVE FACTOR CALCULATIONS
C*******************************************************
C
C THIS SECTION IS USED TO GENERATE THE VARIOUS MOMENTS (0th,1st,2nd,&
C 4th) OF THE AMPLITUDE-FREQUENCY SPECTRUM. THESE CORRESPOND TO
C  THE DIFFERENT STRESS WAVE FACTORS DEFINED BY A. VARY & OTHERS.
C
C   THE SPECTRUM CALCULATED IS THE POWER SPECTRUM DEFINED AS:
C   PS() = AI^2 + AR^2  or FOR THE DHT PS(v)=[H(N-v)^2 + H(v)^2] / 2
C PREVIOUS VERSIONS OF THIS PROGRAM CALCULATED THE AMPLITUDE
C SPECTRUM [ SQRT(PS) ] , WHICH HAS SINCE BEEN CHANGED. OLD RESULTS
C  MAY REFLECT THESE CALCULATIONS.
C
C   A1 = SQRT OF ( SWF0 OR THE ZEROTH MOMENT ).          [OLD SWF]
C   AMO = AREA UNDER THE CURVE                          [NEW SWF]
C*******************************************************
      FT=1.0/((GLEN+1)/(SRATE*1000000))
C
      IF (FRQWNDW.NE."y") THEN
        IWNDLOW=0
        IWNDHGH=(GLEN-1)/2
      ELSE
        IWNDLOW=FRQLOW/FT
        IWNDHGH=FRQHGH/FT
      ENDIF
C
     IF(IWNDHGH.GE.((GLEN-1)/2))IWNDHGH=((GLEN-1)/2)
C
  165  AP = 0.0
      AMO = 0.0
      AM1 = 0.0
      AM2 = 0.0
      AM4 = 0.0
      POWERPW=0.0
      DO 180 I = IWNDLOW,IWNDHGH
        AP = FT * ( PSD(I) + PSD(I+1) )/2.0
        AMO = AMO + AP
        ww = (i*ft)+(ft)/2.0
        am1 = am1 + ap*ww
        am2 = am2 + ap*(ww**2)
        am4 = am4 + ap*(ww**4)
       POWERPW=POWERPW+(AMP(I)**2)
  180  CONTINUE
C
```

```
      a1 = amo**0.5
      b1 = am1 / amo
      c1 = (am2/amo)**0.5
      d1 = (am4/am2)**0.5
      e1=c1/d1
C
C     WRITE THE MOMENT CALCULATIONS TO THE OUTPUT FILE
      write(9,*)
      write(9,*) " FILENAME  -  ",FLNAME
      WRITE(9,*) "FREQ WINDOW LOW = ",IWNDLOW*FT
      WRITE(9,*) "FREQ WINDOW HIGH= ",IWNDHGH*FT
      WRITE(9,*) "TIME TOTAL = ",TTOL
      write(9,*) " M0          = ",AMO,"   SQRT OF M0    = ",A1
      write(9,*) " M1          = ",AM1,"   M1 / M0       = ",B1
      write(9,*) " M2          = ",AM2,"   SQRT OF M2/M0 = ",C1
      write(9,*) " M4          = ",AM4,"   SQRT OF M4/M2 = ",D1
      write(9,*) " SWF3 / SWF4  = ",E1
     WRITE(9,*)" POWERVT     = ",POWERVT,"   POWERPW      =",POWERPW
C
  120 continue
C
  300 CLOSE(7)
      CLOSE(9)
      IF (L2.GT.0) CLOSE(10)
      STOP
      END
C*******************************************************
C              FAST FOURIER TRANSFORM SUBROUTINE
C*******************************************************
C
C  FROM THE BOOK : "An introduction to Random Vibrations and
C                   Spectral Analysis"   BY D. E. Newland
C
C  DELIVERS DFT AS R(I) + i X(I) , FOR I = 0 to N-1
C*********************************************************************
C
      SUBROUTINE FFT(IPOP)
      COMMON V(0:4097),R(0:2047),X(0:2047)
      COMPLEX A(8100),U,W,T
      POP=IPOP
      NB=2**POP
      DO 1000 I=1,NB
      A(I)=V(I-1)
c the -1 accounts for the offset of 1 between the votage and fft arrays
 1000  CONTINUE
      HI = NB
      DO 1100 J = 1,NB
 1100  A(J) = A(J)/NB
```

```
      NBD = NB/2
      NBM = NB-1
      J = 1
      DO 1200 L = 1,NBM
      IF(L.GE.J) GOTO 1300
      T = A(J)
      A(J) = A(L)
      A(L) = T
 1300 K = NBD
 1400 IF(K.GE.J) GOTO 1200
      J = J-K
      K = K/2
      GOTO 1400
 1200 J = J+K
      DO 1225 IZ = 1,18
      HI = HI/2
      IF (HI.EQ. 1) GOTO 1335
 1225 CONTINUE
 1335 NN = IZ
      PI = 3.1415926535893
      DO 1600 M = 1,NN
      U = (1.0,0.0)
      ME = 2**M
      K = ME/2
      W = CMPLX(COS(PI/K),-SIN(PI/K))
      DO 1600 J = 1,K
      DO 1700 L = J,NB,ME
      LPK = L+K
      T = A(LPK)*U
      A(LPK)=A(L)-T
 1700 A(L) = A(L)+T
 1600 U = U*W
C
      DO 5000 II=1,NB
C       R(II)=REAL PART OF A(II)
C       X(II)=IMAG PART OF A(II)
        R(II-1)=REAL(A(II))
        X(II-1)=AIMAG(A(II))
 5000 CONTINUE
C
      RETURN
      END
```

VITA

The author was born on March 11, 1964 in Niagara Falls, New York. He was raised and educated in the Houston, Texas and Newark, Delaware areas. Upon graduating in 1982 from Saint Mark's High School in Wilmington, Delaware he entered the Mechanical Engineering Department of Virginia Polytechnic Institute and State University. In June, 1986, he received his Bachelor of Science Degree in Mechanical Engineering with a Minor in Engineering Science and Mechanics from VPI & SU. He then began work on a Master of Science Degree in Engineering Mechanics at VPI & SU. While working toward this degree, the author also worked at the Hercules Aerospace Corporation, Radford Army Ammunition Plant, in Radford, Virginia as a Mechanical Engineer in the Facilities Engineering Department. Upon completion of this degree, Paul will be joining the Michelin Tire Corporation at the Michelin Americas Research & Development Corporation (MARC) in Greenville, South Carolina as a Design Engineer.